Università degli Studi di Ferrara

DOTTORATO DI RICERCA IN
"SCIENZE DELLA TERRA"

CICLO XXX

COORDINATORE - Prof. Massimo Coltorti

Petrological and geochronological study of magmatic products and mantle xenoliths from Cenozoic Southalpine Magmatic Province (North-East Italy)

Settore Scientifico Disciplinare GEO/07

Dottorando
Dott. Brombin Valentina

Tutori
Prof. Coltorti Massimo

Prof. Bonadiman Costanza

Prof. Marzoli Andrea

Anni 2014/2017

Table of contents

Abstract

The Cenozoic Southalpine Magmatic Province, known as Veneto Volcanic Province (VVP; NE Italy) is one of the widest magmatic areas within the Adria plate. It is formed by five main magmatic districts that are from north-west to south-east: Val d'Adige, Lessini Mts., Marosticano, Berici Hills, and Euganean Hills. Only in this last district volcanic and subvolcanic rocks range from subordinate basalts to prevalently acidic types, mostly quartz-trachytes and rhyolites, while for the rest of the VVP districts the outcropping volcanics are wholly undifferentiated lavas, ranging in composition from mela-nephelinites to quartz-normative tholeiites. Commonly alkaline basalts host mantle peridotites. Despite the extensive petrological studies on this province, the geochronological data of the related magmatic activities for each district are poorly defined or even totally missing. The combination of previous biostratigraphic data with new $^{40}Ar/^{39}Ar$ radioisotopic ages of VVP magmatic products allowed to reconstruct the temporal evolution of the magmatic activity, which was discontinuous and covers a time-span of about 30 Ma (from late Paleocene to early Miocene). In addition, i) new isotropic and anisotropic tomographies for the Alpine region and ii) recent numerical modelling revealing the rarity of the magmatism induced by slab breakoff allow to develop a new model for mechanism triggering the VVP magmatism. This involves the upwelling of toroidal/poloidal flow induced by the progressive retreat and steepness of the subducting European slab after the Adria-Europe continent collision. A likely explanation for the southeastward migration of the magmatism can be accounted for the overidding Adria plate moving faster than the European slab retreatment. The geochemistry of the VVP mafic samples shows a typical OIB signature, as well as positive Ba, Sr, and P anomalies, probably inherited by a carbonatite metasomatized mantle source. This last consideration seems to be confirmed by the geochemical features of the new occurrences of Marosticano mantle xenoliths that reveal an unexpected on-craton type mantle with fingerprint of carbonatitic/CO_2-rich silicatic melt metasomatism. According to the previous studies Val d'Adige and Lessini Mts. mantle xenoliths exhibit characteristics of off-craton lithospheric mantle variably affected by Na-alkaline silicatic metasomatism. However, on- and off-craton VVP mantle portions show similar Archean/Proterozoic Re-Os ages, suggesting that the Marosticano mantle domain could be interpreted as the vestige of an Archean/Proterozoic cratonic keel, whose signature was not erased by the carbonatitic/CO_2-rich silicatic metasomatism, whereas Lessini Mts. and Val d'Adige xenoliths are remnants of circum-cratonic domains compositionally rejuvenated by infiltration of asthenospheric-derived melts, which

upwelling could be induced by the retreatment of the European slab after the Adria/Europe collision.

Introduction and aim of the thesis

Introduction and aim of the thesis

This thesis is focused on the study of Veneto Volcanic Province Sub Continental Lithospheric Mantle (SCLM), through the petrological, geochemical and geochronological characterization of the i) products of Cenozoic Southalpine magmatism and ii) the mantle xenoliths carried out on the surface by the alkaline lavas.

The Cenozoic Southalpine magmatic province (NE Italy), known in literature as Veneto Volcanic Province (VVP; e.g., De Vecchi and Sedea, 1995; Beccaluva et al., 2001, 2007; Macera et al., 2003, 2008; Visonà et al., 2007) is one of the widest magmatic districts of the Adria (or Apulia) plate, the northern continental promontory of the African plate (Beccaluva et al., 2007). From late Paleocene to early Miocene, the VVP magmatic activities developed along a series of eruptive centers orientated NNW-SSE: Val d'Adige, Lessini Mts., Marosticano, Berici Hills, and Euganean Hills. Magma generation appears to have been triggered by decompressional effects related to extensional deformation affecting the Southalpine foreland in response to the general north-south compression during Alpine orogenesis (Beccaluva et al., 2003; 2005). Since the early '90s, extensive petrological studies were carried out on the VVP magmatism, mainly on the basic products; they comprise a wide compositional spectrum including (mela) M-nephelinites, basanites to the west (Val d'Adige and western Lessini Mts.), and predominantly alkali-basalts, transitional basalts and tholeiites to the east (eastern Lessini Mts. and Marosticano) areas (De Vecchi and Sedea, 1995; Beccaluva et al., 2001, 2007; Macera et al., 2003, 2008), only in the Euganean Hills volcanic and subvulcanic rocks range from subordinate basalts to prevalently acidic types, mostly quartz-trachytes and rhyolites (Milani et al., 1999) According to Macera et al. (2003) and Beccaluva et al. (2007) i) the potassic affinity ($Na_2O/K_2O>1$), and ii) the incompatible element distribution (characterized by negative anomalies in Cs, Rb, K and positive anomalies in Nb and Ta) of the VVP volcanics are indices of the intraplate origin from ocean island basalt (OIB)-like mantle source. Despite the deep petrological and geochemical knowledge of the VVP magmatism, the geochronology of the volcanic activities for each district is still poorly defined or even totally missing. Radioisotopic dating were obtained by Borsi and Ferrara (1969), Borsi et al. (1969), and Savelli and Lipparini (1979) with the no longer going in use K-Ar method. Therefore, new high-resolution $^{40}Ar/^{39}Ar$ measurements of basic and acidic lavas from selected key locations of Val d'Adige, Marosticano, Lessini Mts., and Euganean Hills districts were performed in order to i) reconstruct the temporal and geochemical evolution of the VVP magmatism, and ii) understand the interaction between Cenozoic magmatism of the eastern Alps and Alpine orogenesis. These data constitute the backbone of the first

part of my thesis and the results will be submitted in Chemical Geology for publication.

To constrain nature and evolution of the lithospheric mantle source of the VVP magmatic products, mantle peridotites commonly hosted in basanite and nephelinites of various VVP mantle districts were also taken into account. Previous studies of Val d'Adige and Lessini Mts. xenoliths reveal variably depleted mantle domains subsequently enriched by one or more episodes of alkali-silicate metasomatism (Morten et al., 1989; Siena and Coltorti et al., 1989; Beccaluva et al., 2001; Gasperini et al., 2006).

In this frame, a detailed petrological study (major and trace element) and T-$\Delta \log fO_2$ estimates of a newly found suite of mantle xenoliths from the Marosticano district go to building the second part of my thesis along with Re-Os isotopic data from sulfides of Val d'Adige, Lessini Mts., and Marosticano peridotites (Brombin et al., 2018). Re-Os isotopic measurements performed for the first time on the VVP mantle domain, allowed to date the main melting event that the mantle section has undergone, i.e., transformation of fertile astenospheric material into a depleted, buoyant lithosphere (Alard et al., 2002). The manuscript is in preparation.

In summary the thesis is subdivided in five chapters, in addition to the general introduction of the opening section. These are:

Chapter 1: brief introduction to the geological setting and the geodynamic evolution of VVP.

Chapter 2: analytical methods which include i) bulk rock major (XRF) analyses for magmatic products and mantle xenoliths, ii) trace (ICP-MS) analyses for magmatic products, iii) $^{40}Ar/^{39}Ar$ radioisotopic analyses on groundmass and mineral separates of magmatic products, as well as iv) mineral major (EMP) and v) trace (LA-ICP-MS) analyses for peridotites.

Chapter 3: results and discussion of the $^{40}Ar/^{39}Ar$ radioisotopic ages obtained by from the analyses of groundmass and mineral separates of Val d'Adige, Lessini Mts., Marosticano, and Euganean Hills magmatic products.

Chapter 4: petrological characterization of Marosticano mantle xenoliths in term of major and trace element data, and a comparison with peridotites from the nearby VVP districts Val d'Adige and Lessini Mts. (Morten et al., 1989; Siena and Coltorti et al., 1989; Beccaluva et al., 2001; Gasperini et al., 2006).

Chapter 5: final remarks with a general overview of the main outcomes of the present geochemical and geochronological study, sketching a general geodynamic model of VVP region.

References

Alard, O., Griffin, W.L., Pearson, N.J., Lorand, J.-P., O'Reilly, S.Y., 2002. New insights into the Re-Os systematics of sub-continental lithospherica mantle from in situ analysis of sulphides. Earth and Planetary Science Letters 203, 651-663.

Beccaluva, L., Bonadiman, C., Coltorti, M., Salvini, L., Siena, F., 2001. Depletion events, nature of metasomatizing agent and timing of enrichment processes in lithospheric mantle xenoliths from the Veneto Volcanic Province. Journal of Petrology 42, 173-187.

Beccaluva, L., Bianchini, G. et al., 2003. Tertiary nephelinite to tholeiite magma generation in the Veneto volcanic province, Southern Alps. FIST-Geoitalia 2003 (4° Earth Sciences forum), Abstract volume, 189.

Beccaluva, L., Bianchini, G., Bonadiman, C., Coltorti, M., Macciotta, G., Siena, F., Vaccaro, C., 2005. Within-plate Cenozoic volcanism and lithospheric mantle evolution in the western-central Mediterranean area. In Finetti I. (Eds.) Deep Seismic exploration of the Meditterrranean Region (CROP Project), Elsevier, Amsterdam, 641-664.

Beccaluva, L., Bianchini, G., Bonadiman, C., Coltorti, M., Milani, L., Salvini, L., Siena, F., Tassinari, R., 2007. Intraplate lithospheric and sublithospheric components in the Adriatic domain: Nephelinite to tholeiite magma generation in the Paleogene Veneto Volcanic Province, Southern Alps. Geological Society of America 418, 131-152.

Borsi, S., et al. 1969. In Contributo alla conoscenza geologica della regione di Bolca (Monti Lessini), Barbieri, G., Medizza, F.

Borsi, S., Ferrara, G., Piccoli, G., 1969. Determinazioni col metodo K/Ar dell'età delle eruzioni euganee. Rendiconti della Società Italiana di Mineralogia e Petrologia 25, 27-34.

Brombin, V., Bonadiman, C., Coltorti, M., Fahnestock, M.F., Bryce, J.G., Marzoli, A., 2018. Refertilized mantle keel below the Southern Alps domain (North-East Italy): Evidence from Marosticano refractory mantle peridotites. Lithos 300-301, 72-85.

De Vecchi, G., Sedea, R., 1995. The Paleogene basalts of the Veneto region (NE Italy). Memorie di Scienze Geologiche 47, 253-374.

Gasperini, D., Bosch, D., Braga, R., Bondi, M., Macera, P., Morten, L., 2006. Ultramafic xenoliths from the Veneto Volcanic Province (Italy): Petrological and geochemical evidence for multiple metasomatism of the SE Alps mantle lithosphere. Geochemical Journal 40, 377-404.

Macera, P., Gasperini, D., Piromallo, C., Blichert-Toft, J., Bosch, D., Del Moro, A., Martin, S., 2003. Geodynamic implications of deep mantle upwelling in the source of Tertiary volcanics from the Veneto region (Southern-Eastern Alps). Journal of Geodynamics 36, 563-590.

Macera, P., Gasperini, D., Ranalli, G., Mahatsente, R., 2008. Slab detachment and mantle plume upwelling in subduction zones: an example from the Italian South-Eastern Alps. Journal of Geodynamics 45, 32-48.

Milani, L., Beccaluva, L., Coltorti, M., 1999. Petrogenesis and evolution of the Euganean magmatic complex, north eastern Italy. European Journal of Mineralogy 11, 379-399.

Morten, L., Taylor, L.A., Durazzo, A., 1989. Spinel in harzburgite and lherzolite inclusions from the San Giovanni Ilarione Quarry, Lessini Mountains, Veneto Region, Italy. Mineralogy and Petrology 40, 73-89.

Savelli, C., Lipparini, E., 1979. Età K/Ar di basalti del vicentino e la scala dei tempi del Paleogene. Bollettino della Società Geologica Italiana 98, 375-385.

Siena, F., Coltorti, M., 1989. Lithospheric mantle evolution: evidences from ultramafic xenoliths in the Lessinean volcanics (Northern Itlay). Chemical Geology 77, 347-364.

Visonà, D., Caironi, V., Carraro, A., Dallai, L., Fioretti, A.M., Fanning, M., 2007. Zircon megacrysts from basalts of the Venetian Volcani Province (NE Italy): U-Pb, oxygen isotopes and REE data. Lithos 94, 168-180.

Chapter 1.
Geological setting

1. Geological setting

1.1 The magmatic activity of the Veneto Volcanic Province

The central-western Mediterranean area is geologically young, mostly developed during the last 30 Ma. The geological structure and the igneous activity of this area are due to the relative movements of Europe plate and Adria plate (the continental promontory of Africa plate). The convergence between them led to the E- to SE-directed subduction of the Alpine Tethys, started in the eastern Alps, and to the following continental collision triggering Alpine orogenesis from the middle Eocene, ca. 35 Ma (Dal Piaz and Venturelli, 1983; Stampfli et al., 2001; Rosenbaum et al., 2002; Dal Piaz et al., 2003). From the Eocene to Miocene, the Austroalpine and Southalpine Units were interested by orogenic (or subduction-related) and anorogenic (or intraplate-) magmatic activities, respectively. In the Austroalpine Unit the magmatic activity is represented by sub-alkaline and calc-alkaline silicic intrusive bodies ranging in composition from gabbro to monzogranite (i.e., Adamello, Rensen, Monte Alto, Vedrette di Ries, Cima di Vila, Polland; Bellieni, 1977, 1980; Bassi et al., 2008; Bellieni et al., 2010), and basaltic and andesitic dikes with calc-alkaline to shoshonitic affinity (Harangi et al., 2006; Conticelli et al., 2009; Alagna et al., 2010; Bergomi et al., 2015). The plutons and associated dikes are E-W aligned, close to the Periadriatic Line, forming the so-called "Periadriatic magmatism", which activity developed from 42 to 28 Ma (von Blancknburg and Davis, 1995; Rosenberg, 2004; Schaltegger et al., 2009; Schoene et al., 2012; Bergomi et al., 2015).

In contrast, in the eastern Southalpine, the magmatic activity was extrusive to subvolcanic (Beccaluva et al., 2007; Bassi et al., 2008) and its products constitute the Cenozoic Southalpine Magmatic Province known as Veneto Volcanic Province (VVP; Fig. 1) since '90s (e.g., De Vecchi and Sedea, 1995; Beccaluva et al., 2001, 2007; Macera et al., 2003, 2008; Visonà et al., 2007). The VVP represents one example of "low-volcanicity impactogenic rift" (Barberi et al., 1982), which is defined as zone, where small volumes of relatively undifferentiated magmas with a wide range of serial affinity (from tholeiitic to extremely alkaline) erupted from trastensional systems, triggered by a foreland reaction to a major collisional event (Beccaluva et al., 2007). In case of the VVP, the undifferentiated products erupted along NNW-SSE transtensional fault systems (Zampieri, 1995) in response to the general N-S compression along the Alpine Belt (De Vecchi and Sedea, 1995; Milani et al., 1999; Zampieri, 1995; Beccaluva et al., 2003, 2005).

VVP biostratigraphic data suggest that short-lived volcanic pulses occurred in a time span of about 30 Ma, from the late Paleocene to the early Miocene (Barbieri et al., 1991). Today,

the main products (volcaniclastics rocks, explosion breccias, hyaloclastites, lava flows, pillow lavas, lava vents of mafic to ultramafic composition, shallow level intrusions such as sills or laccoliths) are widespread over an elongated NNW-SSE area of about 1500 km^2, defining from west to east five main volcanic districts (Fig. 1): (1) the Val d'Adige district, between Arco and Rovereto; (2) the Lessini Mts. district between Val d'Adige and the Schio-Vicenza tectonic line; (3) the Marosticano district, east of the Schio-Vicenza line; (4) the Berici Hills district, which is separated from (5) the Euganean Hills, the southernmost district, by the Riviera dei Berici line (Beccaluva et al., 2007). Most VVP volcanic products are relatively undifferentiated lavas, and range in composition from nephelinites to quartz (Qz)-normative tholeiitic basalts. They tend to be spatially and temporally distributed, becoming gradually younger and less alkaline toward SE. Differentiated products only occur in the Euganean district, where Qz-trachytes and rhyolites predominate (Milani et al., 1999, and references therein). Nephelinites and basanites commonly carry spinel peridotite mantle xenoliths (Beccaluva et al., 2001; 2007). The petrological and geochemical characterization of both VVP magmatic products and mantle xenoliths allowed to defining the compositional evolution of the related mantle sources. In fact, isotopic signatures, notably $^{206}Pb/^{204}Pb$ and $^{87}Sr/^{86}Sr$ ratios (18.8-19.8 and 0.703-0.704, respectively) led Beccaluva et al. (2001, 2007) to argue that the SCLM beneath the Adria plate has been enriched by metasomatizing agents, likely including FOZO or HIMU components. This signature may be related to the European Asthenospheric Reservoir (EAR; Hoernle et al., 1995), a large mantle upwelling extending from the eastern Atlantic to Europe and the Mediterranean area. Alternatively, Wilson and Patterson (2001), and more recently Lustrino and Wilson (2007) argued that this Cenozoic volcanism is related to diapiric upwelling of small-scale, finger-like, convective instabilities from the base of the upper mantle.

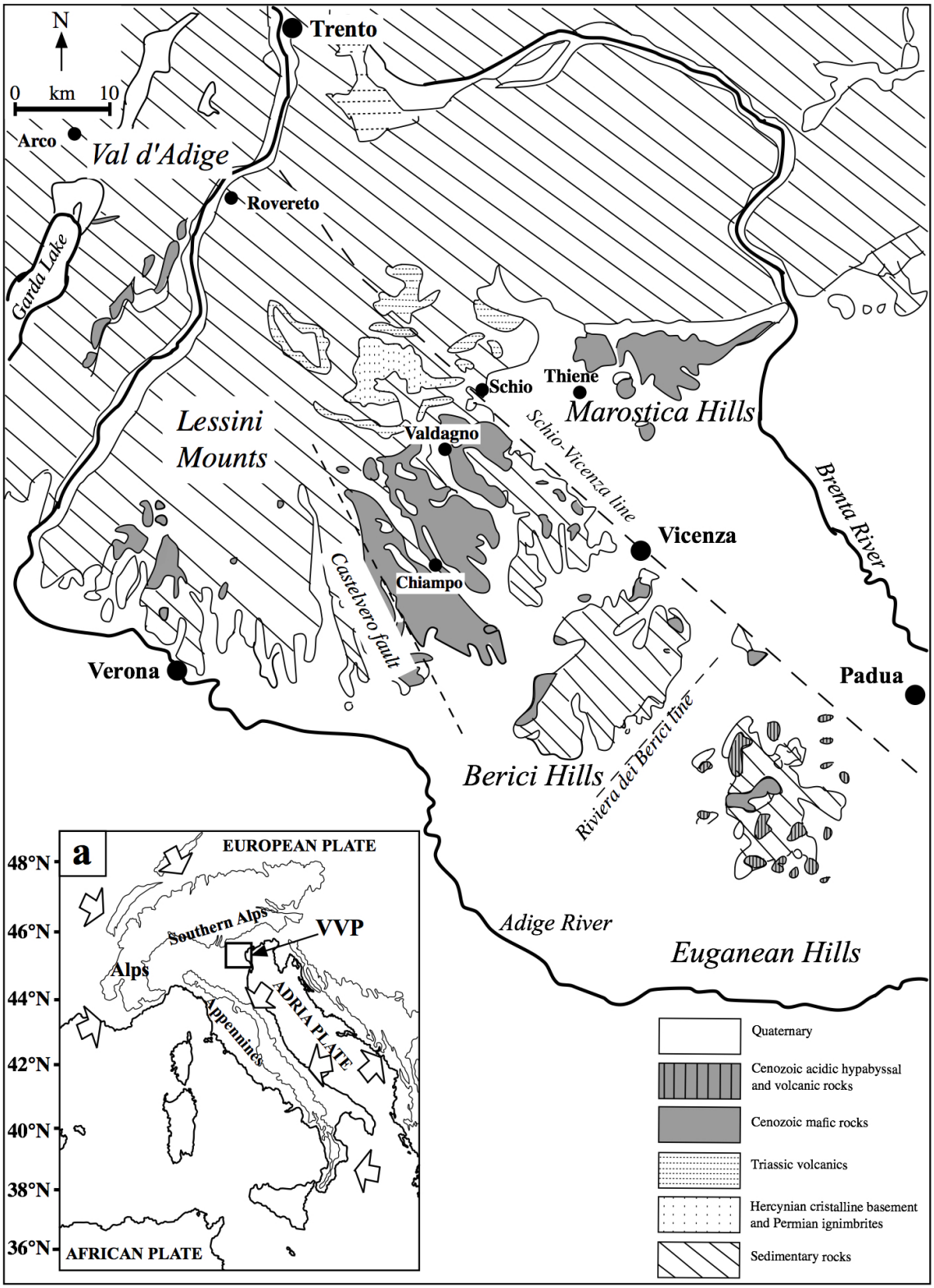

Fig. 1. Geological map of the Veneto Volcanic Province (VVP; De Vecchi and Sedea, 1995) and its five magmatic districts: Val d'Adige, Lessini Mts., Marosticano, Berici Hills, and Euganean Hills. Inset a) Location of VVP in the Italian peninsula, in relation to European, African, and Adria plates. The white arrows show the subduction directions (modified from Carminati and Doglioni, 2012).

1.2 The five VVP magmatic districts

VVP products erupted along the southernmost border of the Jurassic Trento platform, a major structural and paleogeographic domain of the northern Adria margin (Winterer and Bosellini, 1981). The Trento platform was an area of shallow-marine carbonate accumulation until the uppermost Early Jurassic. During the Dogger, it was drowned and subsequently draped by pelagic sediments (Scaglia Rossa) of Late Jurassic to Paleocene age (Bosellini, 1989; Luciani, 1989). During the complex collision between Europe and Adria plates, the former Trento Plateau reacted rigidly and was block-faulted; the submerged platform was segmented into separated blocks, showing variable uplift (Bassi et al., 2008). At the beginning of the Cenozoic, this area was subdivided into two basins roughly separated by the present-day Brenta River. The eastern basin embraced the Belluno and Treviso areas, whereas Monte Baldo, Lessini Mts., Marosticano, Berici Hills, and Euganean Hills belonged to the western basin (Bassi et al., 2008). From late Paleocene to early Miocene, the latter sub-basin was subjected to several pulses of VVP magmatism (Savelli and Lipparini, 1979; Barbieri et al., 1991; Barbieri and Zampieri, 1992; Zampieri, 1995), which allowed the uplift of the seafloor of the highest portions. Since Eocene, these portions acted as centres of initiation of shallow water carbonates, which coalesced to form the carbonate platform "Lessini Shelf", separated from the underlying Upper Cretaceous Scaglia Rossa through hardgrounds and hiatus (Massari and Medizza, 1973; Bosellini, 1989; Luciani, 1989; Barbieri et al., 1991; Zampieri, 2000; Beccaro et al., 2001). Detailed stratigraphic sequences of each district are reported below and shown in Fig. 2.

1.2.1 *Stratigraphy and volcanism in Val d'Adige district: Southern Trentino Alto Adige region and Monte Baldo*

In the Val d'Adige district (Fig. 1), three volcanic pulses are recognized. The oldest event occurred in the late Paleocene as testified by the subaqueous pyroclastics, and epiclastics near Trento (De Vecchi and Sedea, 1995) interbedded with the carbonates of the Scaglia Rossa Formation (Luciani, 1989). The second and volumetrically most important volcanic event occurred during the middle Eocene: subaqueous lava flows were mainly concentrated in the central-northern part of the Monte Baldo and Rovereto area (De Vecchi and Sedea, 1995). The third and last event occurred in the middle Eocene and is represented by minor hyaloclastites and tuffs (De Vecchi and Sedea, 1995). As the first

and third events were mainly phreatomagmatic, the most abundant products from the Val d'Adige district are not-well preserved and extensively altered volcanics, pyroclastics and epiclastics not suitable for radioisotopic measurements. Only in southern Trentino Alto Adige region, in particular along the Monte Baldo ridge, lava flows belonging to the second volcanic event crop out (Luciani, 1989). On Monte Baldo, the Upper Cretaceous Scaglia Rossa is overlapped by Eocene (Ypresian to Lutetian) carbonatic rocks, or by basinal deposits constituted by micritic limestones with planktonic foraminifera (Calcare di Chiusole), as well as slope and platform carbonates (Calcare di Malcesine and Calcare di Torbole). These initial platform sediments were overlaid by basaltic units, which were subaerially erupted in the uppermost Lutetian during a regression event occurred in the Lessini Shelf (Bosellini, 1989; Luciani, 1989). From the middle to late Eocene, the Monte Baldo area was affected by a transgression with formation of a new carbonatic platform (Calcare di Nago) with associated slope (Calcare di Malcesine) and basin deposits (Scaglia Cinerea; e.g., Castellarin and Cita, 1969; Luciani, 1989; Bassi, 2008).

1.2.2 *Stratigraphy and volcanism in Lessini Mts. district*

The Lessini Mts. district is located between the Val d'Adige and the Schio-Vicenza tectonic line (Fig. 1). During the Paleogene, the central-eastern Lessini and western Berici formed a graben system known as "Alpone-Agno graben" (Zampieri, 1995) that influenced the sedimentation on the Lessini Shelf. In fact, since the late Paleocene this structure was bounded toward the west by the east-dipping Castelvero fault (Fig. 1; Barbieri, 1972), that separates two areas characterized by different stratigraphic successions as well as different diffusion and thickness of volcanic products: the western and the eastern Lessini Mts. (Antonelli et al., 1990). On the western Lessini Mts. from Paleocene to Eocene shallow-water marine carbonates dominated (De Zanche and Conterno, 1972; Mietto, 1975; Beschin et al., 1998) as testified by micritic and marly limestones with planctonick foraminifera (Pietra Gallina; Hottinger, 1960) and nummulitic calcarenites (Formazione di Avesa; Sarti, 1980; Ungaro, 2001). During this period, the volcanic activity was weak (De Vecchi and Sedea, 1995) and the magmatic rocks occurred only in isolated necks, breccia necks and rare dykes of basaltic composition (Zampieri, 1995) cross-cutting the middle Eocene sedimentary sequences (De Vecchi and Sedea, 1995). The Oligocene sedimentary and volcanic sequences are lacking (Antonelli et al., 1990), probably due to the emersion of this area (Luciani, 1989).

On the contrary, at the east of the Castelvero fault, from the Paleocene the subsidence was more active, and the eastern Lessini Mts. are characterized by widespread mafic and ultramafic volcanics occuring as hyaloclastites, volcanoclastics, subaqueous and subaerial lava flows, necks and dyke swarms intercalated with marine carbonate deposits (Barbieri and Medizza, 1969; Barbieri, 1972; De Zanche and Conterno, 1972; Beccaro et al., 2001). In the eastern Lessini Mts. sequence, six volcanic phases can be recognized, one from the late Paleocene and the other five from the early to the middle Eocene (De Vecchi and Sedea, 1995; Papazzoni et al., 2014). The first volcanic phase is represented by subaqueous pyroclastic products interbedded between Scaglia Rossa and discontinuous cm-thick lenses of late Paleocene micritic limestone. Subaqueous pyroclastites are the prevalent volcanic products also in the second and third phases, developed during the early Eocene. They are separated from each other by micritic limestone levels. Nummulitic bioclastic calcarenites belonging to the lower part of the "Chiampo Marbles" (Ypresian) separate the third phase of volcanics from those of the other three volcanic phases of middle Eocene. The lowest middle Eocene products are subaqueous pyroclastics, with a maximum thickness of 75 m. The intermediate volcanic level consists of subaqueous pyroclastic deposits, followed by 100 m thick lava flows sometimes emitted in a subaerial environment. The volcanism was exhausted before the late Eocene, when the Priabona Marls were deposited in open marine, deep platform setting. The subaqueous volcanism resumed only in the Aquitanian and was overlaid by coralline calcarenites of Calcari di Lonedo (Savelli and Lipparini, 1979).

1.2.3 *Stratigraphy and volcanism in Marosticano district*

In the Marosticano district the volcanic activity developed discontinuously in the early Oligocene at the same time of the sedimentation of fossiliferous sand, silt, and sandstones (Frascari Ritondale Spano and Bassani, 1973). This rhythmic alternation of volcanic deposits and fossiliferous units, called Salcedo Formation (Frascari Ritondale Spano and Bassani, 1973; Savelli and Lipparini, 1979; De Vecchi and Sedea, 1995), emerged in response to a regression event at the end of the early Oligocene (Frascari Ritondale Spano and Bassani, 1973). During the subaerial conditions of the beginning of Miocene, the volcanics of the last volcanic episode erupted in eastern Marosticano area (Savelli and Lipparini, 1979). These volcanic deposits are overlain by coralline calcarenites of Calcari di Lonedo, that trasgressed onto the Salcedo Formation during the Burdigalian restabilishing the marine conditions (Frascari Ritondale Spano and Bassani, 1973)

1.2.4 *Stratigraphy and volcanism in Euganean Hills district*

From the Eocene to the early Oligocene the Euganean Hills displayed a pelagic environment (Piccoli et al., 1981; Milani et al., 1999). As testified by pelagic marls called "Euganean Marls" deposited above the Ypresian Scaglia Rossa (Massari et al., 1976; Lucchi Garavello, 1980), these basinal conditions continued through the entire early Eocene and extended up to the early Oligocene (De Vecchi and Sedea, 1974; Piccoli et al., 1976). The Euganean Marls are interbedded with mafic volcanics, represented by subaqueous lavas, pillow lavas, pyroclastics, and epiclastics. These products belong to the Eocenic Euganean volcanism (Borsi et al., 1969). Then, according to the previous studies (De Vecchi and Sedea, 1995; Milani et al., 1999; Bartoli et al., 2014), during the lower Oligocene and only in the Euganean Hills, magmatic activity changed suddenly from mafic products to rhyolites, trachytes and subordinately latites. The more acidic rocks were emplaced as subvolcanic bodies with different intrusion mechanism, magma viscosity, internal structure and size (De Vecchi et al., 1976; Piccoli et al., 1976). Intermediate to felsic rocks are considered to have formed by low-pressure fractional crystallization starting from mantle-derived basic magmas, whereas crustal contamination seems to have played a minor role (Milani et al., 1999). The extensive cross-cutting fault system in the Euganean area is considered to have favoured the formation of multiple shallow magma chambers in which mafic magmas accumulated and evolved towards felsic compositions (Milani et al., 1999).

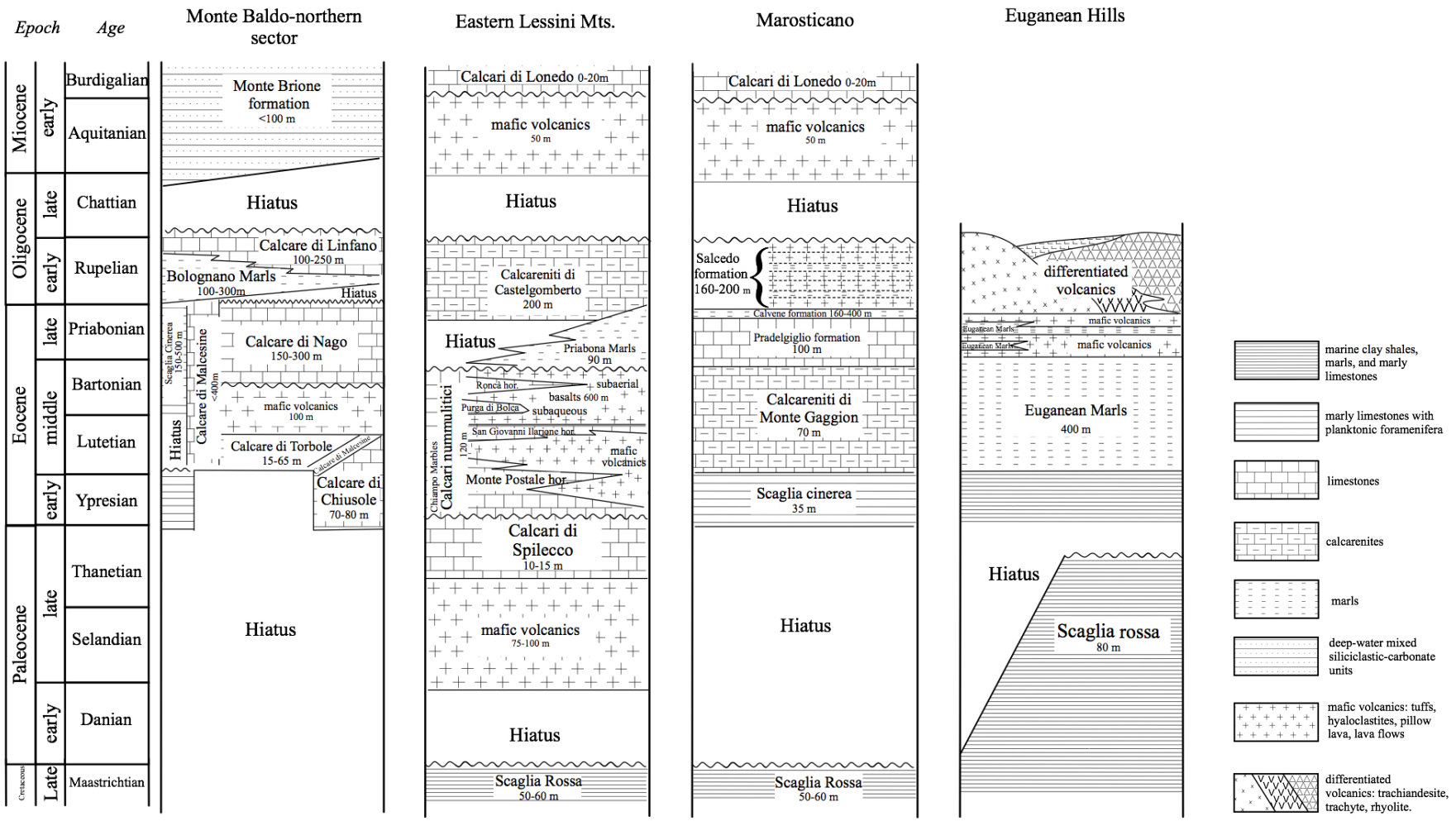

Fig. 2. Upper Cretaceous to lower Miocene stratigraphic record in the Monte Baldo northern sector (Val d'Adige district; Luciani, 1989; De Vecchi and Sedea, 1995), Eastern Lessini Mts. (De Vecchi and Sedea, 1995; Bassi et al., 2008), Marosticano (Frascari Ritondale Spano and Bassani, 1973; De Vecchi and Sedea, 1995; Bassi et al., 2008), and Euganean Hills (Piccoli et al., 1981).

References

Alagna, K.E., Peccerillo, A., Martin S., 2010. Tertiary to present evolution of Orogenic magmatism in Italy. J Virt Expl 36: paper 18. In: Beltrando, M., Peccerillo, A., Mattei, M., Conticelli, S., Doglioni, C. (Eds.) The geology of Italy: tectonics and life along plate margins, 2010.

Antonelli, R., Barbieri, G., Dal Piaz, G.V., Dal Prà, A., De Zanche, V., Grandesso, P., Mietto, P., Sedea, R., Zanferrari, A., 1990. Carta geologica del Veneto. Scala 1:250.000 - una storia di cinquecento milioni di anni. Regione Veneto, SELCA, Firenze, 31 pp. + a geological map.

Barberi, F., Santacroce, R., Varet, J., 1982. Chemical aspects of rift magmatism, in Continental and Oceanic Rifts: American Geophysical Union, Geodynamic Series 8, 223–251.

Barbieri, G., 1972. Sul significato geologico della Faglia di Castelvero (Lessini veronesi), Atti e Memorie Accademia Patavina di Scienze Lettere ed Arti 84, 297- 302.

Barbieri, G., Medizza, F., 1969. Contributo alla conoscenza geologica della regione di Bolca (Monti Lessini). Memorie degli Istituti di Geologia e Mineralogia dell'Università di Padova 27, 1-36.

Barbieri, G., De Zanche, V., Sedea, R., 1991. Evoluzione del semigraben paleogenico Alpone-Agno (Monti Lessini). Rendiconti della Società Geologica Italiana 14, 5-12.

Barbieri, G., Zampieri, D., 1992. Deformazioni sinsedimentarie eoceniche con stile a domino e relativo campo di paleostress (Monti Lessini). Atti Ticinensi di Scienze della Terra 35, 25-31.

Bartoli, O., Meli, S., Bergomi, M.A., Sassi, R., Magaraci, D., Liu, D.Y., 2014. Geochemistry and zircon U-Pb geochronology of magmatic enclaves in trachytes from the Euganean Hills (NE Italy): further constraints on Oligocene magmatism in the eastern Southern Alps. European Journal of Mineralogy 27, 161-174**.**

Bassi, D., Bianchini, G., Mietto, P., Nebelsick, J.H., 2008. Southern Alps: Venetian Pre-Alps. In McCann T. (ed.), The Geology of Central Europe, 2. The Geological Society of London, 1087-1092.Beccaluva, L., Bianchini, G. et al., 2003. Tertiary nephelinite to tholeiite magma generation in the Veneto volcanic province, Southern Alps. FIST-Geoitalia 2003 (4° Earth Sciences forum), Abstract volume, 189.

Beccaluva, L., Bonadiman, C., Coltorti, M., Salvini, L., Siena, F., 2001. Depletion events, nature of metasomatizing agent and timing of enrichment processes in lithospheric mantle xenoliths from the VVP. Journal of Petrology 42, 173-187.

Beccaluva, L., Bianchini, G. et al., 2003. Tertiary nephelinite to tholeiite magma generation in the Veneto volcanic province, Southern Alps. FIST-Geoitalia 2003 (4° Earth Sciences forum), Abstract volume, 189.

Beccaluva, L., Bianchini, G., Bonadiman, C., Coltorti, M., Macciotta, G., Siena, F., Vaccaro, C., 2005. Within-plate Cenozoic volcanism and lithospheric mantle evolution in the western-central Mediterranean area. In Finetti I. (Eds.) Deep Seismic exploration of the Meditterrranean Region (CROP Project), Elsevier, Amsterdam, 641-664.

Beccaluva, L., Bianchini, G., Bonadiman, C., Coltorti, M., 2007. Intraplate lithospheric and sublithospheric components in the Adriatic domain: Nephelinite to tholeiite magma generation in the Paleogene Veneto Volcanic Province, Southern Alps. Geological Society of America 418, 131-152.

Beccaro, L., Fornaciari, E., Mietto, P., Preto, N., 2001. Analisi di facies e ricostruzione paleoambientale della rampa dei "Calcari nummulitici" (Eocene; Monti Lessini orientali - Vicenza): dati preliminari. Studi Trentini di Scienze Naturali - Acta Geologica 76 (1999), 3-16.

Bellieni, G., 1977. Caratteri geobarometrici delle intrusioni granitiche del plutone delle Vedrette di Ries (Rieserferner) (Alto Adige Orientale) alla luce dei sistemi sperimentali Q-Or-Ab-An-H_2O. Rendiconti della Società Italiana di Mineralogia e Petrologia 33, 631-645.

Bellieni, G., 1980. The Cima di Villa (Zinsnock) massif: geochemical features and comparisons with the Vedrette di Ries (Rieserferner) pluton (Eastern Alps, Italy). Neues Jahrbuch für Mineralogie – Abhandlungen 138, 244-258.

Bellieni, G., Fioretti, A.M., Marzoli, A., Visonà, D., 2010. Permo-Paleogene magmatism in the eastern Alps. Rendiconti Fis. Accademia dei Lincei 21, S51-S71.

Bergomi, M.A., Zanchetta, S., Tunesi, A., 2015. The Tertiary dike magmaism in the Southern Alps: geochronological data and geodynamic significance. Internal Journal of Earth Sciences 104, 449-473.

Beschin, C., Busulini, A., De Angeli, A., Tessier, G., Ungaro, S., 1998. Crostacei eocenici di ''Cava Rossi'' presso Monte di Malo (Vicenza-Italia settentrionale). Studi Trentini di Scienze Naturali Acta Geologica, 73 (1996), 7-34.

Borsi, S., et al. 1969. In Contributo alla conoscenza geologica della regione di Bolca (Monti Lessini), Barbieri, G., Medizza, F.

Bosellini, A., 1989. Dynamics of Tethyan carbonate platforms. In Crevello P.D., Wilson J.L., Sarg J.F. & Read J.F. (Eds.), Controls on Carbonate Platform and Basin Platform.

S.E.P.M. Special Publication 44, 3-13.

Carminati, E., Doglioni C., 2012. Alps vs. Appennines: the paradigm of a tectonically asymmetric Earth. Earth Science - Reviews 112, 67-96.

Castellarin, A., Cita, M.B., 1969. Etude de quelques coupe priabonienne dans le Monte Saldo (Prov. Verona et Trento) et discussion de limite de I'etage. Memoires du Bureau des Recherches geologiques et Minieres, Colloque sur l'Eocene 69, 119-140.

Conticelli, S., Guarnieri, L., Farinelli, A., Mattei, M., Avanzinelli, R., Bianchini, G., Boari, E., Tommasini, S., Tiepolo, M., Prelevic, D., Venturelli, G., 2009. Trace-elements and Sr–Nd–Pb isotopes of K-rich, shoshonitic, and calc-alkaline magmatism of the Western Mediterranean region: genesis of ultrapotassic to calcalkaline magmatic association in a post-collisional geodynamic setting. Lithos 107, 69-92.

Dal Piaz, G.V., Venturelli, G., 1983. Brevi riflessioni sul magmatismo post-ofiolitico nel quadro dell'evoluzione spazio-temporale delle Alpi. Memorie Società Geologica Italiana 26, 5–19.

Dal Piaz, G.V., Bistacchi, A., Massironi, M., 2003. Geological outline of the Alps. Episodes 26 (3), 175-181.

De Vecchi, Gp., Sedea, R., 1974. Sui basalti eocenici dei Colli Euganei. Memorie degli Istituti di Geologia e Mineralogia dell'Università di Padova, 31, pp. 25.

De Vecchi, Gp., Gregnanin, A., Piccirillo, E.M., 1976. Aspetti petrogenetici del vulcanesimo terziario Veneto Memorie degli Istituti di Geologia e Mineralogia dell'Università di Padova 30, 1-63.

De Vecchi, Gp., Sedea, R., 1995. The Paleogene basalts of the Veneto region (NE Italy). Memorie di Scienze Geologiche 47, 253-374.

De Zanche, V., Conterno, T., 1972. Contributo alla conoscenza geologica dell'orizzonte eocenico di Roncà nel veronese e nel vicentino. Atti e Memorie dell'Accademia Patavina delle Scienze, Lettere ed Arti 84, 287-295.

Frascari Ritondale Spano, F., Bassani, P., 1973. Ricerche geologiche nei dintorni di Bassano del Grappa (Vicenza). Memorie Museo Trid. Scienze Naturali 19, 65-112.

Harangi, S, Downes, H, Seghedi, I., 2006. Tertiary–Quaternary subduction processes and related magmatism in the Alpine-Mediterranean region. Geological Society, London, Memoirs 32, 167-190.

Hoernle, K., Zhang, Y., Graham, D., 1995. Seismic and geochemical evidence for large-scale mantle upwelling beneath the eastern Atlantic and western and central Europe. Nature 374, 34-39.

Hottinger, L., 1960. Recherches sur les Alvéolines du Paléocène et de l'Eocène. Schweizerische Palaontologische Abhandlungen 75/76, 1-243.

Lucchi Garavello, A.M., 1980. Età e ambienti delle Marne Euganee nei Colli Berici orientali. Annali dell'Università di Ferrara 6, 47-62.

Luciani, V., 1989. Stratigrafia sequenziale del Terziario nella Catena del Monte Baldo (Provincie di Verona e Trento). Memorie di Scienze Geologiche 41, 263-351.

Lustrino, M., Wilson M., 2007. The circum-Mediterranean anorogenic Cenozoic igneous province. Earth-Science Reviews 81, 1-65.

Macera, P., Gasperini, D., Piromallo, C., Blichert-Toft, J., Bosch, D., Del Moro, A., Martin, S., 2003. Geodynamic implications of deep mantle upwelling in the source of Tertiary volcanics from the Veneto region (Southern-Eastern Alps). Journal of Geodynamics 36, 563-590.

Macera, P., Gasperini, D., Ranalli, G., Mahatsente, R., 2008. Slab detachment and mantle plume upwelling in subduction zones: an example from the Italian South-Eastern Alps. Journal of Geodynamics 45, 32-48.

Massari, F., Medizza, F., 1973. Stratigrafia e paleogeografia del Campaniano-Maastrichtiano nelle Alpi Meridionali (con particolare riguardo agli hard ground della Scaglia Rossa Veneta). Memorie degli Istituti di Geologia e Mineralogia dell'Università di Padova 28, 1-63.

Massari, F., Medizza, F., Sedea, R., 1976. L'evoluzione geologica dell'area euganea tra il Giurese superiore e l'Oligocene inferiore. In Piccoli, G. et al. (Eds.) Il sistema idrotermale euganeo-berico e la geologia dei Colli Euganei. Memorie degli Istituti di Geologia e Mineralia, Università di Padova 28, 1-62.

Mietto, P., 1975. La Collezione paleontologica "Dal Lago" e le località fossilifere di Grola Rivagra nell'Eocene vicentino. Memorie degli Istituti di Geologia e Mineralogia dell'Università di Padova 31, 1-28.

Milani, L., Beccaluva, L., Coltorti, M., 1999. Petrogenesis and evolution of the Euganean magmatic complex, north eastern Italy. European Journal of Mineralogy 11, 379-399.

Papazzoni, C.A., Bassi, D., Fornaciari, E., Giusberti, L., Luciani, V., Mietto, P., Roghi, G., Trevisani, E., 2014. Geological and stratigraphical setting of the Bolca. In Papazzoni C.A., Giusberti L., Carnevale G., Roghi G., Bassi D. & Zorzin R. (Eds.), The Bolca Fossil-Lagerstätten: A window into the Eocene World. Rendiconti della Società Paleontologica Italiana 4, 19-28.

Piccoli, G., Bellati, R., Binotti, C., Di Lallo, E., Sedea, R., Dal Prà, A., Cataldi, R., Gatto, G.O., Ghezzi, G., Marchetti, N., Bulgarelli, G., Schiesaro, G., Panichi, C., Tongiorgi, E., Baldi, P., Ferrara, G.C., Massari, F., Medizza, F., Iliceto, V., Norinelli, A., De Vecchi, G., Gregnanin, A., Piccirillo, E.M., Sbettega, G., 1976. Il sistema idrotermale euganeo-berico e la geologia dei Colli Euganei. Memorie degli Istituti di Geologia e Mineralogia dell'Università di Padova, 30, 266 pp.

Piccoli, G., Sedea, R., Bellati, R., Di Lallo, E., Medizza, F., Girardi, A., De Pieri, R., De Vecchi, Gp., Gregnanin, A., Piccirillo, E.M., Norinelli, A., Dal Prà, A., 1981. Note illustrative della carta geologica dei Colli Euganei alla scala 1: 25.000. Memorie di Scienze geologiche 24, 523-546.

Rosenbaum, G., Lister, G.S., Duboz, C., 2002. Relative motions of Africa, Iberia and Europe during Alpine orogeny. Tectonophysics 359, 117-129.

Rosenberg, C.L., 2004. Shear zones and magma ascent: a model based on a review of the Tertiary magmatism in the Alps. Tectonics 23, TC3002, doi:10.1029/2003TC001526.

Sarti, M., 1980. Frane sottomarine e debris flow in una successione carbonatico-torbiditica eocenica (Val d'Avesa, Verona). Annali dell'Università di Ferrara 7, 65-89.

Savelli, C., Lipparini, E. 1979. Età K/Ar di basalti del vicentino e la scala dei tempi del Paleogene. Bollettino della Società Geologica Italiana 98, 375-385.

Schaltegger, U., Brack, P., Ovtcharova, M., Peytcheva, I., Schoene, B., Stracke, A., Marocchi, M., Bargossi, G.M., 2009. Zircon and titanite recording 1.5 million years of magma accretion, crystallization and initial cooling in a composite pluton (southern Adamello batholith, northern Italy). Earth and Planetary Science Letters 286, 208-218.

Schoene, B., Schaltegger, U., Brack, P., Latkoczy, C., Stracke, A., Günther, D., 2012. Rates of magma differentiation and emplacement in a ballooning pluton recorded by U–Pb TIMS-TEA, Adamello batholith, Italy. Earth and Planetary Science Letters 355, 162–173.

Stampfli, G.M., Mosar, J., Favre, P., Pillevuit, A., Vannay, J.C., 2001. Permo-Mesozoic evolution of the western Tethyan realm: the Neotethys/East- Mediterranean connection. In: Ziegler P.A., Cavazza W., Robertson A.H.F. (Eds.). PeriTethys memoir 6: Peritethyan rift/wrench basins and passive margins, vol. 186, Crasquin-Soleau, S., IGCP 369, pp. 51–108, M´em. Museum of Natural History Nat.

Ungaro, S., 2001. Le biofacies paleoceniche ed eoceniche dei Monti Lessini (Veneto, Italia). Annali dell'Università di Ferrara 9, 1-40.

Visonà, D., Caironi, V., Carraro, A., Dallai, L., Fioretti, A.M., Fanning, M., 2007. Zircon megacrysts from basalts of the Venetian Volcani Province (NE Italy): U-Pb, oxygen isotopes and REE data. Lithos, 94, 168-180.

von Blanckenburg, F., Davies, J.H., 1995. Slab breakoff: a model for syncollisional magmatism and tectonics in the Alps. Tectonics 14, 120-131.

Wilson, M., Patterson, R., 2001. Intraplate magmatism related to short-wavelength convective instabilities in the upper mantle: evidence from the Tertiary Quaternary volcanic province of western and central Europe. Geological Society of America Special Paper 352, 37-58.

Winterer, E.J., Bosellini, A., 1981. Subsidence and sedimentation on a Jurassic passive continental margin (Southern Alps, Italy). Bulletin American Association of Petroleum Geologists 65, 394–421.

Zampieri, D., 1995. Tertiary extension in the southern Trento Platform, southern Alps, Italy: Tectonics 14, 645–657.

Zampieri, D., 2000. Segmentation and linkage of the Lessini Mountains normal faults, Southern Alps, Italy. Tectonophysics 319, 19-34.

Chapter 2.
Analytical methods

2. Analytical methods

2.1 Wavelength Dispersive X-Ray Fluorescence Spectrometry (WDXRF)

Bulk rock major and trace element compositions of magmatic products and mantle xenoliths from Val d'Adige, Lessini Mts., and Marosticano districts were determined by Wavelength Dispersive X-Ray Fluorescence Spectrometry (WDXRF) on pressed powder pellets at the Department of Physiscs and Earth Sciences, University of Ferrara (Italy), using an ARL Advant-XP spectrometer, following the full matrix correction method proposed by Lachance and Traill (1966). Accuracy is generally lower than 2% for major oxides and less than 5% for trace element determinations, whereas the detection limits for trace elements range from 1 to 2 ppm. Volatile contents were determined as loss on ignition (LOI) at 1000 °C. Major and trace elements of magmatic products from Euganean Hills district were determined by X-Ray Fluorescence Spectrometry (XRF) on glass bead samples at the Department of Geosciences, University of Padova (Italy), using Phillips PW1404. Analytical uncertainty ranges from 1 to 2% for major elements and from 10 to 15% for trace elements. LOI was measured at 1000 °C.

2.2 Inductively coupled plasma–mass spectrometry (ICP-MS)

Rb, Sr, Y, Zr, Nb, Hf, Ta, Th, U, and Rare Earth elements (REEs) magmatic products from Val d'Adige, Lessini Mts., Marosticano and Euganean Hills districts were determined by Inductively Coupled Plasma–Mass Spectrometry (ICP-MS) using a Thermo Series X-I spectrometer at Department of Physics and Earth Sciences, University of Ferrara. Accuracy and detection limits were determined using several international reference standards, as well as internal standards run as unknowns.

2.3 Analytical procedure for $^{40}Ar/^{39}Ar$ radio-isotopic dating

Basanitic and basaltic samples from Val d'Adige, Lessini Mts., and Marosticano districts lack K-rich minerals suitable for geochronology, therefore $^{40}Ar/^{39}Ar$ analyses were performed on groundmass. The sample fraction (30-40 g) was crushed with a rigorously cleaned steel hydraulic press, sieved to a size fraction of 90-250 μm and rinsed in distilled H_2O to remove any dust or powder. In order to collect only the sample grains constituted by the groundmass, the sample fraction was handpicked under a binocular microscope to remove any phenocrysts (pyroxene and olivine). However, due to the dark color of these

grains it was impossible to clearly observe if inclusions were present, and therefore exclude the possibility of alteration. The grains were leached in dilute HF in order to remove at least the alteration phases along the surface and cracks. Samples were then rinsed in distilled H_2O in an ultrasonic cleaner.

As basaltic trachyandesites, trachyandesites, trachytes, and rhyolites from the Euganean district are characterized by phenocrysts that are good candidates for $^{40}Ar/^{39}Ar$ dating, i.e., plagioclase and amphibole in the most basic sample, and biotite, sanidine, or feldspar in the more acid samples, $^{40}Ar/^{39}Ar$ analyses were performed on mineral separates. The sample fraction (>1kg) was crushed with a rigorously cleaned steel hydraulic press, sieved to size fractions of 150-215 μm and 215-315 μm, and rinsed in distilled H_2O to remove any dust or powder. Phenocrysts were separated from these fractions using a Frantz isodynamic magnetic separator and were hand-picked grain-by-grain under the binocular stereomicroscope. Mineralic separates were further leached using diluted HF (2N) for 5 minutes to remove any potential adhering alteration product within superficial cracks that were not removed during hand picking (Jourdan et al., 2009b) and then were rinsed in distilled H_2O in an ultrasonic cleaner.

The Ar isotopic ratios were measured through laser step-heating with i) MAP 215–50 mass spectrometer and ii) ARGUS VI at Curtin University within the Western Australian Argon Isotope Facility (WAAIF) of the John de Laeter Centre, and iii) Nu Instruments Noblesse magnetic sector noble gas mass spectrometer at the Noble Gas Geochronology Laboratory of the University of Vermont. Irrespective to the instrument used for the analyses, our criteria for the determination of plateau are as follows. Plateaus must include at least 70% of ^{39}Ar. The plateau should be distributed over a minimum of 3 consecutive steps agreeing at 95% confidence level and satisfying a probability of fit (P) of at least 0.05. Plateau ages obtained with MAP 215–50 mass spectrometer and ARGUS VI are given at the 2σ. Plateau ages obtained with Nu Instruments Noblesse magnetic sector noble gas mass spectrometer are given at 1σ level. All the plateau ages are calculated using the mean of all the plateau steps, each weighted by the inverse variance of their individual analytical error. Mini-plateaus are defined similarly except that they include between 50% and 70% of ^{39}Ar. Inverse isochrons include the maximum number of steps with a probability of fit ≥ 0.05. All sources of uncertainties are included in the calculation.

Tthe sample irradiations and the analytical procedures performed are reported in detail below.

2.3.1 *Sample irradiation and analyses for samples analyzed with MAP 215-50 mass spectrometer*

Euganean mineral separates were loaded into five large wells of two 1.9 cm diameter by 0.3 cm depth aluminum discs. In one disc the wells were bracketed by small pits that included GA1550 biotite, while in the other disc, the wells were bracketed by seven pits that included Fish Canyon sanidine (FCs). GA1550 and FCs were used as neutron fluence monitors, adopting an age of 99.738 ± 0.100 Ma and 28.294 ± 0.036 Ma (1σ), respectively (Renne et al., 2011). The discs were Cadmium-shielded (to minimize undesirable nuclear interference reactions) and irradiated for 3 hours in the US Geological Survey nuclear reactor (Denver, USA) in central position. The mean J-values computed from standard grains within the small pits is 0.000661 ± 0.00000099 (0.15%) determined as the average and standard deviation of J-values of the small wells for each irradiation disc. Mass discrimination was monitored using an automated air pipette and provided a mean value ranging from 1.006254 ± 0.00030188 (0.03%) to 1.006589 ± 0.00030198 (0.03%) per dalton (atomic mass unit) relative to an air ratio of 298.56 ± 0.31 (Lee et al., 2006). The correction factors for interfering isotopes were $(^{39}Ar/^{37}Ar)_{Ca}$ = 7.30 × 10^{-4} (± 11%), $(^{36}Ar/^{37}Ar)_{Ca}$ = 2.82 × 10^{-4} (± 1%), and $(^{40}Ar/^{39}Ar)_{K}$ = 6.76 × 10^{-4} (± 32%). At the WAAIF the samples were step-heated using a 110 W Spectron Laser Systems, with a continuous Nd-YAG (IR; 1064 nm) laser rastered over the sample during 1 minute to ensure an homogenously distributed temperature. The gas was purified in a stainless steel extraction line using two SAES AP10 getters, a GP50 getter and a liquid nitrogen condensation trap. Ar isotopes were measured in static mode using a MAP 215-50 mass spectrometer (resolution of ~500; sensitivity of 4x10^{-14} mol/V) with a Balzers SEV 217 electron multiplier mostly using 9 to 10 cycles of peak-hopping. The data acquisition was performed with the Argus program written by M.O. McWilliams and ran under a LabView environment. The raw data were processed using the ArArCALC software (Koppers, 2002) and the ages have been calculated using the decay constants recommended by Renne et al. (2010). Blanks were monitored every 3 to 4 steps and typical ^{40}Ar blanks range from 1 × 10^{-16} to 2 × 10^{-16} mol.

2.3.2 *Sample irradiation and analyses for samples analyzed with ARGUS VI mass spectrometer*

The cleaned groundmass and mineral separates were loaded into several 1.9 cm in diameter by 0.3 cm depth aluminum discs. The discs were then stacked together and placed in quartz tubes. The discs hosting the groundmass included also GA1550 biotite, while the discs hosting plagioclase and amphibole included FCs. GA1550 and FCs were used as neutron fluence monitors, adopting an age of 99.738 ± 0.100 Ma and 28.294 ± 0.036 Ma (1σ), respectively (Renne et al., 2011). The discs were Cd-shielded (to minimize undesirable nuclear interference reactions) and irradiated for 3 hours at the TRIGA Reactor at Oregon State University (USA) The mean J-values computed from standard grains within the small pits range from 0.0008098 (± 0.07%) to 0.0008121 (± 0.11%) for groundmass sample and yielded values of 0.0008098 (± 0.07%) and 0.0008121 (± 0.13%) for the plagioclase and hornblende samples, respectively. For all the samples, the mass discrimination was monitored regularly through the analysis using an automated air pipette and provided the mean value is 0.993485 (±0.02%) per dalton (atomic mass unit) relative to an air ratio of 298.56 ± 0.31 (Lee et al., 2006). The correction factors for interfering isotopes were $(^{39}Ar/^{37}Ar)_{Ca} = 6.95 \times 10^{-4}$ (± 1.3 %), $(^{36}Ar/^{37}Ar)_{Ca} = 2.65 \times 10^{-4}$ (± 0.84 %) and $(^{40}Ar/^{39}Ar)_{K} = 7.30 \times 10^{-4}$ (± 12.4 % ; Renne et al., 2013). At the WAAIF plagioclase, amphibole crystal and groundmass populations were step-heated using a continuous 100 W PhotonMachine© CO_2 (IR, 10.4 μm) laser fired on the crystals during 60 seconds. Each of the standard crystals was fused in a single step.

The gas was purified in an extra low-volume stainless steel extraction line of 240cc and using one SAES AP10 and one GP50 getter. Ar isotopes were measured in static mode using a low volume (600 cc) ARGUS VI mass spectrometer from Thermofisher© set with a permanent resolution of ~200. Measurements were carried out in multi-collection mode using four faradays to measure mass 40 to 37 and a 0-background compact discrete dynode ion counter to measure mass 36. We measured the relative abundance of each mass simultaneously using 10 cycles of peak-hopping and 33 seconds of integration time for each mass. Detectors were calibrated to each other electronically and using Air shot beam signals. The raw data were processed using the ArArCALC software (Koppers, 2002) and the ages have been calculated using the decay constants recommended by Renne et al. (2011). Blanks were monitored every 2 steps.

2.3.3 *Sample irradiation and analyses for samples analyzed with Nu Instruments Noblesse magnetic sector noble gas mass spectrometer*

The cleaned groundmass were loaded into aluminum foil packets, arranged in suprasil vial, and placed in an aluminum canister for irradiation. Samples were irradiated with multigrain aliquots of FCs to act as a flux monitor (age: 28.03 Ma; Renne et al., 1998) to monitor the neutron dose, and CaF_2 and KSO_4 were also irradiated to determine corrections for interfering nuclear reactions. Samples were irradiated for four hours at the Cd-Lined In-Core Irradiation Tube (CLICIT) reactor of Oregon State University, USA. Correction factors used to account for interfering nuclear reactions for the irradiated samples are: $(^{40}Ar/^{39}Ar)_K = 8.87 \times 10^{-3} \pm 5.30 \times 10^{-3}$, $(^{36}Ar/^{37}Ar)_{Ca} = 2.7 \times 10^{-4} \pm 0.2 \times 10^{-4}$, $(^{39}Ar/^{37}Ar)_{Ca} = 6.7 \times 10^{-4} \pm 0.2 \times 10^{-4}$. At the Noble Gas Lab of the University of Vermont, laser step heating for $^{40}Ar/^{39}Ar$ dating was conducted with a Santa Cruz Laser Microfurnace 75 W diode laser system. Flux monitors were loaded into degassed Nb foil packets before being loaded in the wells of the copper planchette sample holder. The volcanic samples were loaded directly into wells of the copper planchette. The gas released during heating was purified with SAES getters and argon isotopes were analyzed on a Nu Instruments Noblesse magnetic sector noble gas mass spectrometer during step-heating analyses. Data from samples and flux monitors were corrected for blanks, mass discrimination, atmospheric argon, neutron-induced interfering isotopes, and the decay of ^{37}Ar and ^{39}Ar. Mass discrimination was calculated by analyzing known aliquots of atmospheric argon for which the measured $^{40}Ar/^{36}Ar$ was compared with an assumed atmospheric value of 298.56 ± 0.31 (Lee et al., 2006). A linear interpolation was used to calculate J factors for samples based on sample position between flux monitor packets in the irradiation tube. All ages were calculated using the isotope decay constants recommended by Steiger and Jäger (1977). The age calculations for inverse isochron and apparent age data were achieved using both an in-house data reduction program and Isoplot 3.0 (Ludwig, 2003).

2.4 Electron Microprobe (EMP)

Major element compositions of minerals (olivine, pyroxene, and spinel) from xenoliths and host lavas were analyzed at the Department of Geosciences, University of Padova (Italy) on Electron MicroProbe (EMP), using ZAF on-line data reduction and matrix correction

procedure. An acceleration voltage of 20 keV and sample currents of 20 nA with 10-20 s counting time on peak position were used. Synthetic oxide standards (MgO, FeO, MnO, ZnO, NiO, Al_2O_3, Cr_2O_3, TiO_2 and SiO_2) were used. Analytical precision is better than ±2% for elements in the range of >10 wt.%, better than 5% for elements in the range 2-10 wt.%, and better than 10% for elements in the range 0.5-2 wt.%.

2.5 Laser Ablation Inductively Coupled Plasma Mass Spectrometry (LA-ICP-MS)

Trace element concentrations in clinopyroxene and orthopyroxene of mantle xenoliths were obtained by Laser Ablation Inductively Coupled Plasma Mass Spectrometry (LA-ICP-MS) at the Department of Earth Sciences, University of New Hampshire (USA) using an Analyte Excite 193 nm excimer laser plumbed into a Nu instruments AttoM high resolution inductively coupled plasma mass spectrometer. Typical spot size was 65 μm, and laser operating conditions were 6.0 mJ at 80% output, fluence of 8.1 J/cm^2 and repetition rate of 5 Hz. Silicate glass MPI-Ding standard, ML3B-G (Jochum et al., 2006), was used as the calibration standard every four sample spots to correct for within-run instrumental drift. Resulting data were then processed with the Iolite software package, using calcium data from EMPA as an internal standard. Precision and accuracy were assessed to be within 10% for ppm-level concentrations by repeated measurements of KH-1 and KL2-G as independent standards.

References

Jochum, K.P., Stoll, B., Herwig, K., Willbold, M., Hofmann, A.W., et al., 2006. MPI-DING reference glasses for in situ microanalysis: new reference values for element concentrations and isotope ratios. Geochemistry Geophysics Geosystems 7.

Jourdan, F., Marzoli, A., Bertrand, H., Cirilli, S., Tanner, L.H., Kontak, D.J., McHone, G., Renne, P.R., Bellieni, G., 2009b. $^{40}Ar/^{39}Ar$ ages of CAMP in North America: Implications for the Triassic–Jurassic boundary and the ^{40}K decay constant bias. Lithos 110, 167-18.

Koppers, A.A.P., 2002. ArArCALC-software for $^{40}Ar/^{39}Ar$ age calculations. Computers & Geosciences 28, 605–619.

Lachance, G.R., Traill, R.J., 1966. Practical solution to the matrix problem in X-ray analysis. Canadian Journal of Spectroscopy 11, 43-48.

Lee, J.-Y., Marti, K., Severinghaus, J.P., Kawamura, K., Yoo, H.-S., Lee, J.B., Kim, J.S., 2006. A redetermination of the isotopic abundance of atmospheric Ar. Geochimica et Cosmochimica Acta 70, 4507-4512.

Ludwig, K.R., 2003. Isoplot/EX, rev. 3.00, a Geochronological Toolkit for Microsoft Excel. Berkeley Geochronology Center Special Publication 4, 71 pp.

Renne, P.R., Swisher, C.C., Deino, A.L., Karner, D.,B., Owens, T.L., Depaolo, D.J., 1998. Intercalibration of standards, absolute ages and uncertainties in $^{40}Ar/^{39}Ar$ dating. Chemical Geology 145, 117–152.

Renne, P.R., Mundil, R., Balco, G., Min, K., Ludwig, K.R., 2010. Joint determination of ^{40}K decay constants and $^{40}Ar^*/^{40}K$ for the Fish Canyon sanidine standard, and improved accuracy for $^{40}Ar/^{39}Ar$ geochronology. Geochimica et Cosmochimica Acta 74, 5349-5367.

Renne, P.R., Balco, G., Ludwig, K.R., Mundil, R., Min, K., 2011. Response to the comment by W.H. Schwarz et al. on "Joint determination of K-40 decay constants and Ar-40*/K-40 for the Fish Canyon sanidine standard, and improved accuracy for Ar-40/Ar-39 geochronology" by P.R. Renne et al. (2010). Geochimica et Cosmochimica Acta 75, 5097-5100.

Renne, P.R., Deino, A.L., Hilgen, F.J., Kuiper, K.F., Mark, D.F., Mitchell, W.S., Morgan, L.E., Mundil, R., Smit, J., 2013. Time scales of critical events around the Cretaceous-Paleogene boundary. Science 339, 684-687.

Steiger, R.H., Jäger, E. 1977. Subcommission on geochronology: Convention on the use of decay constants in geo- and cosmochronology. Earth and Planetary Science Letters 36, 359-362, doi: 10.1016/0012-821X(77)90060-7.

Chapter 3.

The VVP magmatic products

Enclosed manuscript:

The temporal evolution of the Cenozoic Southalpine magmatic Province (North-East Italy): evidence from $^{40}Ar/^{39}Ar$ geochronology. *(in prep.)*

Valentina Brombin[a]*, Andrea Marzoli[b], Guido Roghi [b], Fred Jourdan[c], Massimo Coltorti[a], Costanza Bonadiman[a], Laura E. Webb[d], Sara Callegaro[e], Giuliano Biellieni[b], Giampaolo De Vecchi[b], Roberto Sedea[b]

Affiliations:

[a] Dipartimento di Fisica e di Scienze della Terra, Università di Ferrara, Italy;

[b] Dipartimento di Geoscienze e IGG-CNR, Università di Padova, Italy;

[c] Western Australian Argon Isotope Facility, Department of Applied Geology, JdL Centre, Curtin University, Perth, Western Australia, Australia;

[d] Department of Geology, University of Vermont, Vermont, USA;

[e] Centre for Earth Evolution and Dynamics, University of Oslo, Norway.

3. The VVP magmatic products

3.1. Introduction

Paleogene magmatism within the Alps (North Italy) is variable in time and space reflecting the changing geodynamic framework started since the Early Cretaceous (Bassi et al., 2008). In this time the convergence between Europe and Adria (the continental promontory of Africa) led to the E- to SE-directed subduction of the Alpine Tethys, started in the eastern Alps, and to the following continental collision triggering Alpine orogenesis from the middle Eocene, ca. 35 Ma (Dal Piaz and Venturelli, 1983; Stampfli et al., 2001; Rosenbaum et al., 2002; Dal Piaz et al. 2003). During the Eocene to Miocene, orogenic (or subduction-related) and anorogenic (or intraplate-like) magmatic activity affected the Austroalpine and Southalpine Units, respectively, in the eastern Alps. In the Austroalpine Unit, along the Insubric domains this igneous activity ("Periadriatic magmatism") is testified by i) sub-alkaline and calc-alkaline silicic plutons (i.e., Adamello, Rensen, Monte Alto, Vedrette di Ries, Cima di Vila, Polland; Bellieni 1977, 1980; Bassi et al., 2008; Bellieni et al., 2010) and ii) basaltic and andesitic dikes showing calc-alkaline to shoshonitic affinity (Harangi et al., 2006; Conticelli et al., 2009; Alagna et al., 2010; Bergomi et al., 2015). The plutons were dated as early Oligocene, the so-called "climax" of the Periadritic magmatism (34 to 28 Ma; von Blancknburg and Davis, 1995; Rosenberg, 2004), with the exception of the southern Adamello batholith dated at ca. 42 Ma (e.g., Schaltegger et al., 2009; Schoene et al., 2012) and of coeval periadriatic dikes (42 to 34 Ma; Bergomi et al., 2015).

In the eastern Southalpine, the magmatic activity was extrusive to sub-volcanic (Beccaluva et al., 2007; Bassi et al., 2008). The products of this latter igneous activity constitute the Cenozoic Southalpine Magmatic Province known in literature as Veneto Volcanic Province (VVP; e.g., De Vecchi and Sedea, 1995; Beccaluva et al., 2001, 2007; Macera et al., 2003, 2008; Visonà et al., 2007; Fig. 3), one of the widest magmatic districts of the Adria (or Apulia) plate. The VVP represents one example of "low-volcanicity impactogenic rifts", which are defined as zones, where small volumes of relatively undifferentiated magmas with a wide range of serial affinity (from tholeiitic to extremely alkaline) erupted from trastensional systems, triggered by a foreland reaction to a major collisional event (Beccaluva et al., 2007). In case of the VVP, the magmatic activity developed along NNW-SSE transtensional fault systems (Zampieri, 1995) as response to the general N-S compression along the Alpine Belt (De Vecchi and Sedea, 1995; Milani et al., 1999; Zampieri, 1995; Beccaluva et al., 2003, 2005).

3. The VVP magmatic products

VVP biostratigraphic data suggest that short-lived volcanic pulses occurred over a time span of about 30 Ma, from the late Paleocene to the early Miocene (Barbieri et al., 1991). Today, the main products include volcaniclastics rocks, explosion breccias, hyaloclastites, lava flows, pillow lavas, lava vents of mafic to ultramafic composition, shallow level intrusions such as sills or laccoliths. Those are widespread over an elongated NNW-SSE area of about 1500 km^2, defining from north-west to south-east five main volcanic districts: Val d'Adige, Lessini Mts., Marosticano, Berici Hills, and Euganean Hills (Beccaluva et al., 2007). For most of these districts the lavas are relatively undifferentiated, ranging in composition from mela- (M) nephelinites to quartz (Qz)-normative tholeiites (De Vecchi and Sedea, 1995; Macera et al., 2003; Beccaluva et al., 2007). Commonly alkali-basalts host mantle peridotites (Morten et al., 1989; Siena and Coltorti, 1989; 1993; Beccaluva et al., 2001; Bonadiman et al., 2001; Gasperini et al., 2006; Brombin et al., 2018). Only in the Euganean Hills, the southermost district of the VVP, volcanic and subvolcanic rocks range from subordinate basalts to prevalent acidic types, mostly Qz-trachytes and rhyolites (Milani et al., 1999).

Despite the deep knowledge of the petrological and geochemical aspects of the Alpine Cenozoic magmatism, the geodynamic scenario responsible for the genesis of this magmatism is still debated. The Periadritic and the VVP magmatism have been generally related to the breakoff of the subducted Thetis and European slabs, or to upwelling of plume-like mantle diapirs through a slab window after the continent-continent collision of the Adria and Europe plates occurred in the middle Eocene.

The objective of this study is to combine previous biostratigraphic data with new $^{40}Ar/^{39}Ar$ radioisotopic ages, and major and trace element geochemical data on basic and acidic magmatic rocks from Val d'Adige, Marosticano, Lessini Mts., and Euganean Hills collected from selected key locations to better understand i) the reconstruction of the temporal and geochemical evolution of the VVP magmatism and ii) Adria/Europe geodynamic history necessary to understand the interaction between magmatism and Alpine orogenesis.

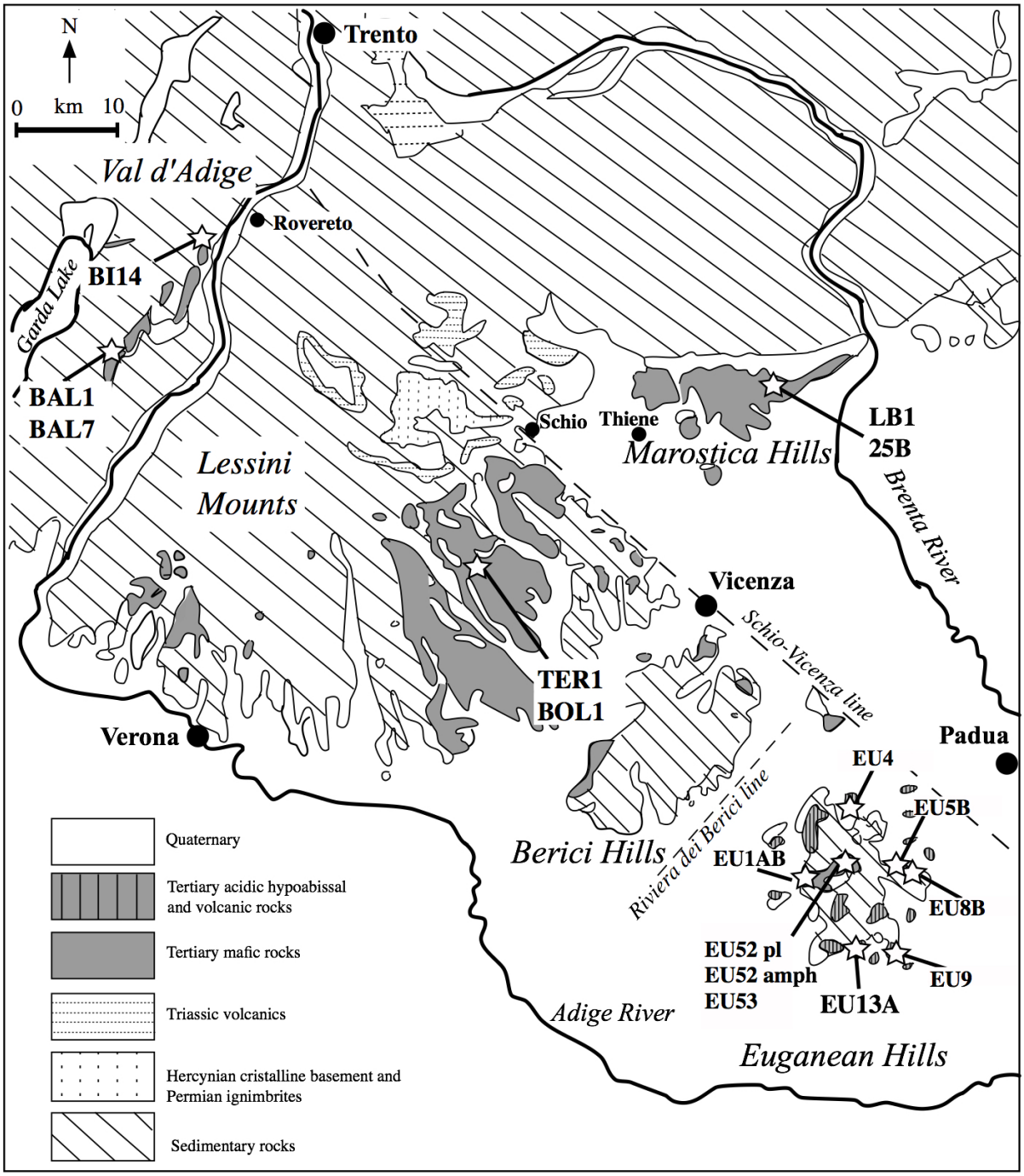

Fig. 3. Geological map of the Veneto Volcanic Province (VVP; De Vecchi and Sedea, 1995), showing the locations of the samples collected for this study.

3.2. Previous geochronological studies of VVP

The Cenozoic VVP products are interbedded at various levels in the Southalpine sedimentary cover that provides the stratigraphic (Paleocene to Miocene) ages of these eruptions that generally decrease towards the south and east (De Vecchi and Sedea, 1995; Beccaluva et al., 2007). The most recently published radioisotopic ages (Fig. 4) are U-Pb ages of inherited zircon hosted in i) a porphyritic basanite lava and in two altered dykes of Lessini Mts. (Visonà et al., 2007) and ii) magmatic enclaves within trachytes of Euganean Hills (Bartoli et al., 2014) districts. These ages were obtained using a sensitive high-resolution ion microprobe (SHRIMP). The calculated ages from Lessini Mts. zircons are all Eocene in age spanning from 51.1 ± 1.5 to 44.9 ± 2.8 Ma (Visonà et al., 2007). Whereas, the Euganean Hills zircons yielded Oligocenic ages of 31.9 ± 1.3 Ma, and 30.6 ± 1.5 Ma. However, as these zircons are inherited, they provide only the pre-eruption ages. Zantendeschi (1994) already dated the Euganean differentiated lavas using the Rb-Sr method, giving eruption ages of trachytes spanning from 32 ± 2 to 28 ± 1 Ma, and rhyolites from 34 ± 2 to 32 ± 1 Ma. But it must be noted that true value of the ^{87}Rb decay constant is still uncertain (Begemann et al., 2001; Schmitz et al., 2003), therefore ages calculated using the Rb-Sr method could not considered reliable. Also previously published K-Ar whole rock analyses (Borsi and Ferrara, 1969; Borsi et al., 1969; Savelli and Lipparini, 1979; Fig. 4) tried to date the VVP magmatism, providing ages for the basic flows (42.5 ± 1.5, 39.9 ± 1.2, and 20.4 ± 0.8 Ma) and necks (Purga di Bolca, 36 Ma no uncertainties are provided by the authors) of the Lessini Mts., for basaltic lavas from the Euganean Hills (42.0 ± 1.5 Ma), and from the Marosticano district (33.7 ± 1.2, 30.0 ± 0.9, and 20.4 Ma ± 0.8 Ma). However, it is well known that the reliability of K-Ar dating technique is questionable, as it is not able to recognize (and correct for) non-atmospheric ^{40}Ar/^{36}Ar ratios and alteration effects (Oostingh et al., 2017).

It is clear that new high-resolution geochronological data are requested to i) complete the state of the art of each VVP district and ii) reconstruct the temporal evolution of the VVP magmatism.

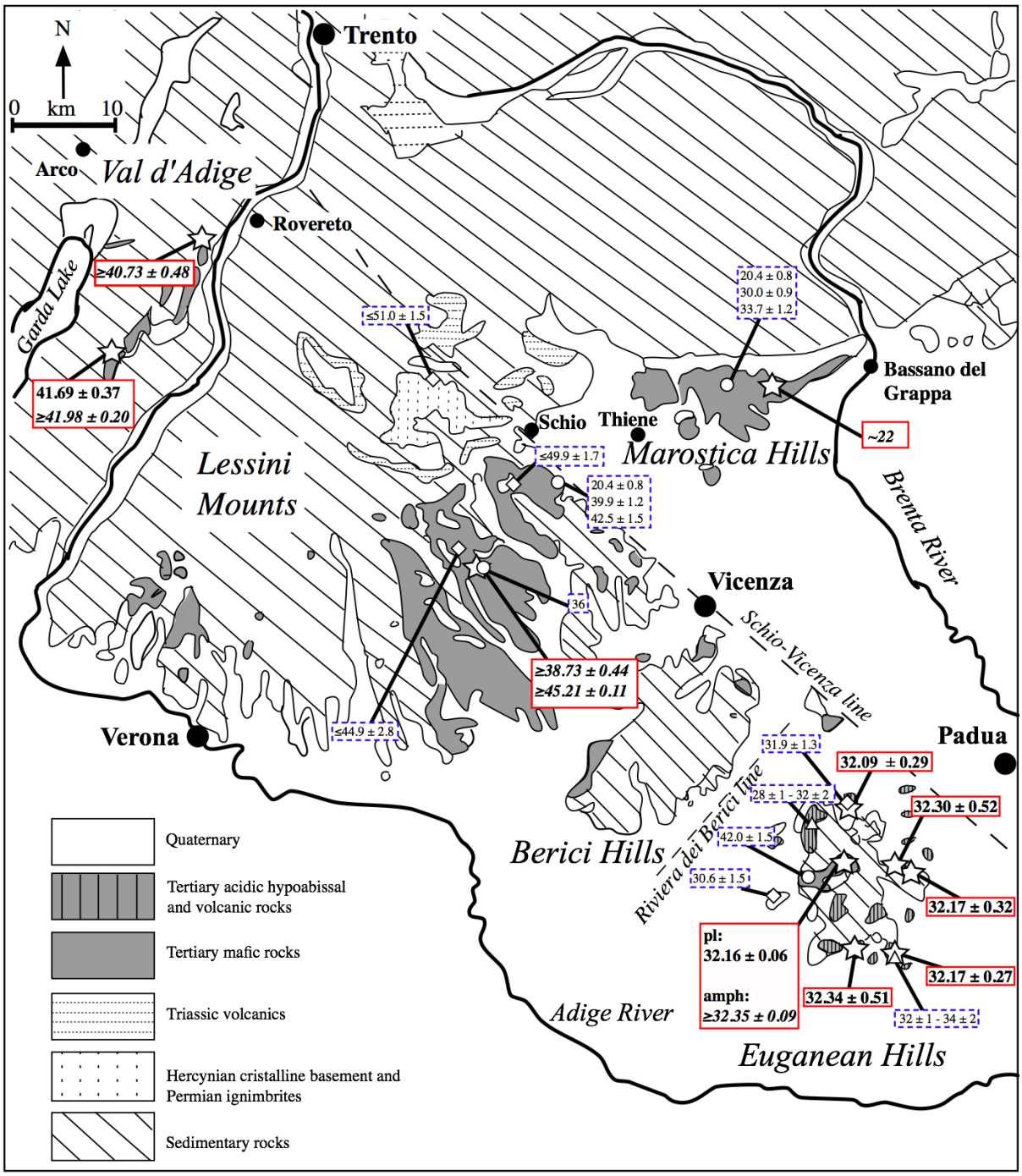

Fig. 4. Ages (in Ma) of the magmatic rocks occuring in the VVP. In blue the literature data, in red this work. Age in italics are derived from mini-plateaus (50-70% ^{39}Ar released) and are considered minimum ages only. Stars are Ar-Ar ages, diamonds are U-Pb ages, triangles are Rb-Sr ages, and circles are K-Ar ages. Ages from Lessini Mts. are from Visonà et al. (2007); Savelli and Lipparini, (1979), and Borsi et al. (1969); ages from Marosticano are from Savelli and Lipparini, (1979); ages from Euganean Hills are from Zantendeschi (1994) and Bartoli et al. (2014).

3.3 Sampling

3.3.1 *Val d'Adige district*

Two of the Val d'Adige district samples, BAL1 and BAL7, were collected in the north-eastern part of Monte Baldo (Table A3.1; Fig. 3). BAL1 was collected near to the top of the subaqueous lava flow interbedded between Calcare di Torbole and Calcare di Nago (Fig. 2), whereas BAL7 was sampled from a thin sill between the Scaglia Rossa and Calcare di Torbole (Fig. 2). The last sample from Val d'Adige district, BI14 (Table A3.2), was collected in the quarry of the locality Isera (Trento), near Rovereto.

3.3.2 *Lessini Mts. district*

The sampling for Lessini Mts. district was focused near the Bolca Fossil-Lagerstätte area. The sample TER1 (Table A3.1; Fig. 3) was collected from a lava flow cropping out in Termine locality, about one kilometer south of Monte Purga. This lava flow is interbedded with red clays of unknown age. The sample BOL1 (Table A3.1; Fig. 3) was collected from the volcanic neck preserved in Purga di Bolca locality. This neck cuts through 10-20 m of freshwater-brackish sediments of probable Ypresian age (Barbieri and Medizza, 1969; Medizza, 1980; Giusberti et al., 2014).

3.3.3 *Marosticano district*

Two samples (LB1 and 25B) were collected at the volcanic neck of Monte Gloso, near the town of Marostica (Table A3.1, b; Fig. 3). The massive volcanic neck cross cuts the middle Oligocene marine sediments of the Salcedo formation (Savelli and Lipparini, 1979; Fig. 2).

3.3.4 *Euganean Hills district*

The Euganean Hills district is the only VVP magmatic centre where basic, intermediate, and acidic lithologies coexist. Therefore, six samples of different lithology were collected in order to define the time enlapsing between the eruptions. EU4, EU5B, EU9, and EU13A represent the most felsic products peculiar of the Euganean Hills. EU4 (Monte Merlo quarry, northern sector of the Euganean Hills; Table A3.1; Fig. 3), EU5B (Monte Alto,

eastern sector; Table A3.1; Fig. 3), EU9 (Monte Ricco, south-eastern sector; Table A3.1; Fig. 3), and EU13A (Monte Cecilia, southern sector; Table A3.1; Fig. 3) were collected from subvolcanic bodies intruded in the Euganean Marls Formation (Oligocene; Piccoli et al., 1981; Fig. 2). EU1AB, EU8A, EU52, and EU53 are the most undifferentiated magmatic products of the Euganean sample suite. EU1AB was collected from an outcrop in the western part of the Euganean Hills and EU8A was collected from a subvolcanic body at Monte Oliveto, in the easternmost part of the Euganean Hills (Table A3.1; Fig. 3). EU52 was sampled from an intrusion cutting a basaltic andesite body at the center of the Euganean district where sample EU53 was collected (Table A3.1; Fig. 3).

3.4 Petrography

BAL7, BI14 (Val d'Adige district), BOL1 (Lessini Mts. district), LB1 and 25B (Marosticano district) are classified as basanites in the total alkali versus silica (TAS) classification (Le Maitre et al., 2002; Fig. 5). These rocks show porphyritic texture with large (up to 2 mm) phenocrysts of euhedral olivine and smaller clinopyroxene (prevalently augite; up to 0.5 mm) as dominant phenocrysts set in a groundmass constituted by acicular plagioclase, clinopyroxene, and oxides. Interestingly, samples from Marosticano district exhibit peridotitic xenoliths of 3-4 mm (Brombin et al., 2018).

BAL1 (Val d'Adige district), TER1 (Lessini Mts. district), and EU1AB (Euganean Hills district) are basalts, while EU53 (Euganean Hills district) is classified as basaltic andesite according to the TAS classification (Fig. 5). They have intergranular texture characterized by elongated and euhedral plagioclase (up to 0.2 mm) and subhedral–anhedral clinopyroxene, olivine and oxides filling spaces between plagioclase crystals. The presence of altered olivine to iddingsite and amygdules indicate were affected by slightly alteration.

EU8B and EU52 (Euganean Hills district) are classified as basaltic trachyandesite in the TAS classification (Fig. 5). The phenocrysts are plagioclase and clinopyroxene in a groundmass of plagioclase and oxides. The plagioclase phenocrysts (up to 2 mm in EU8B and up to 5 mm in EU52) are generally euhedral with sieved-textured center (EU8B) or without alteration (EU52). The clinopyroxene (up to 1 mm) are subhedral with rounded edges. Only EU52 exhibits also large (up to 5 mm) euhedral amphibole without any sign of alteration.

In the TAS classification the sample EU13A (Euganean Hills district) is a trachyandesite (Fig. 5). It contains medium-grained (0.5–1.5 mm) plagioclase, biotite, and clinopyroxene

in a groundmass of plagioclase and oxides. The plagioclase phenocrysts (up to 1.5 mm) are generally euhedral, yet may have a sieved-textured center. The clinopyroxene crystals (1 mm) are subhedral with rounded edges. The biotite (1 mm) are subhedral and partly adsorbed along the rims by oxides.

EU4, EU5B, and EU9 samples (Euganean Hills district) are the most felsic rocks of the analyzed suite. According to the TAS diagram EU4 is a trachyte, whereas EU5B and EU9 are rhyolites (Fig. 5). All of them exhibit glomeroporphyritic texture. The phenocrysts are subhedral and they are predominantly alkali feldspar (up to 5 mm), plagioclase (up to 5 mm), and biotite (1-2 mm) in a groundmass consisting of alkali feldspar and Fe-Ti oxides. Only in sample EU4 phenocysts of amphibole (1-2 mm) are present. The glomerocrysts, up to 1 cm in diameter, are both monomineralic (alkali feldspar) or comprised of plagioclase and alkali feldspar in the same cluster. Crystals within these glomerocrysts are subhedral with rounded corners on the edges of grains.

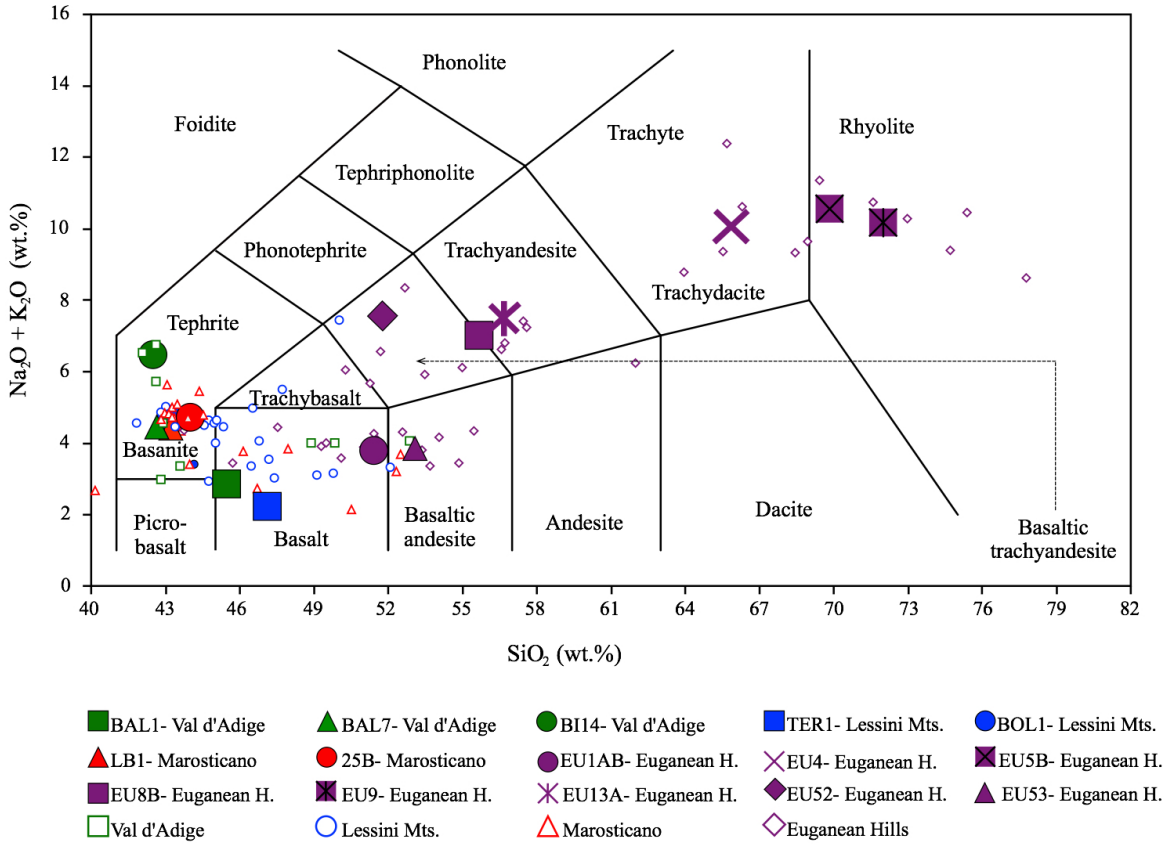

Fig. 5. Total Alkali versus Silica (TAS) classification diagram (Le Maitre et al., 2002) of the Val d'Adige, Lessini Mts., Marosticano, and Euganean Hills of this work (large simbols) and of literature (small simbols). Val d'Adige major compositions are from Beccaluva et al., (2007); Lessini Mts. major compositions are from Macera et al. (2003) and Beccaluva et al. (2007); Marosticano major compositions are from from Macera et al. (2003) and Beccaluva et al. (2007); Euganean Hills compositions are from Macera et al. (2003) and Milani et al. (1999).

3.5 Geochemistry

Major and trace element compositions of the magmatic rocks of this work are reported in Table A3.3-A3.4. On the TAS diagram (Fig. 5), these data overlap with those of literature for the VVP (Milani et al., 1999; Macera et al., 2003; Beccaluva et al., 2007), spanning a wide range of compositions from alkaline to sub-alkaline and including basic and evolved rocks. With increasing SiO_2 content, TiO_2, MgO, FeO_{total}, CaO, and P_2O_5 decrease progressively, whereas K_2O and Na_2O generally increase.

For this study we focused on the geochemistry of mafic samples, since their composition can reveal the features of the mantle source. BAL1, BAL7, BI14, TER1, BOL1, LB1, 25B, EU1AB, EU8B, EU52, and EU53 are heterogeneous in major element composition, with 42.5-55.8 wt.% SiO_2, MgO ranging from 3.1 to 12.3 wt.% and mg# [100 x Mg/(Mg + Fe^{2+})$_{mol}$] from 39.7 to 63.6 reflecting their different degree of evolution (i.e., from basanites to basaltic trachyandesites). The analyzed samples have predominantly alkaline affinities with relatively high K/Na. Since Na_2O/K_2O is comprised between 0.9 and 2.2, the samples classify as potassic, except for BAL1, EU1AB, and EU53 that have a sodic character (Na_2O/K_2O = 3.0; 7.5; 5.2, respectively). Primitive mantle-normalized rare earth element (REE) patterns are generally parallel and display moderate to steep slopes in Val d'Adige, Lessini Mts., and Marosticano samples. These patterns show a strong enrichment in light (L) REE and significant LREE to heavy (H) REE fractionation with $(La/Yb)_N$ between 5.5 and 24.3 (Fig. 6a). Irrespective of the lithology, in primitive mantle-normalized incompatible trace element diagram (Fig. 6b), the mafic samples from Val d'Adige, Lessini Mts., and Marosticano exhibit negative anomalies in Rb, and K, and positive anomalies in Ba, Sr, and P. The Euganean basaltic samples (EU1AB, EU8B, EU52, and EU53) mimic the trace element pattern of the rest of the VVP magmatic samples, but they exhibit different positive and negative anomalies. In particular, they exhibit negative K anomaly, and positive U, and Zr anomalies. Compared to the other analyzed samples, the Euganean basaltic trachyandesites have positive Ba anomaly, but lack positive Sr anomaly, while a slight positive P anomaly is present only in sample EU8B.

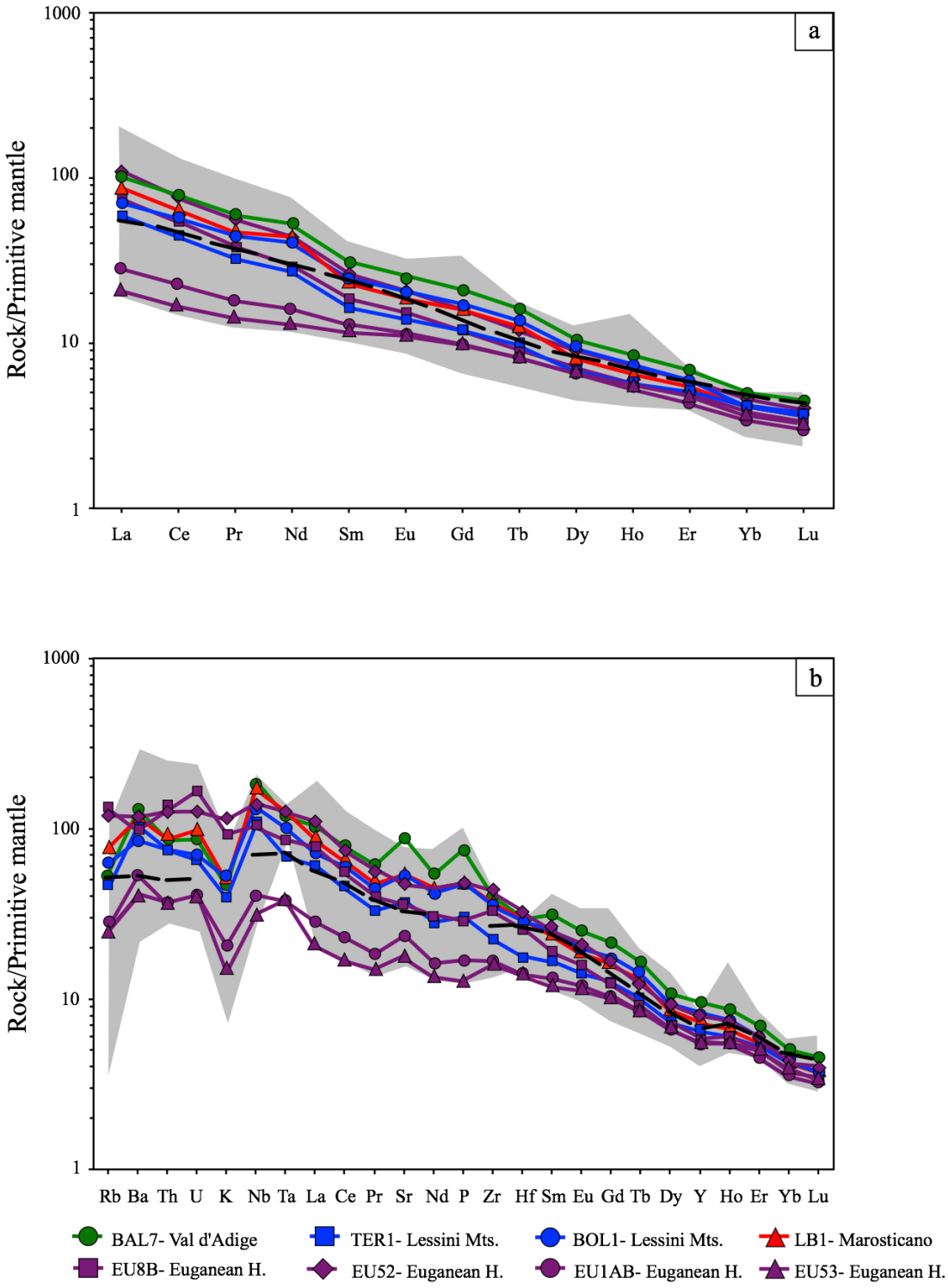

Fig. 6. (a) Primitive mantle-normalized rare earth and (b) trace elements patterns for mafic rocks from Val d'Adige, Lessini Mts., Marosticano, and Euganean Hills. In these diagrams, the patterns of literature samples from Val d'Adige and Lessini Mts. (Macera et al., 2003 and Beccaluva et al., 2007) are represented with a shadowed area. Typical ocean island basalt (OIB; Sun and McDonough, 1989) is indicated with a black dashed line. Primitive mantle values are from McDonough and Sun (1995).

3.6 Results from $^{40}Ar/^{39}Ar$ geochronological analyses

3.6.1 *Results from $^{40}Ar/^{39}Ar$ geochronological analyses obtained from WAAIF*

BAL1, BAL7, TER1, BOL1, and LB1 samples were analyzed with a new generation noble gas multicollector mass spectrometer (ARGUS VI), using groundmass. All ages reported in the text correspond to plateau ages corrected for deviations from the astmospheric $^{40}Ar/^{36}Ar$ ratio of Lee et al. (2006). For most samples the $^{40}Ar/^{36}Ar$ ratios are below the atmospheric values, considered as indication of air fractionation during cooling, especially for young samples (e.g., Oosting et al., 2017). However, since most of the VVP samples $^{40}Ar/^{36}Ar$ ratios are too low for being due to volcanic fractionation, we speculate that low $^{40}Ar/^{36}Ar$ ratios are due to fluid circulation and alteration. Therefore, for the samples with low $^{40}Ar/^{36}Ar$ ratios, the corresponding ages have to be considered as only minimum ages.
BAL1 shows an inverse isochron age of 41.70 ± 0.82 Ma [mean square weighted deviation (MSWD) = 0.78; probability (P) = 69%; Table A3.1; Fig. 7a]. The measured intercept of the inverse isochron indicates an initial $^{40}Ar/^{36}Ar$ value of 266 ± 23, which is slightly below the atmospheric value (298.56 ± 0.31; Lee et al., 2006). Using the $^{40}Ar/^{36}Ar$ intercept value, we calculated a plateau age of 41.69 ± 0.37 Ma (MSWD = 0.39; P = 98%; Table A3.1; Fig. 7b) based on 75% of the total gas. BAL7 yielded an inverse isochron age of 41.95 ± 0.46 Ma (MSWD = 0.82; P = 64; Table A3.1; Fig. 7c). Like the previous sample, the $^{40}Ar/^{36}Ar$ intercept value is slightly below the atmospheric value (264 ± 15 Ma) and allows to calculate a mini-plateau age of 41.98 ± 0.20 Ma (MSWD = 0.25; P = 100%), including 60% of the released ^{39}Ar (Table A3.1; Fig. 7d). Both in BAL1 and BAL7, the K/Ca spectra show patterns typical for basalt rock fragments with relatively high values at the low temperature steps that decrease steadily towards higher temperature steps, indicating that the K-rich phases degassed predominantly at lower temperatures and high Ca/K-phases dominate at higher temperatures (Fig. 7b, d). TER1 and BOL1 are the two samples from Lessini Mts. district and yielded different ages. TER 1 yielded an inverse isochron age of 45.21 ± 0.15 Ma (MSWD = 1; P = 44%; Table A3.1; Fig. 7e). The initial $^{40}Ar/^{36}Ar$ (253± 25) is slightly lower than atmospheric ratio, and defines a mini-plateau age of 45.21 ± 0.11 Ma (MSWD = 0.83; P = 61%) including 57% of the released ^{39}Ar (Table A3.1; Fig. 7f). BOL1 yielded an inverse isochron age of 40.60 ± 1.76 Ma (MSWD = 0.75; P = 74%; Table A3.1; Fig. 7g). The non-radiogenic $^{40}Ar/^{36}Ar$ intercept is 278 ± 19, close to the atmospheric $^{40}Ar/^{36}Ar$ ratio, and it was used to obtain a mini-plateau

age of 38.73 ± 0.44 Ma (MSWD = 0.99; P = 46%) based on 62% of the total gas (Table A3.1; Fig. 7h). This sample shows the lowest K/Ca (0.27 to 0.007) of all analyzed samples (Fig. 7h). LB1, the sample from Marosticano district, did not return isochron and plateau ages. Almost all the steps indicate apparent age between 20.5 and 23.2 Ma (Table A3.1; Fig. 7i, Fig. 7j). The K/Ca diagram shows a monotonically decreasing plot from 1.69 to 0.003 (Fig. 7j).

EU1AB and EU53 from Euganean Hills district were not dated due to the pervasive alteration. EU4, EU5B, EU8B, EU9, and EU13A samples were analyzed with the MAP215-50 mass spetrometer using K-rich mineral separates (i.e., biotite, feldspar, sanidine). Only amphibole and plagioclase of EU52 were analyzed with the ARGUS VI mass spetrometer. Irrespective to the lithology, all Euganean samples analyzed yielded the same age of ca. 32 Ma. The biotite separate of EU4 shows an inverse isochron age of 31.83 ± 0.50 Ma (MSWD = 0.88; P = 57%; Table A3.1; Fig. 7k). The $^{40}Ar/^{36}Ar$ intercept is atmospheric (328 ± 43) and defines a plateau age of 32.09 ± 0.29 Ma (MSWD 0.97; P 48%) based on 100% of the total released gas (Table A3.1; Fig. 7l). The K/Ca spectrum is flat and the high values (157-3762) are consistent with the mineral phase analyzed (Fig. 7l). The sanidine separate of sample EU5B yielded an inverse isochron age of 31.87± 0.79 Ma (MSWD = 0.86; P = 59%; Table A3.1; Fig. 7m) with $^{40}Ar/^{36}Ar$ intercept of 343 ± 58. The calculated plateau age is 32.30 ± 0.52 Ma (MSWD = 1.0; P = 45%) defined by 100% of the released Ar (Table A3.1; Fig. 7n). The K/Ca spectrum is flat with typical ratios for sanidine (Fig. 7n). The inverse age for the feldspar separate of EU8B is 32.11 ± 0.98 Ma (MSWD = 0.85; P = 61%; Table A3.1; Fig. 7o). Using its $^{40}Ar/^{36}Ar$ intercept value (305 ± 99) we obtained a plateau age of 32.17 ± 0.32 Ma (MSWD = 0.79; P = 68%; Table A3.1; Fig. 7p), defined by 100% of the released Ar. The high K/Ca values are consistent with the mineral phase analyzed (Fig. 7p). The sanidine separate of sample EU9 shows inverse isochron ages of 32.02 ± 0.67 Ma (MSWD = 0.51; P = 91%; Table A3.1; Fig. 7q). With the $^{40}Ar/^{36}Ar$ intercept value (315 ± 68) indistinguishable from atmosphere, the calculated plateau age is 32.17 ± 0.27 Ma (MSWD = 0.48; P = 94%; Table A3.1; Fig. 7r), defined by 100% of the gas released. The K/Ca spectrum is flat and exhibits typical values for the mineral phase analyzed (Fig. 7r). For the feldspar separate of the sample EU13A we obtained an inverse isochron age of 31.96 ± 1.13 (MSWD = 0.52; P = 91%; Table A3.1; Fig. 7s). The $^{40}Ar/^{36}Ar$ intercept is atmospheric (349 ± 136) and defines a plateau age of 32.34 ± 0.51 Ma (MSWD = 0.53; P = 91%) that includes 88% of the total ^{39}Ar (Table A3.1; Fig. 7t). Despite their large uncertainties, the K/Ca values are consistent with the

mineral phase analyzed (Fig. 7t). The amphibole separate of EU52 yielded an inverse isochron age of 32.37 ± 0.12 Ma (Table A3.1; Fig. 7u), with $^{40}Ar/^{36}Ar$ intercept (295 ± 14) indistinguishable from atmosphere and yielded a mini-plateau age of 32.35 ± 0.09 Ma (MSWD = 0.48; P = 89%) based on 67% of ^{39}Ar (Table A3.1; Fig. 7v). The K/Ca spectrum is flat and the values (0.098 to 0.104) are low, as expected for amphibole (Fig. 7v). The plagioclase inverse isochron age of EU52 is 32.16 ± 0.08 Ma (MSWD = 0.65; P = 87%, Table A3.1; Fig. 7w). The $^{40}Ar/^{36}Ar$ intercept value is 397 ± 19 and may indicate presence of excess ^{40}Ar. Using this latter value we obtained a 32.16 ± 0.06 Ma (MSWD 0.58; P 93%), based on 99.5% of the gas (Table A3.1; Fig. 7x). It should however be considered that the low K/Ca makes all steps cluster at very low $^{40}Ar/^{36}Ar$ intercepts. The K/Ca values range from 0.079 to 0.114, consistent with the mineral phase analyzed (Fig. 7x).

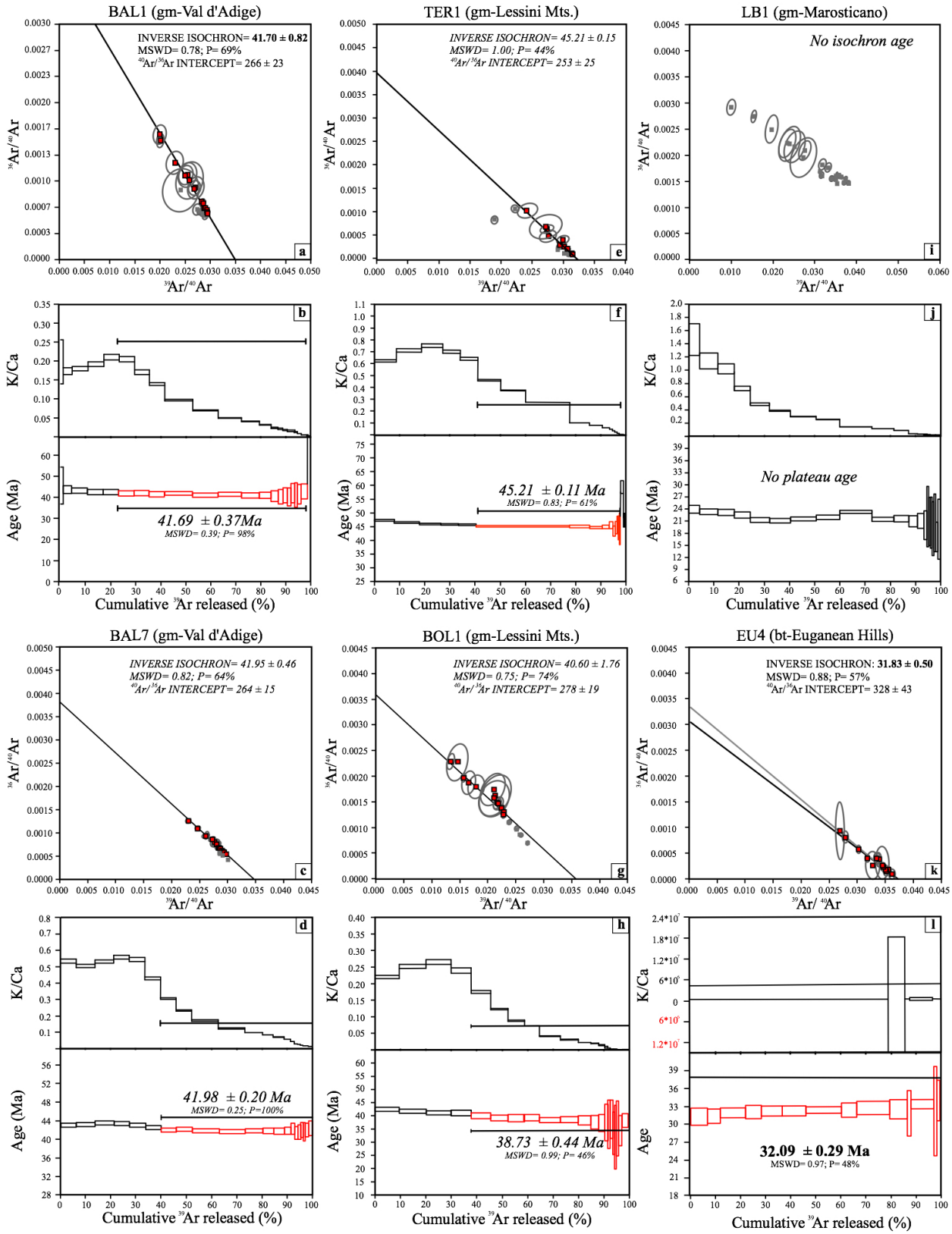
BAL1 (gm-Val d'Adige)
INVERSE ISOCHRON= 41.70 ± 0.82
MSWD= 0.78; P= 69%
40Ar/36Ar INTERCEPT= 266 ± 23
41.69 ± 0.37Ma
MSWD= 0.39; P= 98%
TER1 (gm-Lessini Mts.)
INVERSE ISOCHRON= 45.21 ± 0.15
MSWD= 1.00; P= 44%
40Ar/36Ar INTERCEPT= 253 ± 25
45.21 ± 0.11 Ma
MSWD= 0.83; P= 61%
LB1 (gm-Marosticano)
No isochron age
No plateau age
BAL7 (gm-Val d'Adige)
INVERSE ISOCHRON= 41.95 ± 0.46
MSWD= 0.82; P= 64%
40Ar/35Ar INTERCEPT= 264 ± 15
41.98 ± 0.20 Ma
MSWD= 0.25; P=100%
BOL1 (gm-Lessini Mts.)
INVERSE ISOCHRON= 40.60 ± 1.76
MSWD= 0.75; P= 74%
40Ar/35Ar INTERCEPT= 278 ± 19
38.73 ± 0.44 Ma
MSWD= 0.99; P= 46%
EU4 (bt-Euganean Hills)
INVERSE ISOCHRON: 31.83 ± 0.50
MSWD= 0.88; P= 57%
40Ar/39Ar INTERCEPT= 328 ± 43
32.09 ± 0.29 Ma
MSWD= 0.97; P= 48%
36Ar/40Ar
39Ar/40Ar
K/Ca
Age (Ma)
Age
Cumulative 39Ar released (%)

(continued)

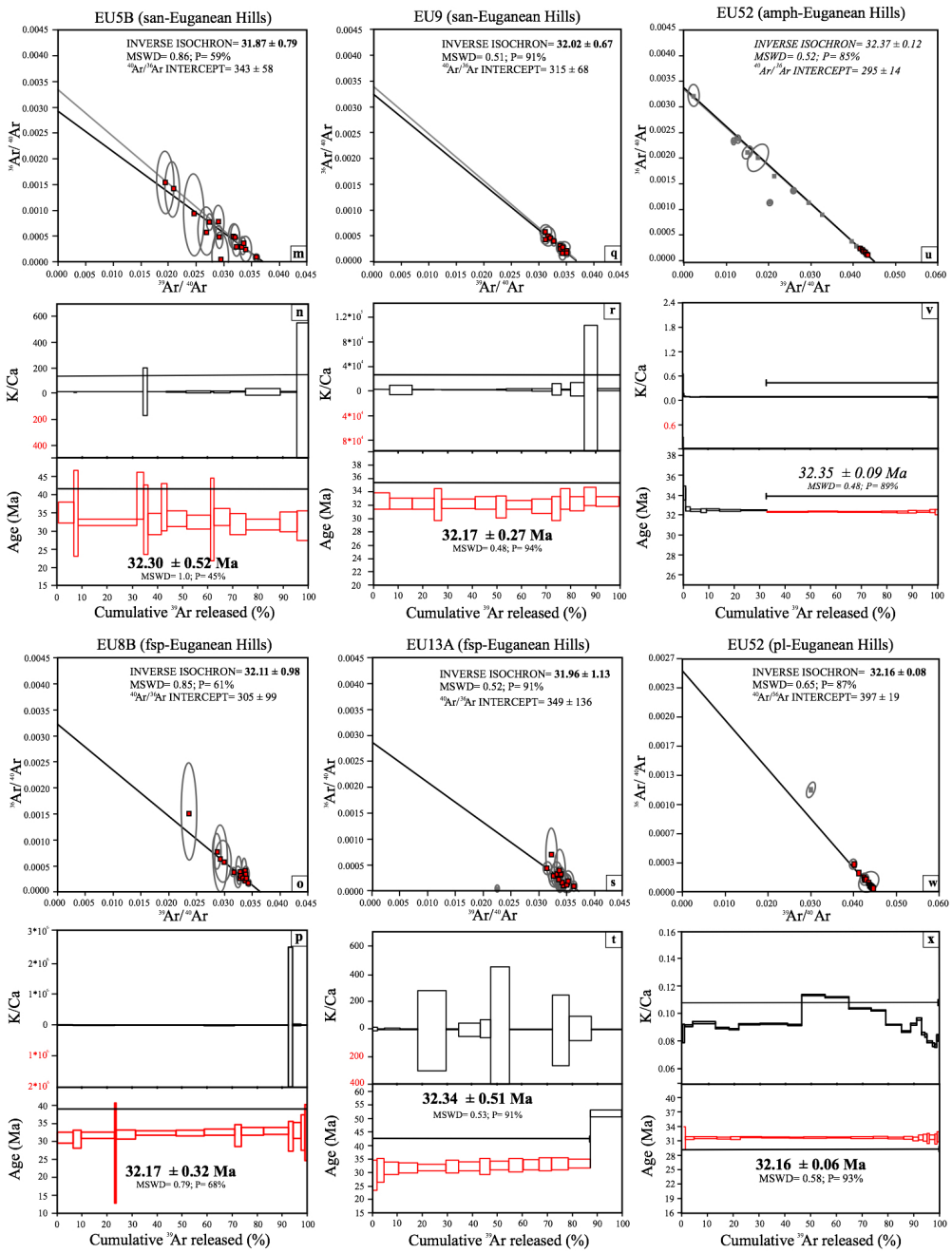

Fig. 7. VVP $^{40}Ar/^{39}Ar$ inverse isochrones and respective apparent age and K/Ca ratio spectra plotted against the cumulative percentage of ^{39}Ar released. Plateau ages (bold) are inverse isochron intercept ($^{40}Ar/^{39}Ar$) corrected. Mini-plateaus (50-70% cumulative ^{39}Ar) are indicated in italics. Mean squared weighted deviation (MSWD) and probability of fit (P) are indicated. Errors on plateau ages are quoted at 2σ and do not include systematic errors (i.e., uncertainties on the age of the monitor and on the decay constant). These plots are obtained at Curtin University within the Western Australian Argon Isotope Facility (WAAIF) of the John de Laeter Centre using ARGUS VI and MAP 215–50 mass spectrometers.

Abbreviations: gm= groundmass; bt= biotite; san= sanidine; fsp= feldspar; pl= plagioclase; amph= amphibole.

3.6.2 *Results from $^{40}Ar/^{39}Ar$ geochronological analyses obtained from Noble Gas Geochronology Laboratory (University of Vermont)*

The samples BI14 and 25B, from Val d'Adige and Marosticano, respectively, were analyzed at the Noble Gas Geochronology Laboratory of the University of Vermont using the Nu Instruments Noblesse magnetic sector noble gas mass spectrometer with the purpose to expand the VVP geochronological dataset. Despite the poor fit of the measured inverse isochrons, the results from these samples are concordant with the Val d'Adige and Marosticano counterparts analyzed at the WAAIF. For the sample BI14 (Val d'Adige district) the $^{40}Ar/^{36}Ar$ intercept of the inverse isochron (207 ± 138; Table A3.2; Fig. 8a) is lower than atmospheric ratio showing that this rock was affected by alteration. This value defines a mini-plateau age (40.73 ± 0.48 Ma; MSWD = 0.80; P = 45%; Table A3.2; Fig. 8b) similar to those calculated from BAL1 and BAL7. In the first three steps the K/Ca ranges from 1.8 to 2.3, while in the last steps decrease from 0.5 to 0.1 (Fig. 8b). As the Marosticano sample LB1, also the sample 25B didn't provide isochron and plateau ages (Table A3.2; Fig. 8c-d). In fact, for both samples, almost all the steps indicate apparent age ca. 22 - 23 Ma.

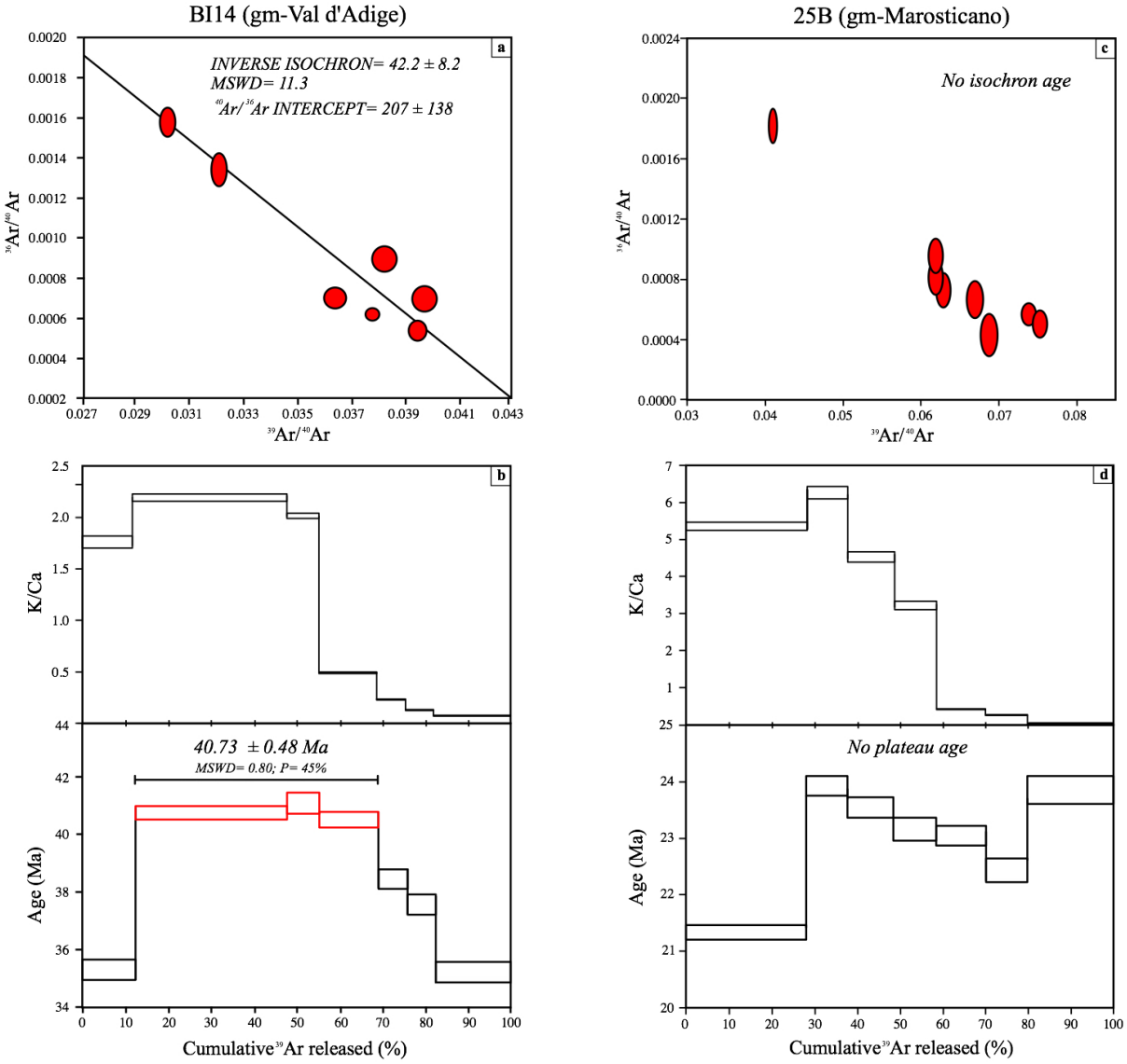

Fig. 8. VVP $^{40}Ar/^{39}Ar$ inverse isochrones and respective apparent age and K/Ca ratio spectra plotted against the cumulative percentage of ^{39}Ar released. Plateau ages (bold) are inverse isochron intercept ($^{40}Ar/^{39}Ar$) corrected. Mini-plateaus (50-70% cumulative ^{39}Ar) are indicated in italics. Mean square weighted deviation (MSWD) and probability of fit (P) are indicated. These plots are obtained at the Noble Gas Geochronology Laboratory of the University of Vermont with Nu Instruments Noblesse magnetic sector noble gas mass spectrometer.

Abbreviations: gm= groundmass

3.7 Discussion

3.7.1 *The mantle source of VVP magmatism*

Although the Cenozoic magmatism of the VVP gave rise to both mafic and felsic magmatic products, for this work we focus on the geochemistry of the poorly evolved rocks in order to provide insights onto the composition and evolution of their mantle source. In particular, trace element compositions of the mafic rocks are used as proxies of nature and evolution of the mantle source(s). The primitive-mantle normalized trace element patterns of VVP mafic samples show i) an increase from Rb to U, ii) a progressive decrease of the incompatible trace elements from Nb, and iii) strong enrichment in LREE compared with HREE [$(La/Yb)_N$: 14.4–22.0] (Fig. 6a, b). These features are observed also in previous studies on the VVP, which interpreted the trace element patterns as the result of an intraplate origin from ocean island basalt (OIB)-like mantle source (Milani et al., 1999; Beccaluva et al., 2007; Macera et al., 2008; Fig. 6a, b). However, VVP patterns of this study are distinguishable from that of the average OIB (McDonough and Sun, 1995) for: i) enrichment in LILE relative to HFSE (Ba/La: 10.7-19.2; average OIB: 9.4), and ii) positive anomalies in Ba, Sr, and P, which are missing only in the Euganean basaltic trachyandesite samples (i.e., EU8B and EU52). In relatively less evolved Euganean rocks, like EU1AB (basalt) and EU53 (tholeiitic basalt), the positive Ba and Sr anomalies are present, but the positive P anomaly is evident only in the basaltic sample.

As the basic rocks are only slightly differentiated, it is unlikely that fractional crystallization modified their incompatible element contents significantly. Specifically, the Ba, Sr, and P contents are unlikely to be affected by the early stage of fractional crystallization that involves olivine and clinopyroxene (Merle et al., 2017). Therefore, Ba, Sr, and P concentrations and enrichment in LREE probably represent source characteristics. These features are commonly observed in carbonatite metasomatized mantle xenoliths (Yaxley et al., 1991; Ionov et al., 1996), which are carried by silicic basaltic melts derived from peridotitic sources (e.g., Price et al., 2010). Beccaluva et al. (2007) have already hypothesized carbonatitic components as important contributors to the mantle source of the VVP alkaline magmas. In addition, in the Marosticano district, on-craton peridotite xenoliths, exhibiting fingerprint of carbonatitic/CO_2-rich silicate melt metasomatism, have been recently described (Brombin et al., 2018).

3.7.2 *The temporal evolution of the magmatic activity of the VVP*

For basaltic rocks older than Quaternary the dating of mineral separates is preferred over groundmass for which separation of altered from fresh grains is difficult during sample preparation (Jourdan et al., 2007; Verati and Jourdan, 2013). Due to the lack of relatively phenocrysts of plagioclase in the VVP basanitic and basaltic samples, groundmass dating was carried out. Therefore, i) the $^{40}Ar/^{36}Ar$ intercepts substantially lower than atmospheric values for VVP whole-rock data (<276.9 ± 19.5; Table A3.1; Fig. 7c, e, g) together with ii) the absence of proper plateau ages (i.e., <70% ^{39}Ar released; Table A3.1-A3.2; Fig. 7d, f, h, j), and iii) their convex K/Ca spectra suggest the presence of alteration phase (Fig. 7b, d, f, h). In this sense, all obtained mini-plateau ages are considered as minimum crystallization ages. In general, ages are consistent with biostratigraphic data, when available. Therefore, we are confident that the reported whole-rock ages are probably not too far off the actual crystallization ages, but we warn that the true age of a rock that yielded a mini-plateau could lie well outside of the 95% confidence level given by the sample uncertainties (e.g., a mini-plateau age of 41.98 ± 0.20 Ma could be associated with an emplacement age of 44 Ma). Only Marosticano whole-rock data do not define isochron or plateau ages (Fig. 7i, j), but biostratigraphic data support an early Miocene eruption. Ages for the Euganean samples were all obtained on mineral separates and are thus of higher quality. All Euganean samples yield statistically robust plateau ages based on > 88% of gas released (Fig. 7l, n, p, r, t, x), only the amphibole separate from EU52 yielded a mini-plateau (defined by 67% of the released gas).

Based on the new age data and considering previously published biostratigraphic data, we reconstructed the temporal evolution of the Cenozoic magmatism occurred in the southeastern alpine domain (Fig. 9). The VVP magmatic activity was discontinuous and took place in several stages, covering a time-span of about 30 Ma (from late Paleocene to early Miocene). The oldest activity was always subaqueous and is thus difficult to date due to the pervasive alteration of the volcanic products. The oldest age from our $^{40}Ar/^{39}Ar$ geochronology study is Lutetian and it was obtained on a basaltic lava flow (TER1≥ 45.21 ± 0.11 Ma; Table A3.1; Fig. 7e, f; Fig. 9) from the Lessini Mts..The basanitic neck of Monte Purga di Bolca cuts this lava flow and records a younger age (BOL1≥ 38.73 ± 0.44 Ma; Bartonian; Table A3.1; Fig. 7g, h; Fig. 9) confirming that volcanism in this district lasted at least 7 Ma and occurred in several pulses. Our $^{40}Ar/^{39}Ar$ ages for Lessini Mts. district are younger than U-Pb age (51.0 ± 1.5 Ma; Fig. 3; Fig. 9) obtained on inherited

zircon megacrysts by Visonà et al. (2007). The Val d'Adige district records similar $^{40}Ar/^{39}Ar$ ages to those obtained for the Lessini Mts. samples presented in this study. In particular at Monte Baldo the lava flow (BAL1) and sill (BAL7) record ages of 41.69 ± 0.37 Ma and 41.98 ± 0.20 Ma, respectively (Table A3.1; Figs. 7a-d). These ages are consistent with biostratigraphic ages for the Calcare di Torbole (Lutetian) and Calcare di Nago (Bartonian-Priabonian), which represent the base and the top of the lava flow, respectively (Fig. 9). Also the other Val d'Adige sample from the basanitic quarry of Isera yields an age (≥40.73 ± 0.48 Ma; Table A3.2; Fig. 8a, b) consistent with the Calcare di Torbole/Calcare di Nago boundary (Fig. 9).

On the contrary, in the other two VVP districts (i.e., Euganean Hills and Marosticano), the magmatic activities are younger. Irrespective to the lithology, the Euganean Hills samples yielded age results that are indistinguishable. In particular, for the basaltic trachyandesite sample (EU52) both amphibole and plagioclase separates were analyzed and the resulting plateau ages are similar: 32.35 ± 0.09 Ma and 32.16 ± 0.06 Ma, respectively (Table A3.1; Fig. 7u-x). The slight difference between the two may be tentatively attributed to the difference of closure temperature of these two minerals with closure temperatures of ca. 550 °C and 300 °C for hornblende and plagioclase respectively. This would suggest a relatively slow cooling of the intrusion with a cooling rate of 1.3 °C/ka from the amphibole to the plagioclase closure temperature. We note that EU52 is intruded in other basic units, which are geochemically equivalent to the late basaltic products of the Euganean Hills. The plateau ages of EU52 overlap that of the other Euganean basaltic trachyandesite (EU8B: 32.17 ± 0.32 Ma; Table A3.1; Fig. 7o, p). The plateau ages for the trachyandesitic, trachytic, and rhyolitic Euganean samples range between 32.09 ± 0.29 and 32.34 ± 0.51 Ma (Table A3.1; Fig. 7l, n, r, t). Therefore, according to our geochronological data both basaltic and acidic magmatism occurred during the Rupelian (lower Oligocene; Fig. 9) during a time-span possibly shorter than 0.2 Ma. Finally, both the Marosticano samples collected in Monte Gloso quarry point to an Aquitanian (early Miocene) eruption age (Table A3.1; Figs. 7i, j, 8c, d; Fig. 9). According to the biostratigraphy, no eruptions occur during in Miocene neither in Val d'Adige nor in Euganean Hills district. Therefore the Miocene magmatic products of Lessini Mts. indicated by the biostratigraphic study (Savelli and Lipparini, 1979; Fig. 3, Fig. 9) and those of Marosticano district (descripted above) represent the most recent known magmatic activity in the VVP.

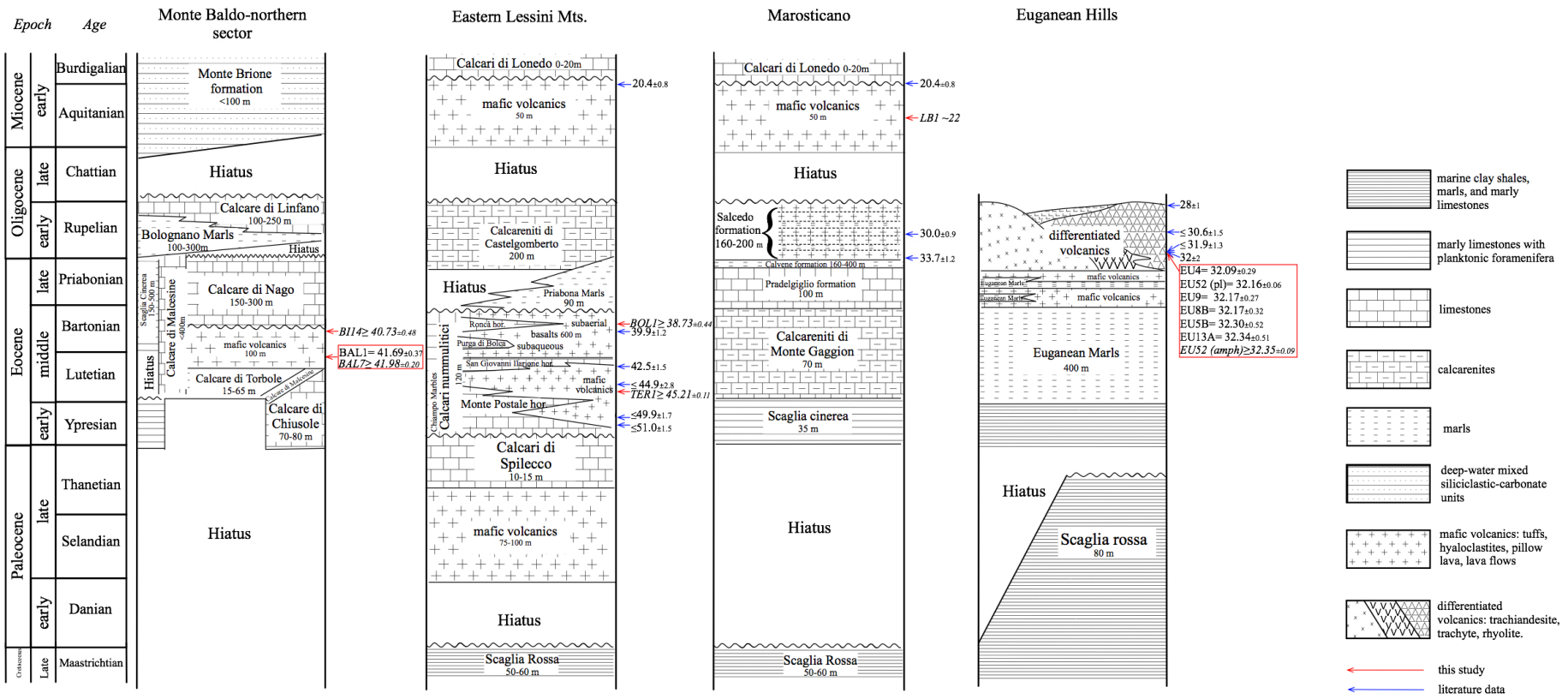

Fig. 9. Upper Cretaceous to lower Miocene stratigraphic records in the Monte Baldo northern sector (Val d'Adige district; Luciani, 1989; De Vecchi and Sedea, 1995), Eastern Lessini Mts. (De Vecchi and Sedea, 1995; Bassi et al., 2008), Marosticano (Frascari Ritondale Spano and Bassani, 1973; De Vecchi and Sedea, 1995; Bassi et al., 2008), and Euganean Hills (Piccoli et al., 1981). Ages and uncertainties are reported in Ma. Ages in italics are derived from mini-plateaus (50-70% ^{39}Ar released) and are considered minimum ages only. Ages derived from inherited (i.e., pre-erupted) zircons from Lessini Mts. and Euganean Hills districts are considered maximum ages. The literature dating for Eastern Lessini Mts. are from Borsi and Ferrara (1969), Savelli and Lipparini, (1979), and Visonà et al. (2007), for Marosticano are from Savelli and Lipparini, (1979), and for Euganean Hills are from Borsi et al. (1969), Zantendeschi (1994), and Bartoli et al. (2014).

3.7.3 *Geodynamic implications of the magmatism in the VVP: two contrasting models*

According to our data the age of the VVP magmatism range from 45.21 ± 0.11 Ma (TER1, Lessini Mts. district) to ca. 22 Ma (LB1, Marosticano district). If we consider also the biostratigraphic evidence for early subacqueous activity in the Lessini Mts. and Val d'Adige, the VVP magmatism probably started from the late Paleocene. Periadritic magmatism from the Central Southern Alps occurred from 42 Ma to 28 Ma (Bergomi at al., 2015 and reference therein) and is characterized by a clear subduction geochemical signature (Bellieni, 1981; Bergomi et al., 2015). Contrasting petrogenetic and geodynamic models are used to explain the Cenozoic magmatism in the Alps (both Periadriatic and VVP). The most quoted is the slab breakoff model (e.g., von Blanckenburg and Davies, 1995; Dal Piaz et al., 2003; Macera et al., 2003; Bergomi et al., 2015). During the middle Eocene (ca. 35 Ma), after the Adria-Europe collision, the subducting oceanic slab detached from the European margin. The breakoff of the subducting slab allowed astenospheric upwelling above the supra-subduction hydrated mantle wedge, causing melting of the subcontinental lithosphere. The occurrence of high velocity anomalies (i.e., "cold" material) observed on tomographic images lying above the mantle transition zone under the Central Alps has been proposed to represent the detached European slab (e.g., Piromallo and Morelli, 2003; Macera et al., 2003; Giacomuzzi et al., 2011; Zhao et al., 2016). The seismic tomography images of Lippitisch et al. (2003) and Piromallo and Morelli (2003) showed also that these high velocity anomalies are discontinuous, reflecting gaps larger than 100 km. The low-velocity anomalies (i.e., "hot" material) below the VVP could represent plume-like mantle diapirs sucked into these lithospheric gaps and upwelled towards shallower levels inducing partial melting of the surrounding subcontinental lithospheric material (Macera et al., 2003). Geochemical and isotopic data of the magmas generated in these areas seem to confirm these observations: the Periadriatic magmatism products (plutons and dikes) are all sub-alkaline and calc-alkaline types, exhibiting trace element signature of subduction-related magmas (high LILE/HFSE, LREE/HFSE ratios, and low-Nb contents; Bellieni, 1981; Bergomi et al., 2015), while the VVP products record an OIB mantle component that was interpreted as sign of possible plume-related origin (Macera et al., 2003). However, our data along with those of literature (Visonà et al., 2007), and the indirect stratigraphic ages suggest that the Cenozoic magmatism started in the late Paleocene, before the supposed slab breakoff. Therefore only the magmatic activity of post-middle Eocene age may be related to slab detachment. Macera et al. (2003)

justified the VVP eruptions at Paleocene time as the result of the mantle diapir action. While Bergomi et al. (2015) supposed the partial melting of supra-subduction mantle wedge in the VVP area in response to the low-angle Alpine subduction, that leads to the shortening in the upper plate and the shift of it to the foreland.

However, recent high-resolution P wave tomography performed by Zhao et al. (2016) shed new light to the geodynamics of the Alpine region. These new images document i) the lateral continuity of the European slab from the Western Alps to the Central Alps, and ii) the downdip slab continuity beneath the Central Alps, ruling out the hypothesis of the slab breakoff as a viable mechanism for Cenozoic magmatism. These observations are confirmed also by the first P wave anisotropic tomography of the Alps performed by Hua et al. (2017). The previous studies performed by Piromallo and Morelli (2003), Macera et al. (2003), Giacomuzzi et al. (2011), and Zhao et al. (2016) are isotropic tomography images that assumed the Earth is isotropic to the propagation of seismic waves. However, it is well known that seismic anisotropy exists in the Earth's interior, due to lattice-preferred orientation and shaped-preferred orientation of minerals (Price, 2010 and reference therein). In the upper mantle, seismic anisotropy is mainly produced by the preferred orientation of olivine crystals induced by mantle flow (e.g., Savage, 1999; Savage and Sheehan, 2000; Park and Levin, 2002; Lucente et al., 2006; Savage et al., 2016). Therefore isotropic tomography simply provides snapshots of the actual crust and the upper mantle structures beneath the Alps (Hua et al., 2017), whereas seismic anisotropy reveals information on the actual upper mantle flow field (Long and Silver, 2008; Hua et al., 2017). The combination of isotropic and anisotropic images allows the reconstruction of the complex mantle structure and dynamics of the Alps and adjacent regions. The isotropic tomography performed by Hua et al. (2017) shows that the subduction mass in the central Alps ranges from 450 to 500 km (planar movement), in accordance with the estimation of the length of an hypothetical continuous subducting slab below the central Alps (Piromallo and Faccenna, 2004), and in contrast with the more reduced slab mass of (planar) 300 km estimated by Piromallo and Faccenna (2004), that was took as evidence of slab breakoff. Whereas, the anisotropic tomography reveals that:

i) a negative radial anisotropy (i.e., $V_{ph}<V_{pv}$, where V_{ph} and V_{pv} are the velocities of P-waves propagating horizontally and vertically, respectively; Zhao et al., 2016), within the high velocity European and Adriatic slab system, drawing two slabs nearly vertical as an effect of the induced movements of the slabs mainly confined in the vertical direction;

ii) a positive radial anisotropy (i.e., $V_{ph}>V_{pv}$) in the low-velocity mantle wedge is recorded, generated by the mantle flow induced by the vertical slab subduction.

These tomographic results provide elements for an alternative model to explain the Alpine geodynamics and related Cenozoic magmatism. Since the closure of Vardar ocean in the Late Cretaceous-early Eocene (Robertson et al., 2013) and the following continent-continent collision, the European slab became not only progressively steeper, but also retreated in response to rollback mechanisms (Singer et al., 2014; Bergomi et al., 2015; Schlunegger and Kissling, 2015). Analytical laboratory solutions, 3D experiments and numerical modelling reproducing the retreating slabs movements show that near the slab lateral edges, the astenospheric material beneath, escapes laterally and upwells frontally producing vigorous toroidal/poloidal mantle flow (i.e., horizontal and vertical rotational vortex-like components of mantle motion; Funiciello et al., 2006; Piromallo et al., 2006; Faccenna et al., 2011). According to these models (Faccenna et al., 2011) the mantle upwelling in the center of the vortex produces decompression melting. We speculate that, in the Alps geological setting, the progressive retreat of the European slab toward west caused the upwelling of a toroidal/poloidal flow, which drove the decompression melting in the mantle wedge beneath the VVP and triggering magmatism at first in the westernmost VVP side (i.e., Val d'Adige-Lessini Mts. domain; ca. 51-45 Ma) and then in the easternmost one (i.e., Marosticano-Euganean Hills domain; ca. 32-30 Ma) (Fig.10). The migration and rejuvenation of the magmatism southeastward can be accounted by considering the forward movement of the overriding Adria plate faster than the retreating slab, allowing the astenospheric upwelling to affect different portions of the overlying lithosphere.

To sum up, compared with the Periadriatic magmatism data set, the geochronological and geochemical data of the VVP magmatism presented in this work allow a rethinking of the geodynamic models and the related mantle processes in the Alpine region. It is clear that we are far from the complete resolution of the geodynamics of the Alps, and highly controversial issues remain. The most relevant concerns the vertical continuity of subducting slabs which imply the presence or not of a slab breakoff beneath the Alps. Unfortunately, this uncertainty in Alpine slab structure prevents to constrain the triggering mechanism of the Cenozoic magmatism (i.e., slab breakoff model or toroidal/poloidal flow model). However, recent numerical modelling reveal that the classic model of slab breakoff and related magmatism could be overestimated, therefore the geodynamic of

many post-collisional areas must be revised. According to Freeburn et al. (2017) the magmatism induced by slab breakoff occurs only when the latter is shallower than the base of the overriding lithosphere. Such processes are not common as slab breakoff occurs typically deeper than the overriding plate thickness (Duretz et al., 2011; van Hunen and Allen, 2011; Freeburn et al., 2017), too deep to generate any decompressional melting of dry upwelling asthenosphere or thermal perturbation within the overriding lithosphere. Therefore alternative mechanisms, like the toroidal/poloidal flow model, must be taking in account to explain the magmatic processes in the post-collisional areas, as the VVP (Fig.10).

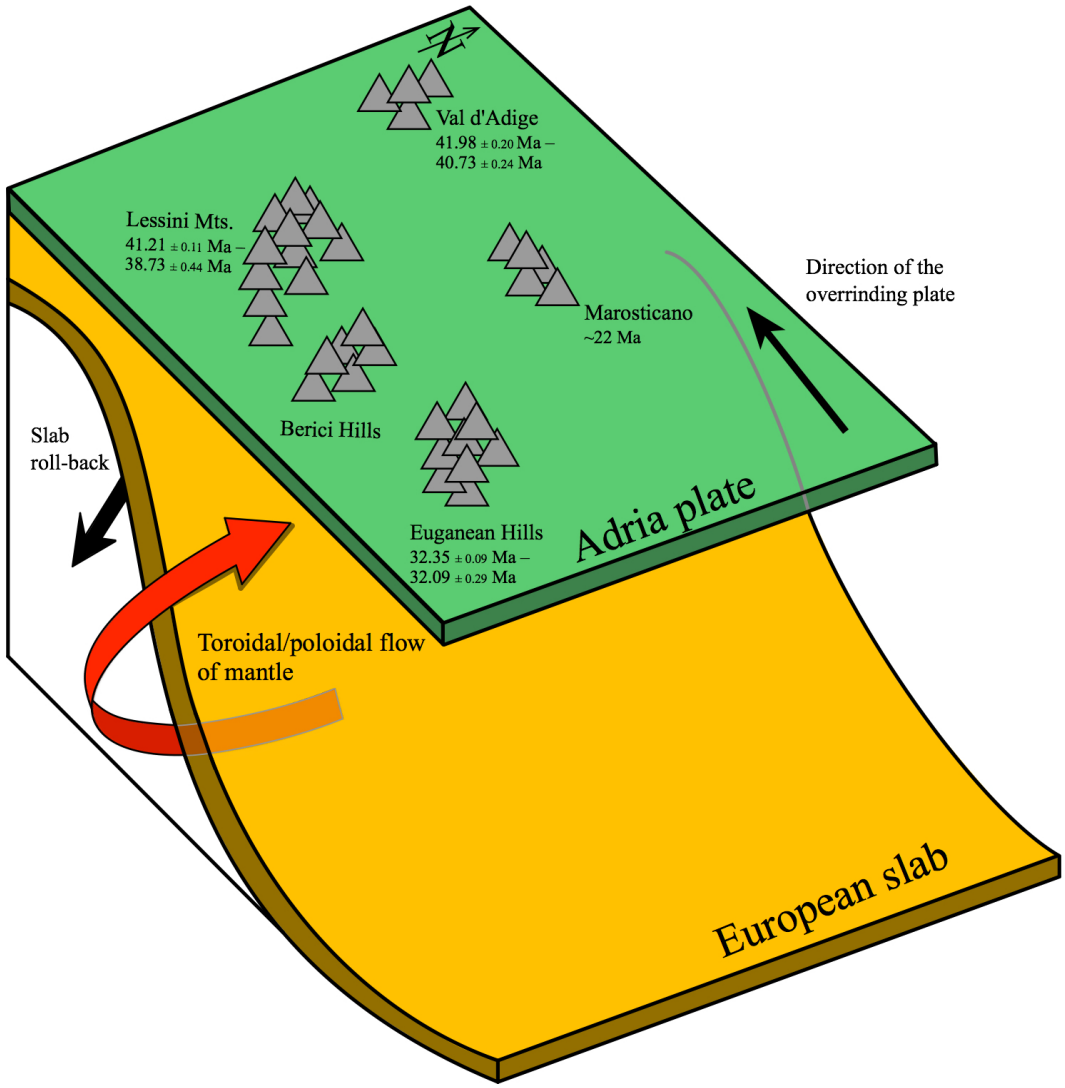

Fig. 10. Schematic model showing toroidal/poloidal flow beneath the Adria plate around the edge of the European slab. See explanation in the text.

3.8 Conclusions

- Bulk rock major and trace elements features of basic and acidic lavas from four VVP magmatic districts (Val d'Adige, Marosticano, Lessini Mts., and Euganean Hills) are comparable to those observed in literature from the same areas and interpretable as the result of a intraplate origin from OIB-like mantle source. The Ba, Sr, and P positive anomalies indicate a mantle source metasomatized by carbonatite/CO_2-rich silicate melts.
- VVP biostratigraphic data and our new high-resolution $^{40}Ar/^{39}Ar$ radioisotopic ages allow the reconstruction of the history of Cenozoic Southalpine magmatism activity, which was discontinuous during a time-span of 30 Ma (from late Paleocene to early Miocene). The first eruptions occurred in the late Paleocene in the western districts (i.e., Val d'Adige and Lessini Mts.). In the early Eocene the magmatic activity went on only in the Lessini Mts. district. The middle Eocene (Lutetian-Bartonian) is considered the climax of the VVP volcanism with basic eruptions in Val d'Adige, Lessini Mts., and Euganean Hills. During the early Oligocene exclusively in Euganean Hills both basic and acidic eruptions occurred, while only basic eruptions occurred in Marosticano. In this latter district, magmatic episodes were recorded until the end of the early Miocene.
- Prior this study, VVP magmatism was interpreted mainly in terms of European slab breakoff, with asthenopheric material rising from the slab gaps and inducing partial melting of the surrounding subcontinental lithospheric material. But, recent high-resolution isotropic and anisotropic tomographic images revealed a continuous nearly vertical subducting European slab. In addition, new numerical modelling reveal that in most cases the slab breakoff occurs too deeply to be an efficient mechanism to induce magmatic processes in post-collisional areas. Therefore, for the Cenozoic VVP magmatism an alternative triggering mechanism must be hypothesized. We proposed a decompression melting of the sublithospheric material beneath the VVP due to the progressive retreatment and steepness of the European slab that produce a "toroidal/poloidal flow" of the beneath mantle. The speculated faster movement of the overriding Adria plate than that of retreating slab explains the migration and rejuvenation of the magmatism southeastward.

References

Alagna, K.E., Peccerillo, A., Martin, S., 2010. Tertiary to present evolution of Orogenic magmatism in Italy. J Virt Expl 36: paper 18. In: Beltrando, M., Peccerillo, A., Mattei, M., Conticelli, S., Doglioni, C. (Eds.) The geology of Italy: tectonics and life along plate margins, 2010.

Barbieri, G., Medizza, F., 1969. Contributo alla conoscenza geologica della regione di Bolca (Monti Lessini). Memorie degli Istituti di Geologia e Mineralogia dell'Università di Padova 27, 1-36.

Barbieri, G., De Zanche, V., Sedea, R., 1991. Evoluzione del semigraben paleogenico Alpone-Agno (Monti Lessini). Rendiconti della Società Geologica Italiana 14, 5-12.

Bartoli, O., Meli S., Bergomi, M.A., Sassi, R., Magaraci, D., Liu, D.Y., 2014. Geochemistry and zircon U-Pb geochronology of magmatic enclaves in trachytes from the Euganean Hills (NE Italy): further constraints on Oligocene magmatism in the eastern Southern Alps. European Journal of Mineralogy, 27, 161-174**.**

Bassi, D., Bianchini, G., Mietto, P., Nebelsick, J.H., 2008. Southern Alps: Venetian Pre-Alps. In McCann T. (ed.), The Geology of Central Europe, 2. The Geological Society of London, 1087-1092.

Beccaluva, L., Bonadiman, C., Coltorti, M., Salvini, L., Siena, F., 2001. Depletion events, nature of metasomatizing agent and timing of enrichment processes in lithospheric mantle xenoliths from the VVP. Journal of Petrology 42, 173-187.

Beccaluva, L., Bianchini, G. et al., 2003. Tertiary nephelinite to tholeiite magma generation in the Veneto volcanic province, Southern Alps. FIST-Geoitalia 2003 (4° Earth Sciences forum), Abstract volume, 189.

Beccaluva, L., Bianchini, G., Bonadiman, C., Coltorti, M., Macciotta, G., Siena, F., Vaccaro, C., 2005. Within-plate Cenozoic volcanism and lithospheric mantle evolution in the western-central Mediterranean area. In Finetti I. (Eds.) Deep Seismic exploration of the Meditterrranean Region (CROP Project), Elsevier, Amsterdam, 641-664.

Beccaluva, L., Bianchini, G., Bonadiman, C., Coltorti, M., 2007. Intraplate lithospheric and sublithospheric components in the Adriatic domain: Nephelinite to tholeiite magma generation in the Paleogene Veneto Volcanic Province, Southern Alps. Geological Society of America 418, 131-152.

Begemann, F., Ludwig, K.R., Lugmair, G.W., Min, K., Nyquisit, L.E., Patchett, P.J., Renne, P.R., Shih, C.-Y., Villa, I.M., Walker R.J., 2001. Call for an improved set of

decay constants for geochronological use. Geochimica et Cosmochimica Acta 65, 111-121.

Bellieni, G., 1977. Caratteri geobarometrici delle intrusioni granitiche del plutone delle Vedrette di Ries (Rieserferner) (Alto Adige Orientale) alla luce dei sistemi sperimentali Q-Or-Ab-An-H_2O. Rendiconti della Società Italiana di Mineralogia e Petrologia 33, 631-645.

Bellieni, G., 1980. The Cima di Villa (Zinsnock) massif: geochemical features and comparisons with the Vedrette di Ries (Rieserferner) pluton (Eastern Alps, Italy). Neues Jahrbuch für Mineralogie – Abhandlungen 138, 244-258.

Bellieni, G., 1981. Classification and nomenclature of basalts. Subcommission on the Systematics of Igneous Rocks, 87.

Bellieni, G., Fioretti, A.M., Marzoli, A., Visonà, ,D., 2010. Permo-Paleogene magmatism in the eastern Alps. Rendiconti Fis. Accademia dei Lincei 21, S51-S71.

Bergomi, M.A., Zanchetta, S., Tunesi, A., 2015. The Tertiary dike magmaism in the Southern Alps: geochronological data and geodynamic significance. Internal Journal of Earth Sciences 104, 449-473.

Bonadiman, C., Coltorti, M., Milani, L., Salvini, L., Siena, F., Tassinari, R., 2001. Metasomatism in the lithospheric mantle and its reltionship to magmatism in the Veneto Volcanic Province, Italy. Periodico di Mineralogia 70, 333-357.

Borsi, S., et al., 1969. In Contributo alla conoscenza geologica della regione di Bolca (Monti Lessini), Barbieri, G., Medizza, F.

Borsi, S., Ferrara, G., Piccoli, G., 1969. Determinazioni col metodo K/Ar dell'età delle eruzioni euganee. Rendiconti della Società Italiana di Mineralogia e Petrologia 25, 27-34.

Brombin, V., Bonadiman, C., Coltorti, M., Fahnestock, M.F., Bryce, J.G., Marzoli, A., 2018. Refertilized mantle keel below the Southern Alps domain (North-East Italy): Evidence from Marosticano refractory mantle peridotites. Lithos 300-301, 72-85.

Conticelli, S., Guarnieri, L., Farinelli, A., Mattei, M., Avanzinelli, R., Bianchini, G., Boari, E., Tommasini S., Tiepolo M., Prelevic D., Venturelli G., 2009. Trace-elements and Sr–Nd–Pb isotopes of K-rich, shoshonitic, and calc-alkaline magmatism of the Western Mediterranean region: genesis of ultrapotassic to calcalkaline magmatic association in a post-collisional geodynamic setting. Lithos 107, 69-92.

Dal Piaz, G.V., Venturelli, G., 1983. Brevi riflessioni sul magmatismo post-ofiolitico nel quadro dell'evoluzione spazio-temporale delle Alpi. Memorie Società Geologica

Italiana 26, 5-19.

Dal Piaz, G.V., Bistacchi, A., Massironi, M., 2003. Geological outline of the Alps. Episodes 26 (3), 175-181.

De Vecchi, G., Sedea, R., 1995. The Paleogene basalts of the Veneto region (NE Italy). Memorie di Scienze Geologiche 47, 253-374.

Duretz, T., Gerya, T.V, May, D.A., 2011. Numerical modelling of spontaneous slab breakoff and subsequent topographic response. Tectonophysics 502, 244-256.

Faccenna, C., Molin, P., Orecchio, B., Olivetti, V., Bellier, O., Funiciello, F., Minelli, L., Piromallo,C., Billi, A., 2011. Topography of the Calabria subduction zone (southern Italy): clues for the orin of Mt. Etna. Tectonics 30, TC1003, doi:10.1029/2010TC002694.

Frascari Ritondale Spano, F., Bassani, P., 1973. Ricerche geologiche nei dintorni di Bassano del Grappa (Vicenza). Memorie Museo Trid. Scienze Naturali 19, 65-112.

Freeburn, R., Bouilhol, P., Maunder, B., Magni, V., van Hunen, J., 2017. Numerical models of the magmatic processes induced by slab breakoff. Earth and Planetary Science Letters 478, 203-213.

Funiciello, F., Moroni, M., Piromallo, C., Faccenna, C., Cenedese, C., Bui, H.A., 2006. Mapping mantle flow during retreating subduction: Laboratory models analyzed by feature tracking, Journal of Geophysical Research 111, B03402, doi:10.1029/2005JB003792.

Gasperini, D., Bosch, D., Braga, R., Bondi, M., Macera, P., Morten, L., 2006. Ultramafic xenoliths from the Veneto Volcanic Province (Italy): Petrological and geochemical evidence for multiple metasomatism of the SE Alps mantle lithospere. Geochemical Journal 40, 377-404.

Giacomuzzi, G., Chiarabbia, C., De Gori, P., 2011. Linking the Alps and Apennines subduction systems: New constraints revealed by high-resolution teleseismic tomography. Earth and Planetary Sciences 301, 531-543.

Giusberti, L., Del Favero, L., Roghi, G., 2014. The Purga di Bolca-Vegroni sites. In Papazzoni, C.A., Giusberti, L., Carnevale, G., Roghi, G., Bassi, D., Zorzin, R., (Eds.), The Bolca Fossil-Lagerstatten: a window into the Eocene world. Rendiconti della Società Paleontologica Italiana 4, 95-103.

Harangi, S., Downes, H., Seghedi, I., 2006. Tertiary–Quaternary subduction processes and related magmatism in the Alpine-Mediterranean region. Geological Society, London, Memoirs 32, 167-190.

Hua, Y., Zhao, D., Xu, Y., 2017. P wave anisotropic tomography of the Alps. Journal of Geophysical Research: Solid Earth 122, 4509-4528.

Ionov, D. A., O'Reilly, S. Y., Kopylova, M. G., Genshaft, Y. S., 1996. Carbonate-bearing mantle peridotite xenoliths from Spitsbergen: phase relationships, mineral compositions and trace element residence. Contributions to Mineralogy and Petrology 125, 375-392.

Jourdan, F., Féraud, G., Bertrand, H., Watkeys, M.K., 2007. From flood basalts to the onset of oceanization: Example from the $^{40}Ar/^{39}Ar$ high-resolution picture of the Karoo large igneous province. Geochemistry, Geophysics, Geosystems 8, Q02002.

Le Maitre, R.W., Streckeisen, A., Zanettin, B., Le Bas, M.J., Bonin, B., Bateman, P. Bellieni, G., Dudek, A., Efremova, S., Keller, J., Lamere, J., Sabine, P.A., Schmid, R., Sorensen, H., Woolley, A.R. (Eds.), 2002. Igneous Rocks: A Classification and Glossary of Terms, Recommendation s of the International Union of Geological Sciences Subcommission of the Systematics of Igneous Rocks. Cambridge University Press, UK.

Lee, J.-Y., Marti, K., Severinghaus, J.P., Kawamura, K., Yoo, H.-S., Lee, J.B., Kim, J.S., 2006. A redetermination of the isotopic abundance of atmospheric Ar. Geochimica et Cosmochimica Acta 70, 4507-4512.

Lippitsch, R., Kissling, E., Ansorge, J., 2003. Upper mantle structure beneath the Alpine orogen from high-resolution teleseismic tomography, Journal of Geophysical Research, 108(B8), 2376, doi:10.1029/2002JB002016.

Long, M.D., Silver, P.G. 2008. The subduction zone flow field from seismic anisotropy: A global view. Science 319, 315-318.

Lucente, F.P., Margheriti, L., Piromallo, C., Barruol, G., 2006. Seismic anisotropy reveals the long route of the slab through the western-central Mediterranean mantle. Earth and Planetary Science Letters, 241 (3–4), 517–529, doi:10.1016/j.epsl.2005.10.041

Luciani, V., 1989. Stratigrafia sequenziale del Terziario nella Catena del Monte Baldo (Provincie di Verona e Trento). Memorie di Scienze Geologiche 41, 263-351.

Macera, P., Gasperini, D., Piromallo, C., Blichert-Toft, J., Bosch, D., Del Moro, A., Martin, S., 2003. Geodynamic implications of deep mantle upwelling in the source of Tertiary volcanics from the Veneto region (Southern-Eastern Alps). Journal of Geodynamics, 36, 563-590.

Macera, P., Gasperini, D., Ranalli, G., Mahatsente, R., 2008. Slab detachment and mantle plume upwelling in subduction zones: an example from the Italian South-Eastern Alps. Journal of Geodynamics 45, 32-48.

McDonough, W.F., Sun, S.S, 1995. The composition of the Earth. Chemical Geology 120, 223-253.

Medizza, F., 1980. Il giacimento della Purga di Bolca (Verona). In I vertebrati fossili italiani. Catalogo della Mostra, Verona: 147-148.

Merle, R., Marzoli, A., Aka, F.T., Chiaradia, J.M., Reisberg, L., Castorina, F., Jourdan, F., Renne, P.R., N'ni, J., Nyobe, J.B., 2017. Mt. Bambouto Volcano, Cameroon Line: Mantle source and Differentiation of Within-plate Alkaline Rocks. Journal of Petrology 58, 933-962.

Milani, L., Beccaluva, L., Coltorti, M., 1999. Petrogenesis and evolution of the Euganean magmatic complex, north eastern Italy. European Journal of Mineralogy 11, 379-399.

Morten, L., Taylor, L.A., Durazzo, A., 1989. Spinel in harzburgite and lherzolite inclusions from the San Giovanni Ilarione Quarry, Lessini Mountains, Veneto Region, Italy. Mineralogy and Petrology 40, 73-89.

Oostingh, K.F., Jourdan, F., Matchan, E.L., Phillips, D., 2017. $^{40}Ar/^{39}Ar$ geochronology reveals rapid change from plume-assisted to stress-dependent volcanism in the Newer Volcanic Province, SE Australia. Geochemistry, Geophysics, Geosystems 18, doi:10.1002/2016GC006601.

Park, J., Levin, V., 2002. Seismic anisotropy: Tracing plate dynamics in the mantle. Science 296, 485-489.

Piccoli, G., Sedea, R., Bellati, R., Di Lallo, E., Medizza, F., Girardi, A., De Pieri, R., De Vecchi, Gp., Gregnanin, A., Piccirillo, E.M., Norinelli, A., Dal Prà, A., 1981. Note illustartive della carta geologica dei Colli Euganei alla scala 1: 25.000. Memorie di Scienze geologiche, Vol. XXXIV, 523-546.

Piromallo, C., Morelli, A., 2003. P wave tomography of the mantle under the Alpine-Mediterranean area. Journal of Geophysical Research 108 (B2), 2065.

Piromallo, C., Faccenna, C., 2004. How deep can we find the traces of Alpine subduction?, Geophysical Research Letters 31, L06605, doi:10.1029/2003GL019288.

Piromallo, C., Becker, T.W., Funiciello, F., Faccenna, C., 2006. Three-dimensional instantaneous mantle flow induced by subduction. Geophysical Research Letters 33, L08304, doi:10.1029/2005GL025390.

Price, G.P., 2010. Mineral Physics. Treatise on Geophysisc Vol.2

Robertson, A.H.F., Trivić, B., Đerić, N., Bucur, I.I., 2013. Tectonic development of the Vardar ocean and its margins: evidence from the Republic of Macedonia and Greek Macedonia. Tectonophysics 595-596, 25-54.

Rosenbaum, G., Lister, G.S., Duboz, C., 2002. Relative motions of Africa, Iberia and Europe during Alpine orogeny. Tectonophysics 359, 117-129.

Rosenberg, C.L., 2004. Shear zones and magma ascent: a model based on a review of the Tertiary magmatism in the Alps. Tectonics 23, TC3002. doi:10.1029/2003TC001526.

Savage, M.K., 1999. Seismic anisotropy and mantle deformation: What have we learned from shear wave splitting?, Rev. Geophys., 37(1), 65-106, doi:10.1029/98RG02075.

Savage, M.K., Sheehan, A.F., 2000. Seismic anisotropy and mantle flow from the Great Basin to the Great Plains, western United States. Journal of Geophysical Research, 105 (B6), 715-734.

Savage, M.K., Aoki, Y., Unglert, K., Ohkura, T., Umakoshi, K., Shimizu, H., Iguchi, M., Tameguri, T., Ohminato, T., Mori, J., 2016. Stress, strain rate and anisotropy in Kyushu, Japan, Earth and Planetary Science Letters, 439, 129-142.

Savelli C., Lipparini E. 1979. Età K/Ar di basalti del vicentino e la scala dei tempi del Paleogene. Bollettino della Società Geologica Italiana 98, 375-385.

Schaltegger, U., Brack, P., Ovtcharova, M., Peytcheva, I., Schoene, B., Stracke, A., Marocchi M., Bargossi G.M., 2009. Zircon and titanite recording 1.5 million years of magma accretion, crystallization and initial cooling in a composite pluton (southern Adamello batholith, northern Italy). Earth and Planetary Science Letters 286, 208-218.

Schlunegger, F., Kissling, E., 2015. Slab rollback orogeny in the Alps and evolution of the Swiss Molasse basin. Nature Communications 6, doi:10.1038/ncomms9605

Schmitz, M.D., Bowring, S.A., Ludwig, K.R., Renne, P.R., 2003. Comment on "Precise K-Ar, $^{40}Ar/^{39}Ar$, Rb-Sr and U/Pb mineral ages from the 27.5 Ma Fish Canyon Tuff reference standard by M.A. Lanphere and H.Baadsgaard. Chemical Geology 199, 277-280.

Schoene, B., Schaltegger, U., Brack, P., Latkoczy, C., Stracke, A., Günther, D., 2012. Rates of magma differentiation and emplacement in a ballooning pluton recorded by U–Pb TIMS-TEA, Adamello batholith, Italy. Earth and Planetary Science Letters 355, 162-173.

Siena, F., Coltorti, M., 1989. Lithospheric mantle evolution: evidences from ultramafic xenoliths in the Lessinean volcanics (Northern Itlay). Chemical Geology 77, 347-364.

Siena, F., Coltorti, M., 1993. Thermobarometric evolution and metasomatic processes of upper mantle in different tectonic settings: evidence from spinel peridotite xenoliths. European Journal of Mineralogy 5, 1073-1090.

Singer, J., Diehl, T., Hunsen, S., Kissiling, E., Duretz, T., 2014. Alpine lithophere slab

rollback causing lower crustal seismicity in northern foreland. Earth and Planetary Science Letters 397, 42-56.

Stampfli, G.M., Mosar, J., Favre, P., Pillevuit, A., Vannay, J.C., 2001. Permo-Mesozoic evolution of the western Tethyan realm: the Neotethys/East- Mediterranean connection. In: Ziegler P.A., Cavazza W., Robertson A.H.F. (Eds.). PeriTethys memoir 6: Peritethyan rift/wrench basins and passive margins, vol. 186, Crasquin-Soleau, S., IGCP 369, pp. 51-108, M´em. Museum of Natural History Nat.

Sun, S.S., McDonough, W.F., 1989. Chemical and isotopic systematics of oceanic basalts: implications for mantle composition and processes. In: Saunders, A.D, Norry, M.J. (Eds). Magmatism in the Oceanic Basins. Geological Society London, Special Publications 42, 313-346.

Verati, C., Jourdan, F., 2013. Modelling effect of sericitization of plagioclase on the ^{40}K/40Ar and ^{40}K/^{39}Ar chronometers: Implication for dating basaltic rocks and mineral deposits, in Jourdan, F., et. al., (Eds.), Advances in ^{40}Ar/^{39}Ar dating: from archaeology to planetary sciences. Geological Society of London Special Publication 378, 155-174.

Visonà, D., Caironi, V., Carraro, A., Dallai, L., Fioretti, A.M., Fanning, M., 2007. Zircon megacrysts from basalts of the Venetian Volcani Province (NE Italy): U-Pb, oxygen isotopes and REE data. Lithos, 94, 168-180.

van Hunen, J., Allen, M.B., 2011. Continental collision and slab break-off: a comparison of 3-D numerical models with observations. Earth and Planetary Science Letters 302, 27-37.

von Blanckenburg, F., Davies, J.H., 1995. Slab breakoff: a model for syncollisional magmatism and tectonics in the Alps. Tectonics 14, 120-131.

Yaxley, G. M., Crawford, A. J., Green, D. H., 1991. Evidence for carbonatite metasomatism in spinel peridotite xenoliths from western Victoria, Australia. Earth and Planetary Science Letters 107, 305-317.

Zampieri, D., 1995, Tertiary extension in the southern Trento Platform, southern Alps, Italy: Tectonics 14, 645-657.

Zantendeschi, C., 1994. New Rb-Sr radiometric data from Colli Euganei (North Eastern Italy). Memorie degli Istituti di Geologia e Mineralogia dell'Università di Padova 46, 17-22.

Zhao, L., Paul, A., Malusà, M.G., Xiaobing, X., Zheng, T., Solarino, S., Guillot, S., Schwartz, S., Dumont, T., Salimbeni, S., Aubert, A., Pondrelli, S., Wang, Q., Zhu, R.,

2016. Continuity of the Alpine slab unraveled by high-resolution P wave tomography. Journal of Geophysical Research: Solid Earth 121, 8720-8737.

APPENDIX A3

Table A3.1. Summary table indicating location, lithology, and $^{40}Ar/^{39}Ar$ results for Val d'Adige, Lessini Mts., Marosticano, and Euganean Hills samples analyzed at Western Australian Argon Isotope Facility (WAAIF).

General characteristics						**Isochron characteristics**					**Plateau characteristics**			
Sample	**District**	**Coordinates**	**Lithology**	**Instrument**	**Separate**	**Inverse isochron age (Ma, ±2σ)**	**n**	**$^{40}Ar/^{36}Ar$ intercept (±2σ)**	**MSWD**	**P (%)**	**Plateau age (Ma, ±2σ)**	**Total ^{39}Ar released (%)**	**MSWD**	**P (%)**
BAL1	Val d'Adige	45°47'02.12"N 10°54'18.26"E	Basalt	ARGUS VI	Groudmass	**41.70 ± 0.82**	16	266 ± 23	0.78	69	**41.69 ± 0.37**	75	0.39	98
BAL7	Val d'Adige	45°44'37.00"N 10°53'04.00"E	Basanite	ARGUS VI	Groudmass	*41.95 ± 0.46*	15	264 ± 15	0.82	64	*41.98 ± 0.20*	60	0.25	100
TER1	Lessini Mts.	45°35'34.05"N 11°12'58.89"E	Basalt	ARGUS VI	Groudmass	*45.21 ± 0.15*	12	253 ± 25	1.00	44	*45.21 ± 0.11*	57	0.83	61
BOL1	Lessini Mts.	45°35'51.84"N 11°12'31.34"E	Basanite	ARGUS VI	Groudmass	*40.60 ± 1.76*	17	278 ± 19	0.75	74	*38.73 ± 0.44*	62	0.99	46
LB1	Marosticano	45°76'72.83"N 11°67'78.97"E	Basanite	ARGUS VI	Groudmass	No isochron age					No plateau age			
EU4	Euganean Hills	45°22'37.30"N 11°42'17.30"E	Trachyte	MAP 215-50	Biotite	**31.83 ± 0.50**	14	328 ± 43	0.88	57	**32.09 ± 0.29**	100	0.97	48
EU5B	Euganean Hills	45°19'16.00"N 11°45'24.00"E	Rhyolite	MAP 215-50	Sanidine	**31.87 ± 0.79**	15	343 ± 58	0.86	59	**32.30 ± 0.52**	100	1.00	45
EU8B	Euganean Hills	45°19'07.80"N 11°46'31.40"E	Basaltic trachyandesite	MAP 215-50	Feldspar	**32.11 ± 0.98**	15	305 ± 99	0.85	61	**32.17 ± 0.32**	100	0.79	68
EU9	Euganean Hills	45°45'01.37"N 11°44'39.85"E	Rhyolite	MAP 215-50	Sanidine	**32.02 ± 0.67**	14	315 ± 68	0.51	91	**32.17 ± 0.27**	100	0.48	94
EU13A	Euganean Hills	45°15'07.02"N 11°41'27.00"E	Trachyandesite	MAP 215-50	Feldspar	**31.96 ± 1.13**	14	349 ± 136	0.52	91	**32.34 ± 0.51**	88	0.53	91
EU52	Euganean Hills	45°32'87.88N 11°68'48.75"E	Basaltic trachyandesite	ARGUS VI	Amphibole	*32.37 ± 0.12*	10	295 ± 14	0.52	85	*32.35 ± 0.09*	67	0.48	89
					Plagioclase	**32.16 ± 0.08**	21	397 ± 19	0.65	87	**32.16 ± 0.06**	100	0.58	93

Data in italics are derived from mini-plateaus (50-70% ^{39}Ar released) and are considered minimum ages only, bold font represents statistically significant plateau ages. Mean square weighted deviation (MSWD) for isochron, plateau, and mini-plateau, number of analyses included in the isochron, $^{40}Ar/^{36}Ar$ intercept, percentage of ^{39}Ar degassed used in the plateau calculation, probability (P) for plateau and mini-plateau, are indicate. Analytical uncertainties on the ages and $^{40}Ar/^{36}Ar$ intercept are quoted at 2 sigma (2σ) confidence levels.

Table A3.2. Summary table indicating location, lithology, and $^{40}Ar/^{39}Ar$ results for Val d'Adige, and Marosticano samples analyzed at the Noble Gas Geochronology Laboratory of the University of Vermont with Nu Instruments Noblesse magnetic sector noble gas mass spectrometer.

General characteristics					**Isochron characteristics**				**Plateau characteristics**			
Sample	**District**	**Coordinates**	**Lithology**	**Separate**	**Inverse isochron age (Ma, ±2σ)**	**n**	**$^{40}Ar/^{36}Ar$ intercept (±2σ)**	**MSWD**	**Plateau age (Ma, ±2σ)**	**Total ^{39}Ar released (%)**	**MSWD**	**P (%)**
BI14	Val d'Adige	45°47'02.12"N 10°54'18.26"E	Basanite	Groudmass	*42.2 ± 8.2*	7	207 ± 138	11.3	*40.73 ± 0.48*	57	0.8	45
25B	Marosticano	45°76'72.83"N 11°67'78.97"E	Basanite	Groudmass	No isochron age				No plateau age			

Data in italics are derived from mini-plateaus (50-70% ^{39}Ar released) and are considered minimum ages only. Mean square weighted deviation (MSWD) for isochron, plateau, and mini-plateau, number of analyses included in the isochron, $^{40}Ar/^{36}Ar$ intercept, percentage of ^{39}Ar degassed used in the plateau calculation, probability (P) for plateau and mini-plateau, are indicate. Analytical uncertainties on the ages and $^{40}Ar/^{36}Ar$ intercept are quoted at 2 sigma (2σ) confidence levels.

Table A3.3. Whole-rock major (wt.%), composition of magmatic products from Val d'Adige, Lessini Mts., Marosticano, and Euganean Hills.

Sample	**BAL1**	**BAL7**	**BI14**	**TER1**	**BOL1**	**LB1**	**25B**	**EU1AB**	**EU4**	**EU5B**	**EU8B**	**EU9**	**EU13A**	**EU52**	**EU53**
Rock	Basalt	Basanite	Basanite	Basalt	Basanite	Basanite	Basanite	Basalt	Trachyte	Rhyolite	Basaltic trachy-andesite	Rhyolite	Trachy-andesite	Basaltic trachy-andesite	Basaltic andesite
District	Val d'Adige	Val d'Adige	Val d'Adige	Lessini Mts.	Lessini Mts.	Marosticano	Marosticano	Euganean Hills	Euganean Hills	Euganean Hills	Euganean Hills	Euganean Hills	Euganean Hills	Euganean Hills	Euganean Hills
SiO_2	45.42	42.62	42.51	47.11	43.00	43.22	44.02	51.82	65.52	69.86	55.63	72.00	56.90	51.80	53.22
TiO_2	2.67	3.71	3.26	2.71	3.44	3.47	3.12	2.44	0.69	0.39	2.01	0.32	2.00	2.76	2.37
Al_2O_3	14.15	13.04	14.82	13.08	13.21	11.52	12.80	14.80	16.51	15.41	15.53	14.81	15.68	16.32	14.83
Fe_2O_3	14.17	14.56	12.10	10.64	14.35	13.12	10.95	11.09	3.71	2.05	8.82	1.26	7.27	10.45	11.24
MnO	0.19	0.19	0.17	0.35	0.19	0.19	0.16	0.12	0.06	0.09	0.13	0.03	0.09	0.12	0.12
MgO	6.73	8.96	8.37	10.41	9.55	11.29	12.26	6.23	0.72	0.17	3.41	0.14	3.14	3.86	6.22
CaO	10.08	11.03	10.46	9.60	10.23	11.85	10.89	9.47	1.59	0.65	6.47	0.49	5.68	6.13	8.66
Na_2O	2.17	3.09	5.04	1.05	3.06	3.06	3.22	3.09	5.23	4.80	4.23	4.63	4.11	4.36	3.24
K_2O	0.73	1.37	1.44	1.13	1.45	1.36	1.53	0.59	5.11	5.77	2.68	5.56	3.59	3.24	0.43
P_2O_5	0.68	1.53	1.83	0.62	0.97	0.97	1.06	0.35	0.30	0.07	0.59	0.03	0.57	0.97	0.26
Tot	96.99	100.10	100.00	96.70	99.45	100.05	100.00	100.00	99.44	99.26	99.50	99.27	99.03	100.00	100.59
mg#	45.85	52.31	55.22	63.56	54.26	60.53	66.62	50.03	25.70	12.88	40.80	16.53	43.50	39.70	49.66

mg#= 100 x $Mg/(Mg+Fe^{2+})_{mol}$

Table A3.4. Trace element (ppm) composition of magmatic products from Val d'Adige, Lessini Mts., Marosticano, and Euganean Hills.

Sample	**BAL7**	**TER1**	**BOL1**	**LB1**	**EU1AB**	**EU4**	**EU8B**	**EU9**	**EU13A**	**EU52**	**EU53**
Rock	Basanite	Basalt	Basanite	Basanite	Basalt	Trachyte	Basaltic trachy-andesite	Rhyolite	Trachy-andesite	Basaltic trachy-andesite	Basaltic andesite
District	Val d'Adige	Lessini Mts.	Lessini Mts.	Marosticano	Euganean Hills	Euganean Hills	Euganean Hills	Euganean Hills	Euganean Hills	Euganean Hills	Euganean Hills
Rb	29.58	27.78	37.44	46.63	17.00	134.82	79.76	161.33	89.50	71.03	15.00
Ba	860	664	553	777	348	586	643	130	768	777	264
Th	6.80	5.87	5.99	6.85	2.95	19.32	10.91	24.70	10.14	10.08	2.85
U	1.77	1.34	1.42	2.00	0.83	3.53	3.37	5.79	3.06	2.56	0.82
Nb	123.86	74.31	91.44	118.61	28.00	125.52	71.32	136.56	79.96	96.63	21.00
Ta	4.47	2.52	3.74	4.67	1.38	6.28	3.17	7.76	4.19	4.64	1.43
La	66.79	38.99	47.02	57.51	18.42	77.29	49.87	113.83	66.28	72.35	13.74
Ce	130.97	75.82	96.05	108.88	38.48	124.90	92.56	205.60	121.68	127.46	28.45
Pr	15.46	8.37	11.51	12.08	4.68	12.64	9.75	18.25	14.74	14.37	3.71
Sr	1744.33	736.83	1060.08	1071.06	473.00	372.22	695.46	68.55	714.44	929.12	349.00
Nd	67.44	35.63	52.01	53.26	20.37	45.83	37.53	60.25	52.39	55.93	16.88
Zr	413.96	235.59	354.19	381.54	175.00	110.57	348.89	163.95	386.70	456.25	168.00
Hf	8.29	5.01	7.58	7.91	3.93	2.99	7.30	5.28	8.23	9.11	4.03
Sm	12.61	6.73	10.14	9.68	5.36	7.91	7.68	9.51	10.43	10.85	4.85
Eu	3.86	2.16	3.13	2.91	1.83	2.22	2.43	1.83	3.00	3.25	1.75
Gd	11.70	6.66	9.32	8.92	5.55	5.73	6.57	6.66	8.67	8.82	5.47
Tb	1.64	0.99	1.38	1.27	0.83	0.80	0.91	0.98	1.24	1.19	0.85
Dy	7.20	4.63	6.23	5.61	4.48	4.34	4.89	5.54	6.58	6.15	4.77
Y	40.75	28.66	35.40	31.46	24.10	20.32	24.32	29.33	38.84	34.64	23.96
Ho	1.28	0.88	1.10	1.00	0.83	0.73	0.86	0.98	1.20	1.10	0.88
Er	3.05	2.22	2.62	2.42	1.97	1.74	2.18	2.69	3.04	2.64	2.20
Yb	2.21	1.84	1.93	1.78	1.56	1.34	1.72	2.41	2.49	2.03	1.70
Lu	0.31	0.27	0.27	0.25	0.21	0.18	0.23	0.34	0.34	0.27	0.23

Chapter 4.

The VVP mantle xenoliths

Enclosed:

Brombin, V., Bonadiman, C., Coltorti, M., Fahnestock, M.F., Bryce, J.G., Marzoli, A., 2018. Refertilized mantle keel below the Southern Alps domain (North-East Italy): Evidence from Marosticano refractory mantle peridotites. Lithos 300-301, 72-85.

4. The VVP mantle xenoliths

4.1. Introduction

The stability of continents is intimately linked to the underlying sub-continental lithospheric mantle (SCLM). Peridotite xenoliths hosted in intraplate basaltic rocks provide a useful way to evaluate the petrological features and evolution of the SCLM in terms of mineral compositions, modal abundance and fluid modification (Liu et al., 2015).

The mantle xenoliths occurring in Veneto Volcanic Province (VVP; SE Alps, NE Italy, Fig. 11) afford a means to understand further the "big" picture of the SCLM beneath the Adria plate, the African promontory of the central-western Mediterranean area. In the Cretaceous, the VVP region was involved in convergence between Africa and Eurasia plates, inducing subduction processes of the latter southeastward (Schmid et al., 1997; von Blanckenburg and Davies, 1995). In spite of the immense quantity of seismic, structural, petrologic, and geochemical data compiled over at least five decades, the Adria plate (Fig. 11) remains an enigmatic aspect of the geodynamic evolution of the Africa-Eurasia collision system (Carminati and Doglioni, 2012; Lustrino, et al., 2011). It has been considered either to be in crustal continuity with the African mainland or separated from the latter by an oceanic plate (Catalano et al., 2000; Lustrino et al., 2011; Muttoni et al., 2001; Schmid et al., 2008). Mantle xenoliths from a few VVP localities previously investigated (Lessini Mts. and Val d'Adige localities; Fig. 11) reveal variably depleted mantle domains, which were subsequently enriched by one or more episodes of metasomatism as recorded by widespread interstitial recrystallized glassy patches (Beccaluva et al., 2001; Gasperini et al., 2006; Morten et al., 1989; Siena and Coltorti, 1989).

In this paper, we describe results from a petrological and geochemical study of a newly discovered occurrence of mantle xenoliths from the Marostica Hills (Fig. 11), in the Marosticano district of the VVP. We then interpret our findings to constrain the mantle domain underlying the northern (continental) sector of the Adria plate, with the ultimate goal of gaining insight into dynamic processes at work during plate boundary interactions.

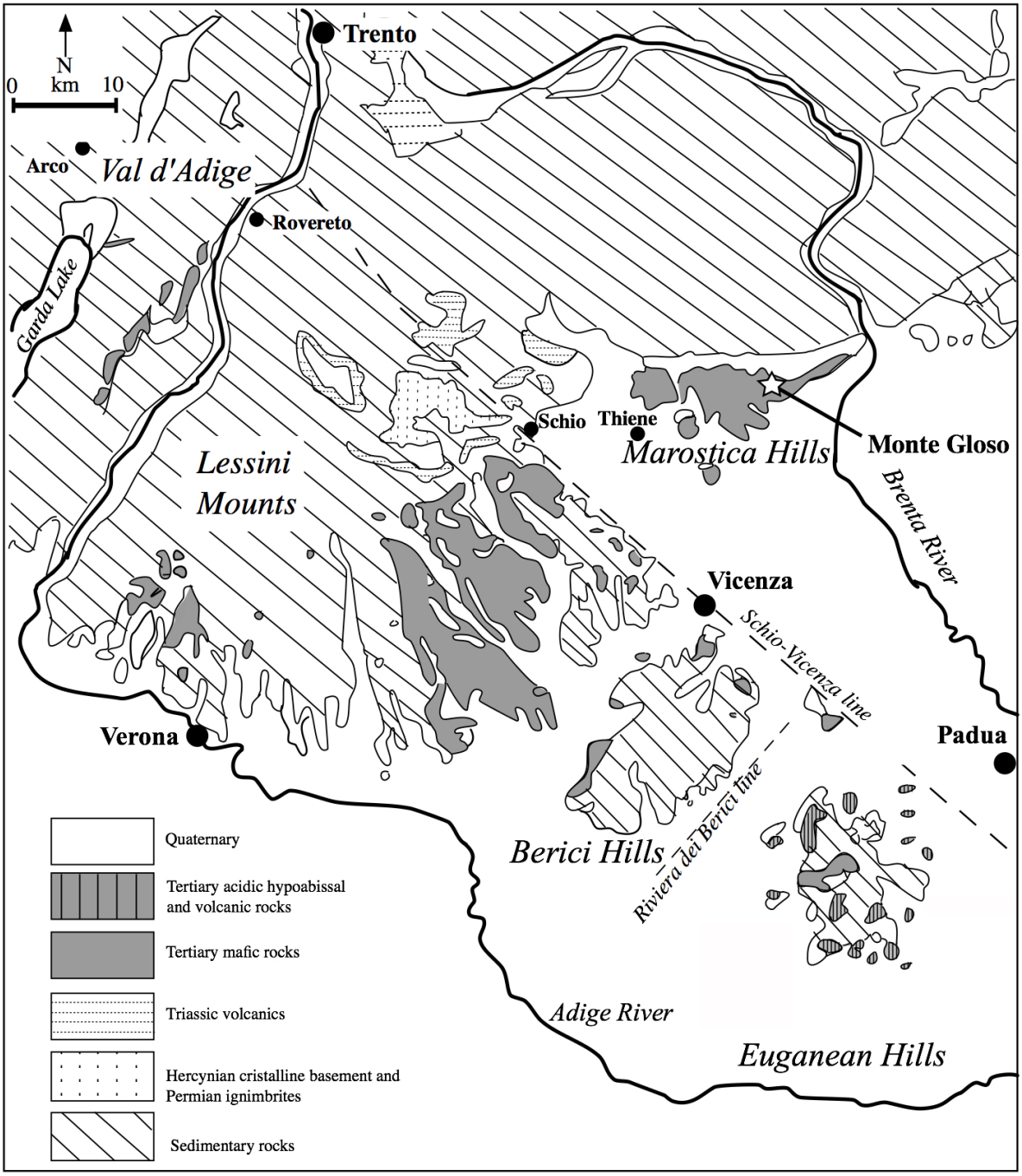

Fig. 11. Geological map of the Veneto Volcanic Province (VVP; De Vecchi and Sedea, 1995), showing the location of Monte Gloso (MG), xenolith site in Marosticano magmatic district. Inset a) Location of VVP in the Italian peninsula, in relation to European, African, and Adria plates. The white arrows show the subduction directions (modified from Carminati and Doglioni, 2012).

4.2 Petrography

The Marosticano xenoliths were sampled in the quarry of Monte Gloso (MG), a few kilometers east of Marostica (Fig. 11). The basanitic host lavas show a porphyritic texture with phenocrysts of olivine, clinopyroxene, and magnetite set in a fine-grained groundmass composed of clinopyroxene, plagioclase, and oxides. The xenoliths are generally subrounded or (more rarely) angular, ranging in size from a few up to 10 cm. Heavy fracturing and alteration are present throughout of the suite. Only five samples were sufficiently fresh to permit a complete petrological characterization. These samples also showed no evidence of host magma infiltration.

The Marosticano xenoliths are peridotites with complete spinel facies equilibration. They display a coarse-grained protogranular texture following the nomenclature of Mercier and Nicolas (1975). Two of the five investigated xenoliths are harzburgites with 4% clinopyroxene, one is low-clinopyroxene (6%) lherzolite and two are lherzolites with 9-13% clinopyroxene (Table 1). In two out of three lherzolites, orthopyroxene is modally scarce (12-14%) as compared to typical peridotites (e.g., Streckeisen, 1974). All Marosticano peridotites are characterized by large crystals of olivine and orthopyroxene (up to 2 mm across; Fig. 12a) with smaller grains of clinopyroxene (0.5-1 mm in size) and spinel (up to 1 mm across). Spinel are typically present in holly-leaf or lobate forms, while olivine and pyroxene crystals display curvilinear grain boundaries. Kinking is common in olivine, while orthopyroxene contain exsolution lamellae and, rarely, exhibit sieved rims. Clinopyroxene are always smaller in size with respect to orthopyroxene and show large cloudy portions.

Several types of pyrometamorphic textures are superimposed on these features. They consist of (1) cloudy, spongy clinopyroxene crystals: the recrystallized portion generally replaces the whole crystal, in rare cases it covers only the rim zones (Fig. 12b); (2) reaction areas made up of small crystals of olivine, clinopyroxene, vermicular spinel, and rare glass (Fig. 12c, d); (3) brown to pale yellow glassy patches containing secondary crystals of olivine, clinopyroxene, and spinel. The secondary paragenesis is generally too small to be analyzed by Electron MicroProbe (EMP) and therefore was not considered for *in-situ* analysis.

Table 1: Modal (%) compositions of Marosticano (MG) spinel peridotite xenoliths.

	Lherzolites			Harzburgites	
Samples	MG1	MG6	MG16	MG13	MG14
Ol	73	74	70	63	73
Opx	12	14	20	31	19
Cpx	13	9	6	4	4
Sp	2	3	4	2	4
Gl	trace	trace		trace	trace
Alteration	trace	trace	trace	trace	trace

Ol= olivine; Opx= orthopyroxene; Cpx= clinopyroxene; Sp= spinel; Gl= glass.

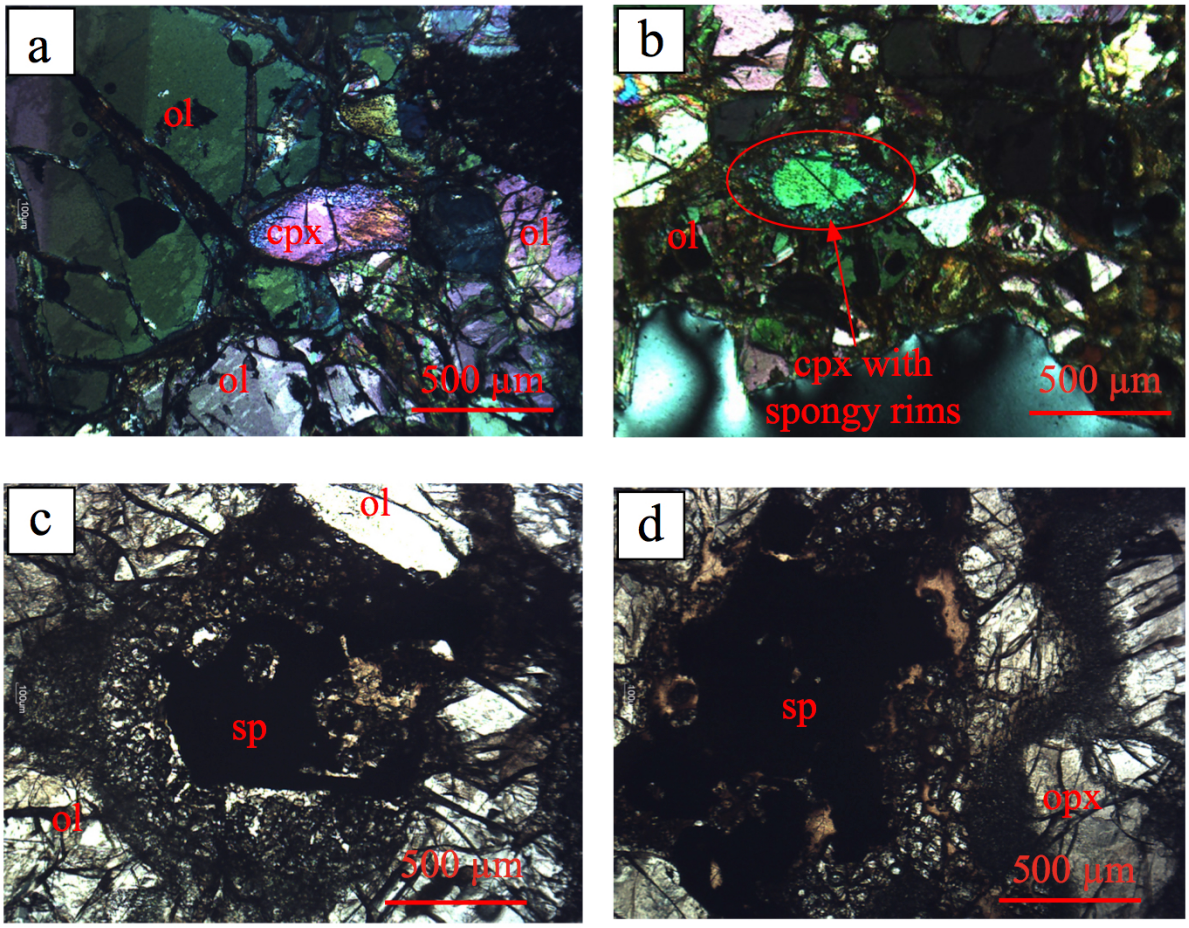

Fig. 12. Photomicrographs of representative microtextures of MG xenoliths. (a) large kinked olivine near clear clinopyroxene; (b) clinopyroxene with cloudy, spongy rims; (c) reaction areas surrounding spinel, constituted by small crystals of olivine, clinopyroxene, spinel, and rare glass; (d) orthopyroxene and spinel shearing reaction rims composed of secondary clinopyroxene and olivine.

4.3 Mineral Chemistry

Within each xenolith, minerals are generally homogeneous in composition with no significant chemical variation between core and rims of the same crystal. The latter is observed only for spongy crystals and grains close to reaction areas (Fig. 12). When these areas are near the contact with host basanites, olivine and clinopyroxene core and rim analyses were performed and compared with olivine and clinopyroxene phenocrysts in order to ensure they are not the result of host magma infiltration. Representative analyses of phases are reported in Tables A4.1-A4.6.

4.3.1 *Major element composition*

Olivine is chemically unzoned in Monte Gloso (MG) lherzolites and harzburgites. It shows a narrow compositional range with Fo contents [=100 x $Mg/(Mg+Fe)_{mol}$] varying from 91.3 to 92.2 for lherzolites and from 90.5 to 92.5 for harzburgites (Fig. 13a), with high Ni contents (2600-3620 ppm and 2670-3540 ppm in lherzolites and harzburgites, respectively). Though conspicuous variability of Ni in olivine within individual samples may suggest potential interaction between MG xenoliths and the host magma, the invariant Fo contents for each sample are inconsistent with melt-xenolith reaction. Specifically, it is noteworthy, that olivine phenocrysts from the host lavas have Fo values ranging from 86.1 to 87.2 and Ni contents from 2240 to 2251 ppm, suggesting that melt-xenolith reaction may explain only a small proportion of the variable Ni contents found in the MG xenolith suite (Fig. 13b).

Orthopyroxene from unreacted core to reacted rims is chemically unzoned and frequently contains elongate oriented rods of exsolved clinopyroxene. Orthopyroxene mg# [=100 x $Mg/(Mg+Fe)_{mol}$] values vary from 91.2 to 92.8 for both lherzolites and harzburgites, like the coexisting olivine grains. Contents of Al_2O_3 are highly variable in lherzolites (1.68-4.18 wt.%) whereas a more restricted range is shown by harzburgites (1.78-2.60 wt.%), reflecting a common "harzburgitic" melting degree, or limited temperature-dependent subsolidus exchange with spinel (Brey et al., 1999) (Fig. 13c). Lherzolite TiO_2 contents are more variable (<0.07 wt.%) than those in harzburgites (<0.03 wt.%).

By texture the most reactive phase, clinopyroxene bears evident compositional heterogeneity within each individual sample for most compositional features except mg#. Along with the coexisting olivine and orthopyroxene, mg# of clinopyroxene ranges from

91.0 to 93.3 across all lithologies. By contrast, Al_2O_3, Cr_2O_3, and to lesser extent Na_2O, are highly variable in both lherzolite and harzburgite clinopyroxene (Fig. 13d, e). Lherzolites generally show a larger range in Al_2O_3 (1.73-4.53 wt.%), Cr_2O_3 (0.72-1.64 wt.%), and Na_2O (0.49-1.89 wt.%) compared to harzburgites (Al_2O_3= 0.63 to 3.79 wt.%; Cr_2O_3= 0.89-1.52 wt.%; Na_2O= 0.35-1.18 wt.%; Fig. 13). The high chromium contents classify these crystals as chromiferous clinopyroxene (Morimoto, 1988) with TiO_2 always less than 0.60 wt.% (Fig. 13f). Clinopyroxene mg# values in both lherzolite and harzburgite are not correlated with Al_2O_3, Na_2O, and TiO_2 distribution as would be expected for a mantle residual trend or, in turn, for alkaline basic-ultrabasic magma fractionation lines (Fig. 13d-f). Accordingly, we interpret negligible, if any, interactions between peridotites and basanitic host lavas.

Large compositional variations are exhibited in spinel, with overlapping values cr# [=100 x Cr /$(Cr+Al)_{mol}$] and mg# for both lherzolite and harzburgite. However, cr# and mg# are homogenous within each individual sample with the exception of harzburgite MG13 (Fig. 13g). Across the samples, cr# and mg# vary from Cr-rich in harzburgite (cr#= 38.3-67.2; mg#= 56.2-69.6) to Al-rich types in lherzolite (cr#= 30.4-52.7; mg#= 62.2-75.9).

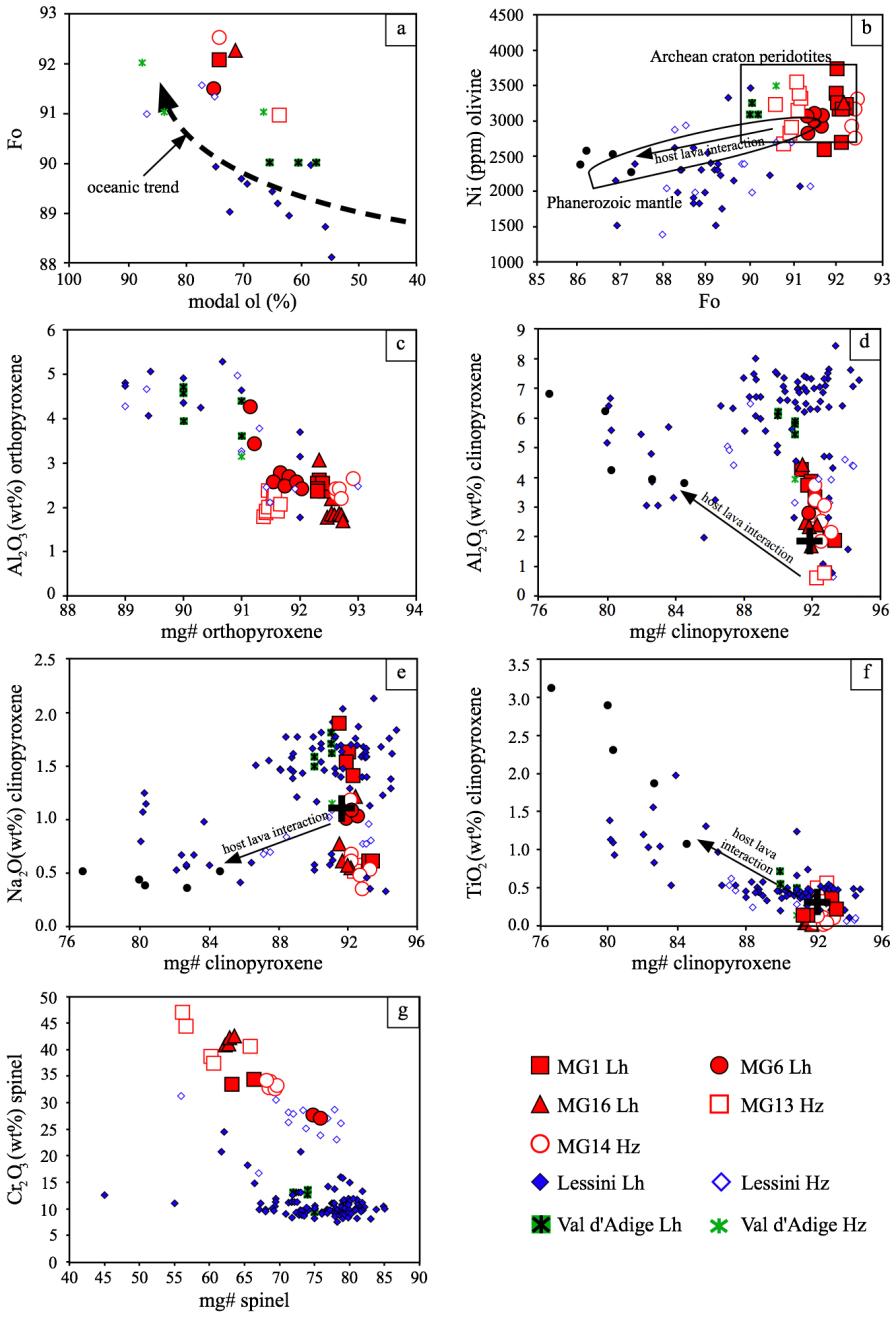

Fig. 13. (a) Forsterite [Fo= 100 x Mg/(Mg+Fe)$_{mol}$] compositions versus modal olivine for VVP mantle peridotites; the "oceanic trend" is from Boyd (1989). (b) Ni (ppm) versus Fo of olivines; fields from Archean craton both garnet and spinel peridotites (Kelemen et al., 1998), and Phanerozoic mantle array (Takahashi, 1987) are also plotted; (c-f) mineral major element oxides versus mg# [= 100 x Mg/(Mg+Fe)$_{mol}$]. In b, d, e, f hypothetical trends of mineral-host lava interations are also shown. Filled and open symbols are for Marosticano lherzolite (Lh) and harzburgite (Hz), respectively. For comparison Lessini Mts. (Beccaluva et al., 2001; Gasperini et al., 2006; Morten et al., 1989; Siena and Coltorti, 1989) and Val d'Adige (Gasperini et al., 2006) xenoliths, and host lava phenocrysts (black dots; this study) and crystallized clinopyroxene from silica-bearing carbonatite melts (black crosses; Dasgupta et al., 2009) are also reported.

4.3.2 *Pyroxene trace element contents*

Representative *in-situ* (LA-ICP-MS) trace element analyses of both pyroxenes are reported in Tables A4.5-A4.6. The values are shown in chondrite-normalized incompatible trace elements (Fig. 14a, b; 15a, b) and rare earth element (REE) diagrams (Fig. 15c, d). In order to characterize the "original" features of the MG lithospheric domain prior to the metasomatic event, trace element contents of both orthopyroxene and unreacted clinopyroxene cores were considered. One sample (MG13 harzburgite) has only orthopyroxene with rare clinopyroxene crystals occurring in reaction areas, where their small size (<30 μm) prevent high resolved quantitative analysis.

Both lherzolites and harzburgites bear orthopyroxene with heavy (H) REE contents in a narrow range [$(Tb/Lu)_N$ in lherzolites= 0.05-0.44; in harzburgites= 0.13-0.47] but large light (L) - middle (M) REE variability between grain to grain and sample to sample (e.g., Eu_N). MG16 lherzolite shows distinctive orthopyroxene REE contents with nearly flat M-HREE [$(Dy/Lu)_N$= 0.39-0.49] and LREE downward convex enrichments [$(La/Nd)_N$= 0.27-0.79; Fig. 14a]. MG1, MG6 lherzolites and MG14 harzburgite preserve residual M-HREE signatures [$(Dy/Lu)_N$= 0.18-0.37; Fig. 14a, b] typical of the spinel stability field after melt extraction co-existing with an apparent LREE enrichment [$(La/Nd)_N$= 1.05-13.1]. In turn, orthopyroxene of MG13 harzburgite show an overall M-HREE enrichment [$(Dy/Lu)_N$= 0.41-0.42; Fig. 14b]. Finally, Ti shows both positive and negative anomalies in both xenolith rock types.

Across all lithologies MG clinopyroxene have an overall high REE content (ΣREE=185-621 ppm) and distinctive LREE enrichment relative to HREE [La up to 100 times chondritic; $(La/Yb)_N$ in lherzolites = 9.58-26.68; $(La/Yb)_N$ in harzburgites = 13.88-19.24].

The geochemical data, taken together, allow for two groups of clinopyroxene compositions to be defined. Group-1 includes clinopyroxene of MG1, MG6 lherzolites, and MG13, MG14 harzburgites, which show almost flat M-HREE patterns [$(Sm/Lu)_N$= 1.31-4.76] with abrupt (more than one order of magnitude) LREE-enrichments [$(La/Nd)_N$= 1.53-6.18]. Almost all these clinopyroxene display a positive Eu anomaly ($\{Eu_N/[(Sm+Gd)_N/2]\}$= 1.07-1.68) (Fig. 15c). In turn, group-2 is defined by clinopyroxene of MG16 lherzolite only, which show distinctive convex upward REE patterns with a steep negative slope from Nd to Lu ($(Nd/Lu)_N$= 14.0-18.0) and a maximum at Pr_N (114-143; Fig. 15d).

The entire MG clinopyroxene population has variable high Th and U contents (Th and U up to 3.03 and 0.63 ppm, respectively) with negative Ti and high field strength elements

(HFSE; e.g., Nb, Ta, Zr, and Hf) anomalies, the most evident being the Zr anomaly in harzburgites with Zr* $\{Zr_N/[(Nd+Hf)_N/2]\}$= 0.09-0.24 (Fig. 15a, b). It should be noted that MG unreacted clinopyroxene have trace elements contents similar or even higher than those of primary and secondary clinopyroxene from mantle xenoliths of the Lessini Mts. (Beccaluva et al., 2001; Fig. 16).

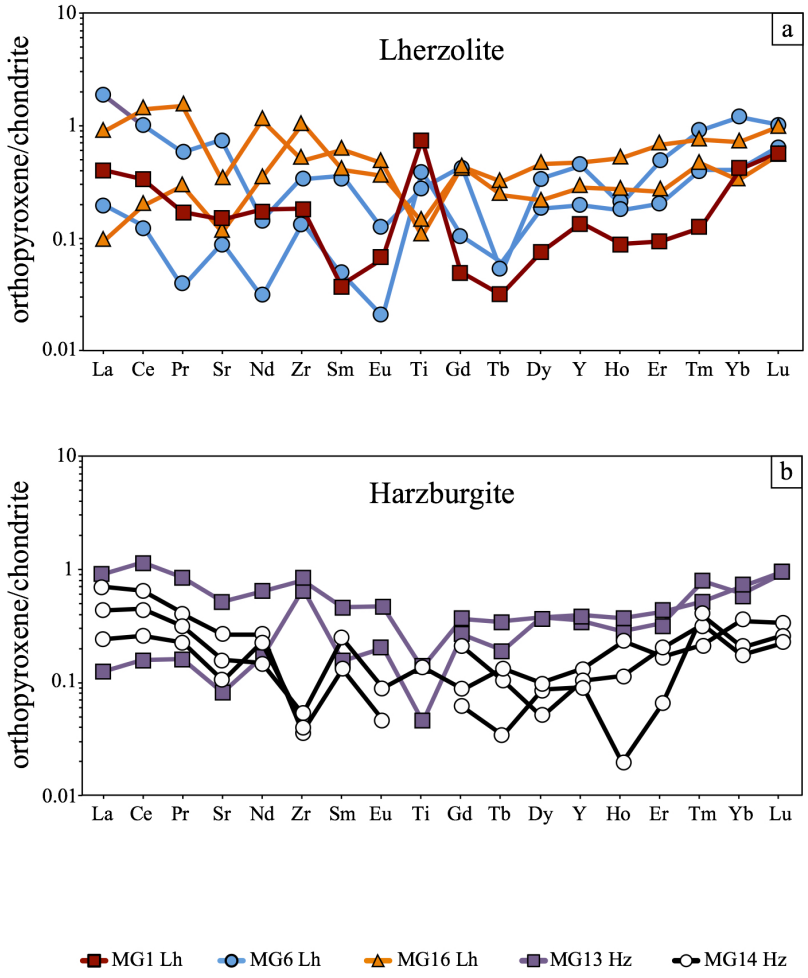

Fig. 14. Chondrite-normalized (Sun and McDonough, 1989) incompatible trace elements distribution of orthopyroxene from MG lherzolites (a) and harzburgites (b). Abbreviations and symbols as in Fig. 13.

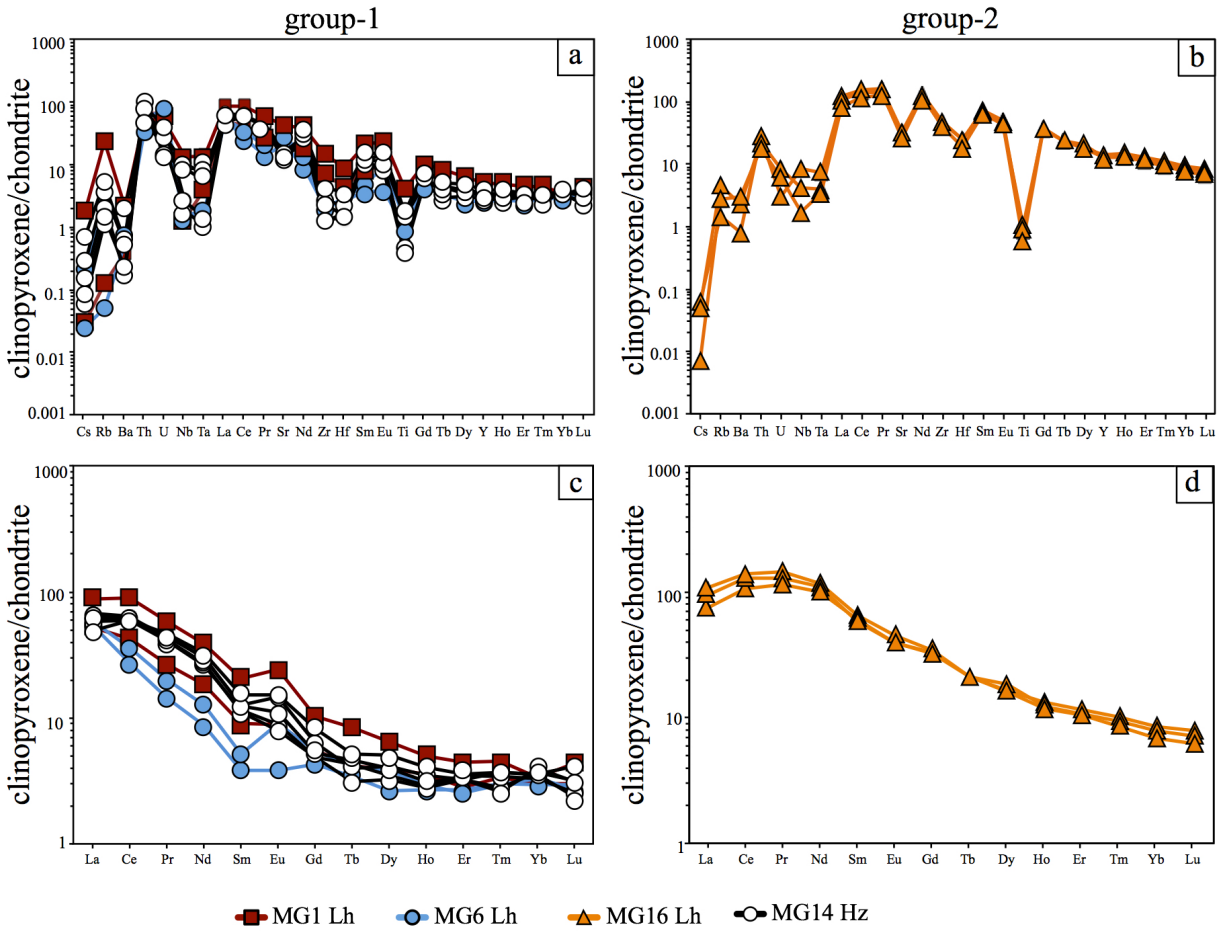

Fig. 15. Chondrite-normalized (Sun and McDonough, 1989) incompatibile trace elements distributions of group-1 clinopyroxene (a) and group-2 clinopyroxene (b). Chondrite-normalized (Sun and McDonough, 1989) REE patterns of group-1 clinopyroxene (c) and group-2 clinopyroxene (d).

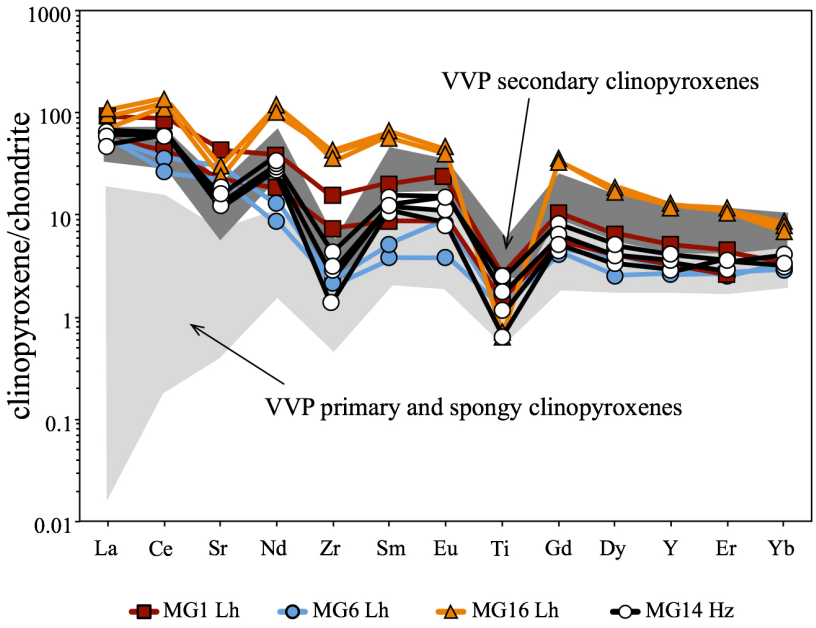

Fig. 16. Trace element compositions of MG clinopyroxene (this study) compared with the overall VVP clinopyroxene, shadowed areas: data from Beccaluva et al. (2001). Abbreviations and symbols as in Fig. 13.

4.4 Geothermobarometry

To estimate the temperature conditions under which the MG spinel lherzolites and harzburgites were equilibrated, we used the two-pyroxene geothermometer based on Fe/Mg exchange of Brey and Köhler (1990), which we will denote as T_{BK}. Olivine-spinel geothermometers of Wells (1977) and Taylor (1998) were also applied for comparative purposes and are denoted as T_W and T_T, respectively. For the thermobarometric calculations, we considered only cores of unreacted orthopyroxene and clinopyroxene grains that were in close contact.

Though some studies provide barometry, mainly based on the Ca distribution of olivine and clinopyroxene (e.g., Köhler and Brey, 1990), determining appropriate barometry in spinel peridotites (Medaris, 1999; O'Reilly et al., 1977) is challenging. Therefore, we assume the equilibrium pressure from experimental stability phase relationships (Caldeira and Munhá, 2002). Taking into account the absence of amphiboles (which could modify the peridotite mineral stability fields) and the presence of spinel as the sole aluminum bearing phase, an upper limit of 2.1 GPa and a lower limit of 0.9 GPa are set (Caldeira and

Munhá, 2002; Green and Hibberson, 1970; Green and Ringwood, 1970; O'Neill and Wall, 1987; Siena and Coltorti, 1989). This pressure approximation agrees with the maximum depth of the local SCLM, constrained by seismic profiles (Carminati and Doglioni, 2012) to fall within the 1.5-2.0 GPa range. The pyroxene Fe/Mg exchange is largely dependent on temperature (Brey and Köhler, 1990; Wells, 1977; Wood and Banno, 1973) and is relatively insensitive to pressure; temperatures calculated at 1.0 GPa and 2.0 GPa show only minor variations (<10°C). Accordingly, primarily for comparative purposes, temperature calculations were made at a fixed pressure of 1.5 GPa.

4.4.1 *Equilibration temperatures*

MG spinel lherzolites record residual temperatures in the range of 923-1058°C. The highest value (MG16) is comparable with those recorded by the two MG harzburgites (MG13: 1117 ± 20°; MG14: 1033 ± 30°C; Table 2). This is in agreement with low clinopyroxene content (6%), which could reflect a residual character analogous to harzburgites. We compared MG peridotites equilibration temperatures with those from the nearby districts of Lessini Mts. and Val d'Adige calculated with the Wells (1977) and Taylor (1998) geothermometers (Gasperini et al., 2006).

For comparison, equilibration temperatures of a few Lessini Mts. and Val d'Adige peridotites were recalculated together with MG samples of this work applying the three thermobarometric models (Table 2). We observed that: i) as seen in other geothermobarometric studies (e.g., Greenfield et al., 2013), T_T values are always lower than T_{BK} and T_W; ii) with the exception of one sample from Lessini Mts., differences between T_{BK} and T_W within each sample are negligible (<20°C); iii) T_T diverges from T_{BK} by 2 to 78°C and diverges from T_W by 19 to 78°C.

Taking this into account, the T_{BK} range of 923-1117°C recorded by MG peridotites is higher than most of Val d'Adige (T_{BK}= 896-902°C) and Lessini Mts. (T_{BK}= 885-975°C) xenoliths.

Within the entire VVP mantle domain, the high equilibration temperatures recorded by MG mantle xenoliths are only comparable to those of the highly metasomatized Lessini Mts. peridotites (1130 ± 60°C; Fig. 17).

4.4.2 *Oxygen fugacity*

Oxygen fugacities (fO_2) of Marosticano peridotites were estimated using the method of Ballhaus et al. (1991) and temperatures provided by the Brey-Köhler thermometer (T_{BK}). Calculated fO_2 values are plotted in Fig. 17 in logarithmic units with respect to the fayalite-magnetite-quartz (FMQ) buffer ($\Delta \log fO_2$). Estimates for the two spinel harzburgites range from +0.6 to +0.9, while for the spinel lherzolites the range is wider (-0.6 to +1.1), with MG6 lherzolite being the most reduced sample. With the exception of the latter xenolith, MG peridotites are more oxidized than Val d'Adige lherzolites [$\Delta \log fO_2$ (FMQ) from +0.2 to +0.3 as calculated for compositions from Gasperini et al., 2006 and T_{BK}; Table 2 and Fig. 17]. The Lessini Mts. peridotites also yield more variability in the recorded redox conditions [$\Delta \log fO_2$ (FMQ) from -1 to +1, calculated from data of Gasperini et al., 2006; Table 2] encompassing the entire range of Marosticano and Val d'Adige samples (Fig. 17).

Table 2: Average temperature (T) and oxygen fugacity reported as $\Delta logfO_2$ (FMQ) for MG spinel peridotites from Marosticano, Val d'Adige and Lessini Mts. calculated at 1.5 GPa. Estimated temperatures are from geothermometers of Brey and Köhler (1990), T_{BK}; Taylor (1998), T_T; and Wells (1977), T_W. $\Delta logfO_2$ (FMQ) is calculated from the method of Ballhaus et al. (1991) using T_{BK}. T_{BK} and $\Delta logfO_2$ (FMQ) of spinel peridotites from Val d'Adige and Lessini Mts. were re-calculated from data of Gasperini et al. (2006). CO_2 mole fractions are determined by equation of Stagno and Frost (2010) using the estimated T_{BK} and $\Delta logfO_2$ (FMQ).

	n	Average T_{BK} (°C)	2σ uncertainty T_{BK} (°C)	Average T_T (°C)	2σ uncertainty T_T (°C)	Average T_W (°C)	2σ uncertainty T_W (°C)	Average $\Delta logfO_2$ (FMQ)	2σ uncertainty $\Delta logfO_2$ (FMQ)	CO_2 mole fractions	2σ uncertainty CO_2 mole fractions
Marosticano											
MG1 Lh	2	949	*36*	912	*60*	954	*46*	1.1	*0.00*	1.19	*0.27*
MG6 Lh	2	923	*25*	898	*12*	940	*12*	-0.6	*0.08*	0.02	*0.01*
MG16 Lh	2	1058	*21*	1022	*19*	1041	*10*	0.8	*0.08*	1.03	*0.28*
Marosticano											
MG13 Hz	2	1117	*20*	1069	*22*	1109	*22*	0.9	*0.44*	0.83	*0.00*
MG14 Hz	3	1033	*30*	1010	*28*	1029	*29*	0.6	*0.12*	0.65	*0.08*
Val d'Adige											
56B Lh	1	902		836		914		0.3			
F56-7 Lh	1	966		888		956		0.2			
Val d'Adige											
F56-5 Hz	1	896		842		909					
Lessini Mts.											
25 Lh	1	975		969		998		-0.1			
25C Lh	1	885		883		926					

n= number of analyses per sample; Lh= lherzolite; Hz= harzburgite.

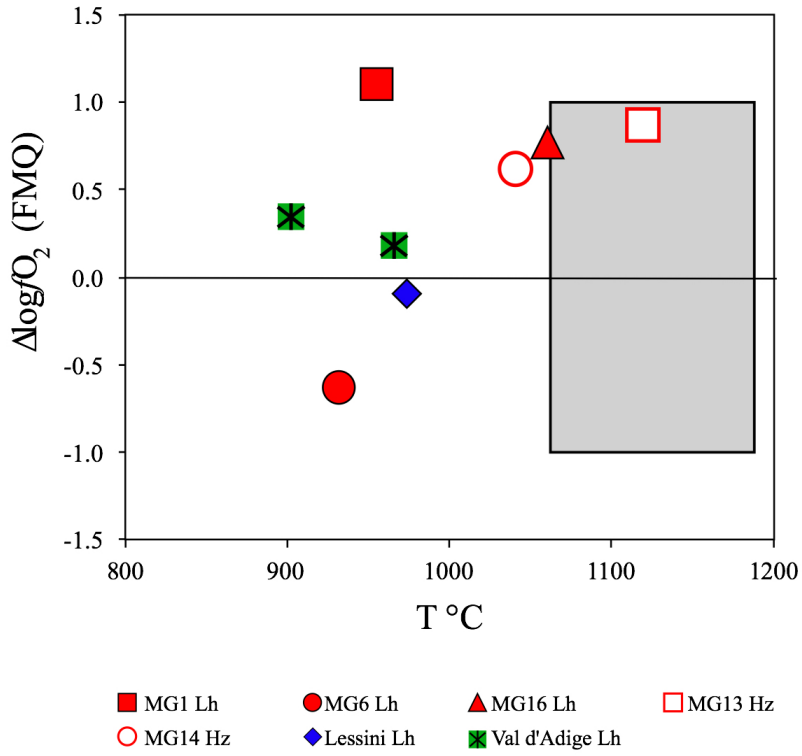

Fig. 17. Temperatures and fO_2 relative to the buffer reaction fayalite-quartz-magnetite (ΔlogfO_2 FQM). Temperatures are calculated using the approach of Brey and Köhler (1990). ΔlogfO_2 (FMQ) estimates are calculated with the formula of Ballhaus et al. (1991). P is fixed at 1.5 GPa. Filled and open symbols are for lherzolite (Lh) and harzburgite (Hz), respectively. T-fO_2 conditions of Lessini and Val d'Adige lherzolites are calculated using major element data from Gasperini et al., 2006. Shadowed area represents the T-fO_2 range of highly metasomatized Lessini xenoliths previously reported in Siena and Coltorti (1993).

4.5 Discussion

4.5.1 *A cratonic origin?*

The highly refractory bulk composition of lherzolites (Al_2O_3 <1.03 wt.%, mg#= 90.3-91.6; Table 3), associated with low Al_2O_3 contents, high mg# values in both pyroxenes and spinel of MG peridotites (Fig. 13c-d) testify for a large extraction of basaltic melts from the Marosticano mantle domain which appears the most residual of the entire VVP (e.g., Lessini Mts. lherzolites: Al_2O_3 >2.52 wt.%, mg#= 85.8-89.9). Peridotites with refractory composition are expected in Phanerozoic and Proterozoic off-craton mantle and ophiolites. They generally follow the so-called "residual or oceanic trend", explained as an extraction of basaltic components, resulting in an increase of Fo content in olivine accompanied by

increased olivine modal content (Boyd, 1989). Refractory peridotites characterize also the cratonic mantle, but they rarely follow the oceanic trend (Bernstein et al, 2007; Boyd, 1989; Boyd et al., 1997; Ionov et al., 2010). They are characterized by olivine with generally high Fo content (~91-94) at extremely variable modal olivine content (~40-75%). In particular, the high Fo of olivine in spinel bearing (shallow) cratonic peridotites with relatively low orthopyroxene modal contents (<20%; e.g., Tanzanian, Greenland, and Slave Cratons) are indicative of high degrees (~30 to 50%) of partial melting in thermal regime active only till Archean/early Proterozoic time (Ionov et al., 2010; Walter, 2003).

In the Boyd diagram (Boyd, 1989; Boyd et al., 1997) MG olivines plot off the oceanic trend (Fig. 13a), and follow the general behavior of cratonic olivine (i.e., Kapvaal, Tanzanian, Greenland and Slave Cratons). In comparison most of the Val d'Adige and Lessini Mts. peridotites exhibit lower olivine modal contents at lower Fo following the oceanic trend (Fig. 13a). Marosticano olivine also have Ni values higher than those of Lessini Mts. but similar to those of Val d'Adige (Fig. 13b).

In association with high Fo olivine, MG peridotites show high mg# orthopyroxene in the range of 12-30% modal contents (Table 1), out of any "ideal" Phanerozoic (abyssal, oceanic and continental) off-craton melting trend (Niu, 2004; Pelorosso et al., 2016). Instead, they reflect a general olivine-orthopyroxene behavior recorded in "shallow" (garnet-free) cratonic mantle and interpreted as physical segregation of olivine and orthopyroxene in high-pressure melting residuum and polybaric re-equilibration (Bernstein et al., 2007; Ionov et al., 2010). In addition, trace element distributions in orthopyroxene from MG16 lherzolite and MG13 harzburgite show almost flat M-HREE profiles [i.e., $(Dy/Yb)_N$], consistent with an original subsolidus equilibrium with garnet (Bonadiman et al., 2005). In garnet lherzolites at progressively decreasing sub-solidus T (1300-900°C), the presence of orthopyroxene decreases the total REE contents with equal M-HREE solid-solid partition coefficients (Sun and Liang, 2014). In turn, orthopyroxene of MG1, MG6 lherzolites, and MG14 harzburgite seem to be originally equilibrated in the spinel stability field showing the typical steep slope for M-HREE at comparable subsolidus temperature (1000-900°C; Sun and Liang, 2014; Fig. 14a, b).

Spinel, the distinctive phase of the great majority of off-craton mantle xenoliths, has cr# (30-67) which suggests a residual component neither coherent with the oceanic residual trend (i.e., "OSMA"; Arai, 1994a, 1994b) nor with the more fertile VVP-mantle fragment (cr#= 9-12). On the other hand, Marosticano spinel mimic the tendency observed for spinel coexisting with olivine in shallow on-craton (garnet-free) xenoliths (Bernstein et al., 2007).

In this refractory P-T system, spinel cr# of 60.0, together with the olivine Fo content of 91.5, would suggest strong (or complete) clinopyroxene consumption by high degrees of partial melting (>25%; Bernstein et al., 2007; Bonadiman et al., 2005; Hellebrand et al., 2001; Scott et al., 2016; Walter, 2003) that are typical of the Archean or early Proterozoic mantle (Walter, 2003). Accordingly, we suggest that the partial melting occurred at high melting T and thus more likely in an old mantle thermal regime. Subsequently, the Marosticano mantle was enriched, forming the observed clinopyroxene (modal contents 4-13%) in MG xenoliths. These are thus secondary in nature in agreement with several studies demonstrating that most clinopyroxene in on-craton mantle may have a metasomatic legacy (Grégoire et al., 2003; Pearson et al., 2003; Simon et al., 2003; 2007). In summary, Marosticano xenoliths are characterized by cratonic fingerprints according to major and trace element compositions of the peridotite phases, and Re-Os geochronological modeling (T model age= 2.1-2.9; Brombin et al., in prep.). These geochemical characteristics are evident only for the Marosticano mantle fragment, whereas the rest of the VVP mantle studied heretofore demonstrates off-craton SCLM.

The sole, intriguing link between on-craton and off-craton VVP mantle is the similarity of the Re-Os ages, ranging between 1.9 to 2.1 Ga, with a unique value at 3.1 Ga for the entire VVP domain. These results speak in favor for a continuum geodynamic set, which includes on-craton and off-craton mantle portions, as more frequently reported.

Cratonic signatures in off-craton spinel mantle xenoliths derived from intraplate volcanic areas are recognized in a few mantle xenolith populations, e.g., in Massif Central (France; Lenoir et al., 2000), West Otago (New Zealand; Liu et al., 2015; Scott et al., 2014a, 2014b, 2016) and Cape Verde (Bonadiman et al., 2005; Coltorti et al., 2010). In the Massif Central, two contrasting shallow lithospheric domains are faced. Relatively refractory (i.e., Al_2O_3 <2.0 wt.%) and highly fertile (i.e., Al_2O_3 >4.0 wt.%) harzburgites and lherzolites are interpreted as reminiscent of cratonic and circumcratonic SCLM domains, respectively (Lenoir et al., 2000). West Otago spinel peridotites with high variable Re depletion Os model ages (0.5-2.7 Ga) would represent relicts of Archean depleted mantle residues recycled through the asthenosphere over Ga timescales along with more fertile convecting mantle. Therefore, different remnants of shallow lithospheric domains are incorporated within the young (<300 Ma) Zealandia microplate (Liu et al., 2015; McCoy-West et al., 2013).

It is important to note that “shallow” (garnet-free) cratonic mantle is not exclusive of continental setting. Cape Verde Islands lie in the Atlantic Ocean but have Archean spinel

mantle xenoliths that record garnet bearing precursors as well as K-rich metasomatism (Bonadiman et al., 2005), thus suggesting the involvement of ancient geochemical reservoir in the genesis of oceanic basalts (Coltorti et al., 2010).

Although Archean cratons are considered ancient continental nuclei characterized by tectonic inactivity for at least the past 2 Ga and low heat flow, recent studies show that their highly refractory mantle roots are intensively modified over time by mechanical destructions (lithospheric thinning and incipient rifting) and by episodic rejuvenation events (Foley, 2008; Tang et al., 2013; Zhang et al., 2009a; Zhang et al., 2012). The Wyoming Craton and North China Craton are well-known examples of complete chemical rejuvenation by varying degrees of refertilization (Eggler and Furlong, 1991; Fan and Menzies, 1992; Tang et al., 2008, 2012, 2013). In turn, other cratons might not have yet suffered large-scale removal of their ancient keels but are in the early stages of disruption due to the efficiency of extensive regime (Foley, 2008). We recall that Lessini Mts. and Val d'Adige xenoliths are generally fertile lherzolites with both clinopyroxene and orthopyroxene coherently showing the typical LREE-depleted, MREE flat and steep H-LREE fractionated patterns respectively (Beccaluva et al., 2001; Lenoir et al., 2000). These features are in chemical contrast with the refractory nature and the LREE enrichments of Marosticano xenolith population. These differences could be interpreted in terms of compositional rejuvenation of the circumcratonic domains. Lessini Mts. and Val d'Adige xenoliths may be fragments of the ancient SCLM, strongly refertilized by infiltration of asthenosphere-derived melts, rather than newly accreted "off-craton" SCLM. By contrast, Marosticano domain could be interpreted as the vestige of an old (Archean?) SCLM block that underwent depletion via melt extraction and was afterward pervasively metasomatized, a process, that was not, however, able to erase fully the original cratonic nature.

Table 3: Bulk rock major element (wt%) compositions of Marosticano lherzolites (Lh).

Sample	MG1 Lh	MG6 Lh
SiO_2	44.66	46.94
TiO_2	0.02	0.02
Al_2O_3	0.41	1.03
Fe_2O_3	0.00	0.00
FeO	7.44	8.15
MnO	0.11	0.12
MgO	45.72	42.61
CaO	1.57	1.12
Na_2O	0.00	0.00
K_2O	0.07	0.02
P_2O_5	0.00	0.00
Tot	100.00	100.00
mg#	91.64	90.31

$mg\# = 100 \times Mg/(Mg+Fe)_{mol}$

4.5.2 *Metasomatic origin of clinopyroxene in Marosticano xenoliths*

Despite the general refractory features of MG peridotites, a superimposed metasomatic process is manifested by major and trace element geochemistry of both pyroxenes. Trace element compositions of Marosticano clinopyroxene show variable enrichment characteristics, inconsistent with a residual origin after melt extraction (e.g., Sun et al., 2012). They exhibit a notable LREE-enrichment (Fig. 15c, d), a fractionated REE pattern and a general HFSE depletion (Fig. 15a, b) with respect to the chondrite model of trace element abundances (Sun and McDonough, 1989). Taken together, these signatures confirm that clinopyroxene is a phase either formed by a reaction of a residual peridotite with metasomatic melts or it is a new phase directly crystallized from the metasomatic agents.

As nearby VVP districts (i.e., Lessini Mts. and Val d'Adige) are thought to have been affected by silicate metasomatism (Beccaluva et al., 2001), we first evaluated whether the MG mantle segment could also be explained by the same type of metasomatism. Taking into account only Lessini Mts. and Val d'Adige samples that show clinopyroxene modal contents and two-pyroxene mg# values comparable to those of MG xenoliths, trace element compositions of MG clinopyroxene are significantly enriched compared to the

primary, spongy, and secondary VVP clinopyroxene (Fig. 16). This suggests that MG peridotites were infiltrated by a metasomatic agent distinct from that affecting the rest of the VVP region. However, both group-1 and group-2 clinopyroxene are more enriched in LREE (Fig. 15c, d) and depleted in Ti and HFSE (e.g., Zr; Fig. 15a, b), arguing against a "pure" alkaline silicate metasomatism and favoring instead the contribution of a carbonatic component. Interestingly, experimentally produced silica-bearing carbonatite melts crystallize clinopyroxene with major element composition similar to both MG group-1 and group-2 clinopyroxene (Fig. 13d-f).

Enrichment in LREE accompanied by strong HFSE depletion (Fig. 15a, b) of group-1 and group-2 clinopyroxene are notably assigned to an effect of the clinopyroxene/carbonatite partitioning as shown by experimental and empirical data by Dasgupta et al. (2009), Dixon et al. (2008), Gudfinnsson and Presnall (2005), and Pokhilenko et al. (2015). This geochemical effect has been observed in various carbonatite metasomatized mantle xenoliths from both oceanic and continental settings (i.e., Spitsbergen, Ionov, 1998; North China Craton; Sun et al., 2012; New Zealand, Scott et al., 2016; Comores Archipelago; Coltorti et al, 1999). Group-2 clinopyroxene also demonstrate steep M-HREE fractionated patterns, and they have remarkably higher LREE contents with respect to clinopyroxene formed by a carbonatitic/CO_2-rich silicate melt experimentally obtained at pressure of 6.6 GPa in equilibrium with garnet (Dasgupta et al., 2009; Fig. 18). The calculated $D_{La}^{\text{clinopyroxene/carbonatite}}$ at this pressure is 0.006 but systematically increases with decreasing pressure and with the spinel content (Dasgupta et al., 2009). Therefore, if we consider REE clinopyroxene/carbonatite partition coefficients calculated for 2 GPa and 1100-1150°C (e.g., $D_{La}^{\text{clinopyroxene/carbonatite}}$ of 0.09; Klemme et al., 1995) we can reproduce the general shape of the REE pattern of both MG clinopyroxene groups (Fig. 18). The chief distinction between group-1 and group-2 clinopyroxene is that the former shows a less steep, or flat, HREE pattern indicating chromatographic fractionation of a metasomatic agent interacting with different peridotitic wallrocks (Ionov et al., 2002; Sen et al., 1993). In this scenario, the concentration fronts of the migrating melts are controlled by ion-exchange with the peridotitic matrix. In general, the fronts of the more incompatible elements (i.e., LREE) travel faster than those of less incompatible ones (i.e., M-HREE) producing enrichments in LREE and depletion or flatness in HREE of the whole rock depending on the original peridotitic matrix (Ionov et al., 2002). In this frame, the group-1 clinopyroxene record a continuum incorporation of REE from the carbonatitic melt into a possible residual (primary?) clinopyroxene (Ionov et al., 2002; Pokhilenko et al., 2015;

Sen et al., 1993). On the contrary, the convex-upward REE patterns of group-2 clinopyroxene may reflect nearly complete equilibration between the peridotite matrix (mainly olivine-orthopyroxene) and the metasomatic melt (Dasgupta et al., 2009; Dixon et al., 2008).

In anhydrous garnet-free peridotites, restitic orthopyroxene is the counterpart of clinopyroxene to accommodate changes in the geochemical budget. The only evidence of metasomatic effects in the MG orthopyroxene is their high Ti content (up to 281 ppm), a chemical feature incongruous with their low Al_2O_3 (Scott et al., 2016; Fig. 19) and the carbonatitic enrichment described for the clinopyroxene. This can be explained by the action of CO_2-rich silicate melts which could primarily impart a carbonatite-like trace element signature in clinopyroxene (i.e., L-REE) hiding the potential effects of silicate melts (i.e., Ti enrichment), that in turn is magnified in the residual orthopyroxene (Scott, et al., 2016). Spinel facies clinopyroxene prefers most trace elements, including Ti, compared to orthopyroxene; however, relative to elements with slightly larger and smaller atomic radii (Eu and Dy), Ti is slightly less favorably partitioned into clinopyroxene (Eggins et al., 1998; Scott, et al., 2016). This nuance leads to the formation of small negative Ti anomaly in clinopyroxene and a corresponding positive anomaly in orthopyroxene (Scott et al., 2016). Consequently, both negative and positive Ti anomalies observed in MG orthopyroxene could be due to a chromatographic fractionation effect during the interaction between carbonatite/CO_2-rich silicate melts and a peridotitic wallrock where clinopyroxene was or was not present (Ionov et al., 2002; Scott et al., 2016; Sen et al., 1993).

Though we cannot resolve if this metasomatism initially occurred in the garnet stability field and continued in shallower portions of the MG mantle, we can assume that the product of such metasomatism may be stabilized at P conditions of the spinel stability field. Accordingly, we interpret the geochemical characteristics (major and trace elements) acquired by MG pyroxenes as consistent with the resulting clinopyroxene formed by the interaction of a carbonatitic melt with cratonic flavored ambient peridotite (Griffin et al., 1999; Spengler et al., 2006). Notably, experimental studies (e.g., Dasgupta and Hirschmann, 2006; Dasgupta et al., 2007; Green, 2015; Hammouda and Keshav, 2015; Hirose, 1997) suggest that a carbon-rich peridotite is necessary to form alkaline and in particular ultra-alkaline mantle melts. Similarly, carbonatitic components have been hypothesized as important contributors to VVP alkaline- to ultra-alkaline magmas, the hosting lavas that ferry VVP mantle xenoliths to the surface (Beccaluva et al., 2007).

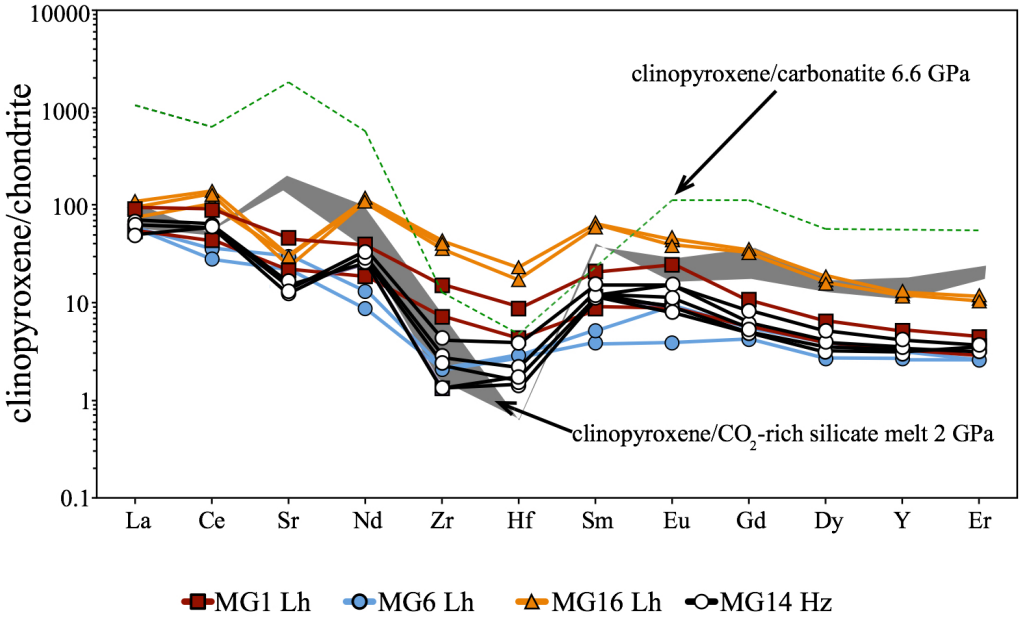

Fig. 18. REE patterns of MG clinopyroxene (this study) compared with i) clinopyroxene experimentally equilibrated with carbonatite melt obtained at pressure of 6.6 GPa in equilibrium with garnet (Dasgupta et al., 2009); dashed line; ii) modeled clinopyroxene formed by a carbonatitic/CO_2-rich silicate melt applying $D^{clinopyroxene/carbonatite}$ calculated at pressure of 2 GPa and temperature of 1100-1150°C (Klemme et al., 1995); shadowed area. Chondrite values are from Sun and McDonough (1989). Abbreviations and symbols as in Fig. 13.

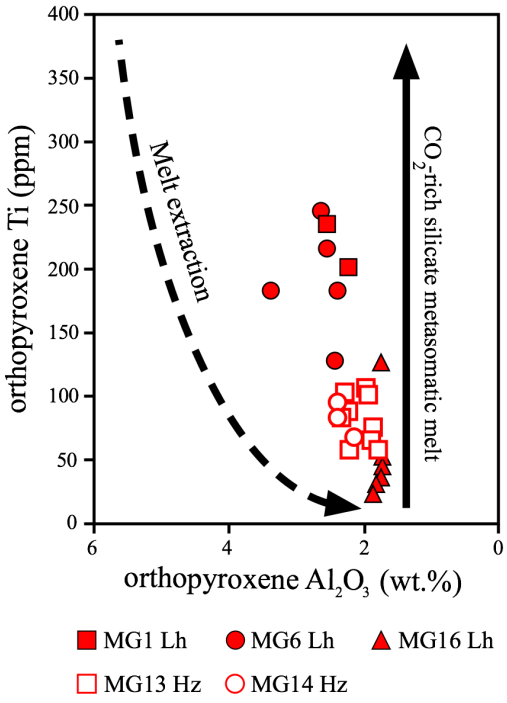

Fig. 19. Orthopyroxene Ti (ppm) and Al_2O_3 (wt.%) contents with respect to melt extraction (dashed line) and CO_2-rich metasomatic enrichment (solid line) trends (from Scott el al., 2016). Abbreviations and symbols as in Fig. 13.

4.5.3 *Relationships between carbonatite/CO_2-rich silicate metasomatism and fO_2 conditions*

As carbonatitic/CO_2-rich silicate melts contain large amounts of dissolved fluids, they are able to mobilize volatile elements (C, O, H, but also Na and K as lithophile elements); accordingly, their interaction with the peridotite matrix may affect the redox conditions (Dasgupta et al., 2013). MG peridotites represent a cratonic "enclave" of continental mantle of the Adria plate that was later pervaded by carbonatite metasomatism. The high fO_2 (Fig. 17), comparable with the other VVP mantle occurrences and within the range of the SCLM (Foley, 2011), is not compatible with a cratonic origin but requires a late oxidation event, preserved until the xenolith exhumation by Cenozoic host lavas. Volatile mass transport occurs mostly by fluid and silicate (with prevailing H_2O) or carbonate (with prevailing CO_2) melts as function of the redox state of the mantle (Foley, 2008, 2011; Frost and McCammon et al., 2008; Pokhilenko et al., 2015). Assuming the relatively high oxidizing conditions of Marosticano peridotites were due to CO_2-bearing melts, we calculated CO_2 mole fractions of such melts using the equation of Stagno and Frost (2010). We obtained CO_2 mole fractions close to 1.0, taking into account the T-fO_2 values independently calculated from the silicate parageneses (Table 2). High CO_2 mole fractions are also evident in the diagram of fO_2 as a function of potential temperatures (Goncharov et al., 2012), where almost all the Marosticano peridotites straddle the field for carbonatite and CO_2 fluid (Fig. 20). This may suggest that the Marosticano geothermobarometric conditions record this matrix/carbonatitic melt interaction, rather than the T-fO_2 values of the initial cratonic lithospheric mantle.

The variable redox states may also influence the Eu oxidation state (Eu^{3+} or Eu^{2+}; Henderson, 1984) and may explain why this element is enriched in group-1 clinopyroxene. In oxidized magmas Eu is an incompatible element in its trivalent form (Eu^{3+}), while in reduced magmas it is preferentially incorporated into plagioclase in its divalent form (Eu^{2+}). This ion-exchange process explains the negative Eu anomaly in many terrestrial basalts showing plagioclase as liquid phase. However, Eu speciation is highly sensitive to small redox variations. Thus the different accommodation of Eu in minerals may change rapidly (McLennan, 2001).

Almost all group-1 clinopyroxene have M-HREE flat profiles demonstrating positive Eu anomalies (Fig. 15a, c). This Eu anomaly is not accompanied by a positive K or Sr anomaly, that could be assigned to the melting of pre-existing phlogopite and plagioclase

in the protolith (Marchesi et al., 2013; Tang et al., 2017), neither of which were observed in any Marosticano xenolith. In other xenolith suites, examination of the Eu content in garnet and clinopyroxene in eclogites led to the suggestion that the positive Eu anomaly results from the interplay between crystal chemistry and redox conditions during metasomatism (Griffin and O'Reilly, 2007). Karner et al. (2010) determined the Eu partition coefficient between augite and melt ($D_{Eu}^{\text{clinopyroxene/carbonatite}}$) in samples crystallized from a highly Eu-spiked Martian basalt at different fO_2 conditions. These authors observed that $D_{Eu}^{\text{augite/melt}}$ steadily increases with fO_2 since Eu^{3+} is more compatible than Eu^{2+} in the pyroxene structure; thus increasing fO_2 leads to greater Eu^{3+}/Eu^{2+} in the melt, allowing for more Eu (total) to partition into the clinopyroxene. It is worth noting that positive Eu anomaly is occasionally observed in clinopyroxene from metasomatized suboceanic mantle or subcontinental cratonic mantle in both spinel and garnet stability fields irrespective of the nature of the metasomatic melts (e.g., xenoliths from Loch Roag, North Atlantic Craton, Northern Scotland, Hughes et al., 2015; from Siberian Craton, Pearson et al., 1995; Slave Craton, Heaman et al., 2002; Kaapval craton, Jacob et al., 2003). On the basis of these considerations, we suggest that small variations in the redox conditions may induce Eu to modify its solid/solid, solid/melt partitioning behaviors, without less noticeable effects on large-scale geochemical process.

The interaction between the Marosticano residual mantle with a carbonatite/CO_2-rich silicate melt is explained by a possible chromatographic fractionation effect only in group-1 clinopyroxene bearing peridotite. This leads to a "local" variation of fO_2 oxidizing conditions and by consequence to a "local" increase of Eu^{3+}/Eu^{2+} in the melt and to higher Eu concentration in the newly formed clinopyroxene. Group-2 clinopyroxene is suggested to crystallize from the carbonatitic/CO_2-rich silicate melts that control the environmental redox condition.

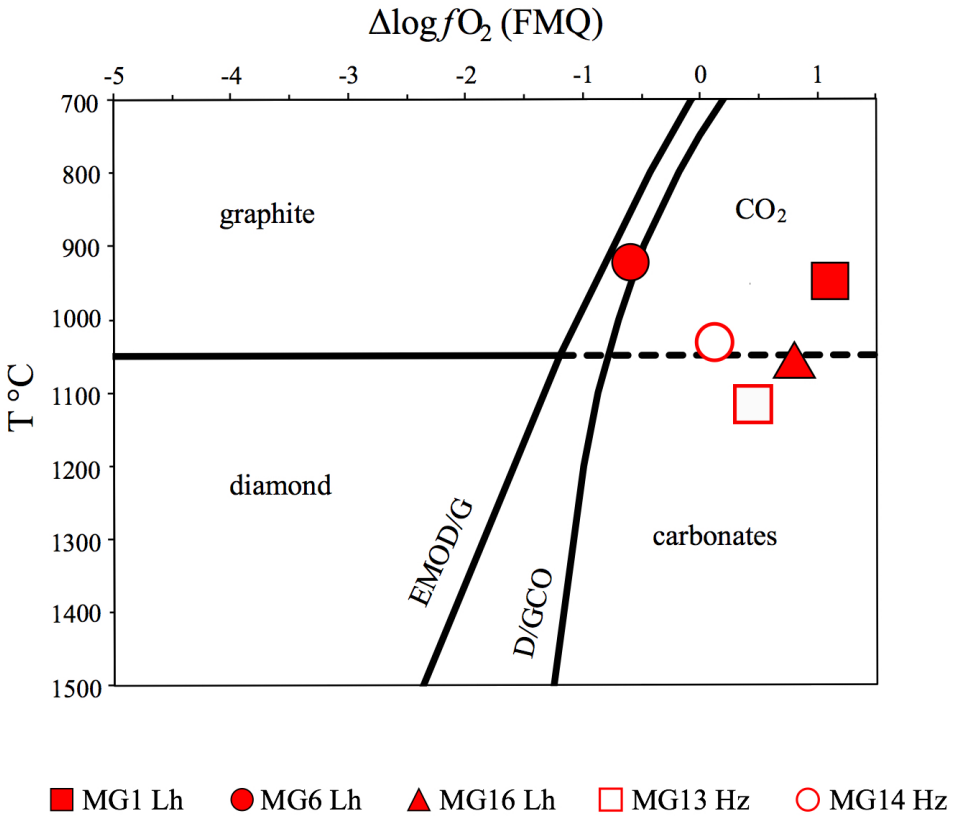

Fig. 20. Oxygen fugacity (ΔlogfO_2 FMQ) versus temperature for MG xenoliths. Stability fields of diamond, graphite and carbonates are delineated by the buffer reactions and the enstatite-magnesite-olivine-diamond/graphite (EMOD/G) and diamond/graphite-CO (D/GCO) (Goncharov et al., 2012 and references therein). Almost all the Marosticano peridotites straddle the fields for carbonatite and CO_2 fluid suggesting that the Marosticano geothermobarometric conditions record the interaction between matrix and carbonatite/CO_2-rich silicate melts. Abbreviations and symbols as in Fig. 13.

4.6 Conclusions

- Petrological and geochemical features of the newly discovered Marosticano peridotite xenoliths indicate that they represent a mantle segment geochemically distinctive from the other VVP peridotites (e.g., Lessini Mts. and Val d'Adige), contributing to enlarge the knowledge of spatial heterogeneity within the mantle of this region.
- Marosticano lherzolites and clinopyroxene bearing harzburgites demonstrate complete spinel facies equilibration. Mineral major and trace elements features are comparable to those observed for on-craton peridotites worldwide.
- Marosticano clinopyroxene are secondary in nature and they exhibit a substantive LREE enrichment, a fractionated REE pattern with positive Eu anomaly, almost flat

(group-1 clinopyroxene) or steep (group-2 clinopyroxene) HREE patterns, and a remarkable HFSE depletion. These characteristics are attributed to a chromatographic separation of a metasomatic agent with high carbonatitic/CO_2-rich silicatic components.

- Marosticano samples record relatively high oxidation conditions anomalous for a proper cratonic environment, but similar to those of the VVP off-craton xenoliths (e.g., Lessini Mts.). These T-fO_2 relationships are probably due to the oxidizing nature of CO_2-rich circulating fluids.
- The variable, but generally high, redox states of the Marosticano xenoliths could be responsible for the positive Eu anomaly of group-1 clinopyroxene. As higher fO_2 leads to higher Eu^{3+}/Eu^{2+} in the melt increasing the element partitioning in clinopyroxene, the positive Eu anomaly could result from the relatively high redox conditions of the Marosticano mantle fragment during the formation of group-1 clinopyroxene. On the contrary, group-2 clinopyroxene that do not exhibit positive Eu anomaly may show the fingerprint of a carbonatitic/CO_2-rich silicate melt metasomatism, therefore still preserving the original redox conditions.
- Within the SCLM sampled by VVP magmatism, only Marosticano xenoliths show evidence of carbonatitic metasomatic overprinting of a likely cratonic mantle domain. All the other mantle VVP mantle xenoliths exhibit characteristics of off-craton lithospheric mantle variably affected by Na-alkaline silicatic metasomatism.
- The lithospheric mantle beneath the Adria plate as sketched in Fig. 21 has been affected by complex refertilization processes, related to a geodynamic scenario dominated by extension-related magmatism in response to the near active collision between Eurasia and Africa plates.
- The geochemical features of Marosticano mantle xenoliths introduce a cratonic component in the geodynamic evolution of the Adria plate system in the general frame of the geodynamical reconstruction of the Africa/Eurasia collision. From our current study, together with literature data, we interpret that the cratonic keel is preserved only in the Marosticano district, while Lessini Mts. and Val d'Adige mantle domains could be circumcratonic portions refertilized by infiltration of asthenospheric-derived melts (Fig. 21).

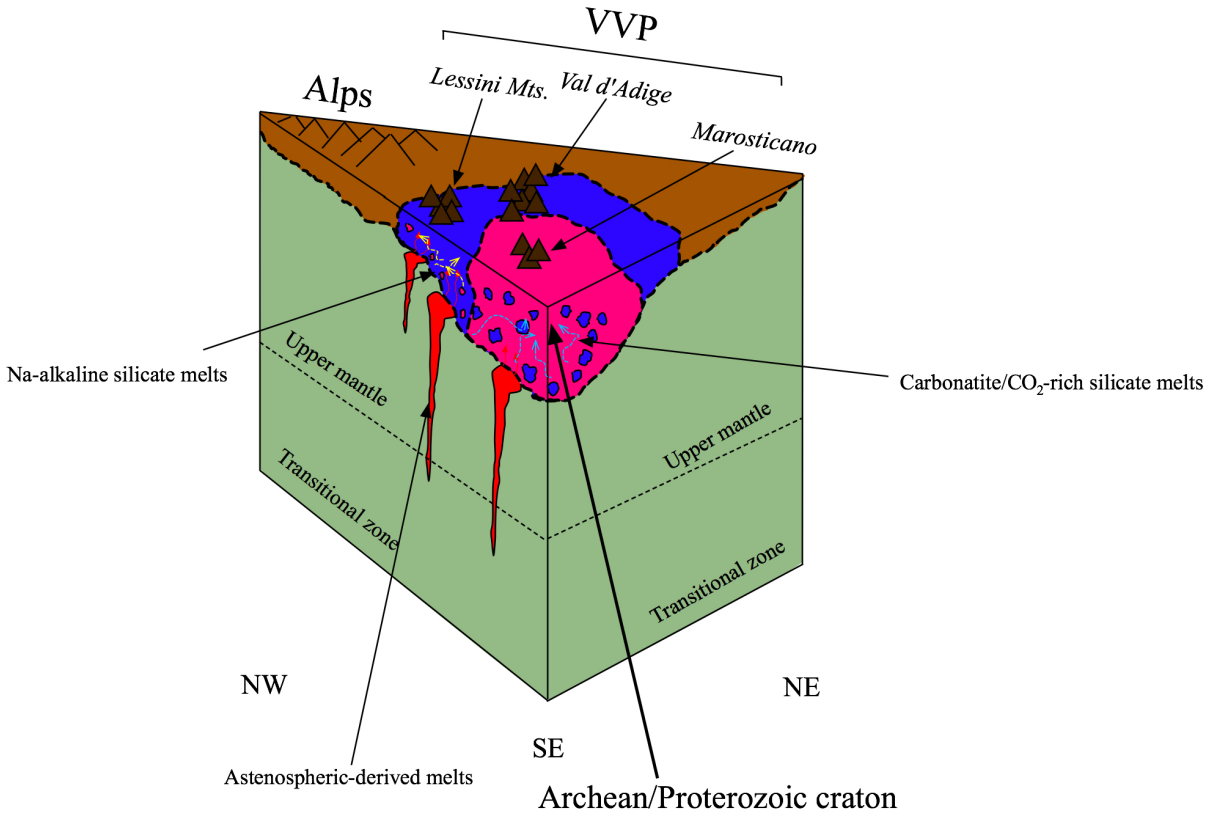

Fig. 21. Schematic model of processes significant in the evolution of the lithospheric mantle beneath Veneto Volcanic Province (VVP) during the European/Adria collision. The cratonic keel, variably affected by carbonatite/CO_2-rich silicate metasomatism, is preserved only in Marosticano district (purple area) while Lessini Mts. and Val d'Adige mantle domains are circumcratonic portions (blue zones) refertilized by astenospheric-derived melts (red-upwelling "fingers"). The rejuvenated mantle is subsequently metasomatized by Na-alkaline silicate melts (Beccaluva et al., 2001; Gasperini et al., 2006; Morten et al., 1989; Siena and Coltorti, 1989).

Acknowledgments

R. Carampin (I.G.G-C.N.R. Padova) is thanked for analytical assistance during the EMP analyses.

The Italian National Research Program PRIN_2015/prot. 20158A9 (CB-AM) and the IUSS Mobility Research Programme of the University of Ferrara (VB scholarship for Abroad Mobility for Long Period) supported this research. H. Downes and E.-R. Neumann are also thanked for helping us to clarify and strengthen the early version of the manuscript. We appreciate the critical reviews of J.M. Scott and an anonymous referee for their constructive comments on a previous version of this paper and Andrew Kerr for his thoughtful suggestions and editorial handling.

References

Ansorge, J., Blundell, D., Müller, S., 1992. Europe's lithospheric structure, in Blundell D., Freeman, R., Müller, S. (Eds.), A Continent Revealed: The European Geotraverse. Cambridge University Press, New York, p. 275.

Arai, S., 1994a. Characterization of spinel peridotites by olivine-spinel compositional relationships; review and interpretation. Chemical Geology 113, 191-204.

Arai, S., 1994b. Compositional variation of olivine chromian spinel in Mg-rich magmas as a guide to their residual spinel peridotites. Journal of Volcanology and Geothermal Research 59, 279-293.

Ballhaus, C., Berry, R., Green, D., 1991. High pressure experimental calibration of the olivine-orthopyroxene-spinel oxygen geobarometer: implications for the oxidation state of the upper mantle. Contributions to Mineralogy and Petrology 107, 27-40.

Beccaluva, L., Bonadiman, C., Coltorti, M., Salvini, L., Siena, F., 2001. Depletion events, nature of metasomatizing agent and timing of enrichment processes in lithospheric mantle xenoliths from the Veneto Volcanic Province. Journal of Petrology 42, 173-187.

Beccaluva, L., Bianchini, G., Bonadiman, C., Coltorti, M., Milani, L., Salvini, L., Siena, F., Tassinari, R., 2007. Intraplate lithospheric and sublithospheric components in the Adriatic domain: Nephelinite to tholeiite magma generation in the Paleogene Veneto Volcanic Province, Southern Alps. Geological Society of America 418, 131-152.

Bernstein, S., Kelemen, P.B., Hanghøj, K., 2007. Consistent olivine Mg# in cratonic mantle reflects Archean mantle melting to the exhaustion of orthopyroxene. Geology 35, 459-462.

Bonadiman, C., Beccaluva, L., Coltorti, M., Siena F., 2005. Kimberlite-like metasomatism and "garnet signature" in spinel-peridotite xenoliths from Sal, Cape Verde Archipelago: relics of a subcontinental mantle domain within the Atlantic Oceanic Lithosphere? Journal of Petrology 46, 2465-2493.

Boyd, F.R., 1989. Compositional distinction between oceanic and cratonic lithosphere. Earth and Planetary Science Letters 96, 15-26.

Boyd, F.R., Pokhilenko, N.P., Pearson, D.G., Mertzman, S.A., Sobolev, N.V., Finger, L.W., 1997. Composition of the Siberian cratonic mantle: evidence from Udachnaya peridotite xenoliths. Contributions to Mineralogy and Petrology 128, 228-246.

Brey, G.P., Köhler, T.P., 1990. Geothermobarometry in four-phase lherzolites II. New thermobarometers, and practical assessment of existing thermobarometers. Journal of Petrology 31, 1353-1378.

Brey, G.P., Doroshev, A.M., Girnis, A.V., Turkin, A.I., 1999. Garnet-spinel-orthopyroxene equilibria in the FeO-MgO-Al_2O_3-SiO_2-Cr_2O_3 system; I, composition and molar volumes of minerals. European Journal of Mineralogy 11, 599-617.

Caldeira, R., Munhá J.M., 2002. Petrology of ultramafic nodules from Sao Tomé Island, Cameroon Volcanic Line (oceanic sector). Journal of African Earth Sciences 34, 231-246.

Carminati, E., Doglioni, C., 2012. Alps vs Apennines: the paradigm of a tectonically asymmetric Earth. Earth-Science Reviews 112, 67-96.

Catalano, R., Doglioni, C., Merlini, S., 2000. On the Mesozoic Ionian basin. Geophysical Journal International 144, 49-64.

Coltorti, M., Bonadiman, C., Hinton, R.W., Siena, F., Upton, B.G.J., 1999. Carbonatite metasomatism of the oceanic upper mantle: evidence from clinopyroxenes and glasses in ultramafic xenoliths of Grande Comore, Indian Ocean. Journal of Petrology 40, 133-165.

Coltorti, M., Bonadiman, C., O'Reilly S.Y., Griffin, W.L., Pearson, N.J., 2010. Buoyant ancient continental mantle embedded in oceanic lithosphere (Sal Island, Cape Verde Archipelago). Lithos 120, 223-233.

Dasgupta, R., Hirschmann, M.M., 2006. Melting in the Earth's deep upper mantle caused by carbon dioxide. Nature 440, 659-662.

Dasgupta, R., Hirschmann, M.M., Smith, N.D., 2007. Partial melting experiments of peridotite+CO_2 at 3GPa and genesis of alkali ocean island basalts. Journal of Petrology 48, 2093-2124.

Dasgupta, R., Hirschmann, M.M., McDonough, W.F., Spiegelman, M., Withers, A.C., 2009. Trace element partitioning between garnet lherzolite and carbonatite at 6.6 and 8.6 GPa with applications to the geochemistry of the mantle and of mantle-derived melts. Chemical Geology 2009, 57-77.

Dasgupta, R., Mallik, A., Tsuno, K., Withers, A.C., Hirth, G., Hirschmann M.M., 2013. Carbon-dioxide-rich silicate melt in the Earth's upper mantle. Nature 493, 211-215.

De Vecchi, G., Sedea, R., 1995. The Paleogene basalts of the Veneto region (NE Italy). Memorie di Scienze Geologiche 47, 253-374.

Dixon, J., Clague, D.A., Cousens, B., Monsalve, M.L., Uhl, J., 2008. Carbonatite and silicate melt metasomatism of the mantle surrounding the Hawaiian plume: evidence from volatiles, trace elements, and radiogenic isotopes in rejuvenated-stage lavas from Niihau, Hawaii. Geochemistry, Geophysics, Geosystems 9.

Eggins, S.M., Rudnick, R.L., McDonough, W.F., 1998. The composition of peridotites and their minerals: a laser-ablation ICP-MS study. Earth and Planetary Science Letters 3, 247-254.

Eggler, D.H., Furlong, K.P., 1991. Destruction of subcratonic mantle keel: the Wyoming Province. 5th Kimberlite Conference Extended Abstracts, 85-87.

Fan, W.M., Menzies, M.A., 1992. Destruction of aged lower lithosphere and accretion of asthenosphere mantle beneath eastern China. Geotectonica et Metallogenia 16, 171-180.

Foley, S.F., 2008. Rejuvenation and erosion of the cratonic lithosphere. Nature Geoscience 1, 503-510.

Foley, S.F., 2011. A reappraisal of redox melting in the Earth's mantle as a function of tectonic setting and time. Journal of Petrology 52, 1363-1391.

Frost, D.J., McCammon, C.A. 2008. The redox state of Earth's Mantle. Annual Review of Earth and Planetary Sciences 36, 389-420.

Gasperini, D., Bosch, D., Braga, R., Bondi, M., Macera, P., Morten, L., 2006. Ultramafic xenoliths from the Veneto Volcanic Province (Italy): Petrological and geochemical evidence for multiple metasomatism of the SE Alps mantle lithosphere. Geochemical Journal 40, 377-404.

Giese, P., Buness, H., 1992. Moho depth, atlas map 2, in In Blundell, D., Freeman, R., Müller, S., (Eds.), A Continent Revealed: The European Geotraverse. New York, Cambridge University Press, p. 275.

Goncharov, A.G., Ionov, D.A., Doucet, L.S, Pokhilenko, L.N., 2012. Thermal state, oxygen fugacity and C-O-H fluid speciation in cratonic lithospheric mantle: New data on peridotite xenoliths from the Udachnaya kimberlite, Siberia. Earth and Planetary Science Letters 357-358, 99-110.

Green, D.H., 2015. Experimental petrology of peridotites, including effects of water and carbon on melting in the Earth's upper mantle. Physics and Chemistry of Minerals 42, 95-122.

Green, D.H., Hibberson, W., 1970. The instability of plagioclase in peridotite at high pressure. Lithos 3, 209-221.

Green, D.H., Ringwood, A.E., 1970. Mineralogy of peridotitic compositions under upper-mantle conditions. Physics of the Earth and Planetary Interiors 3, 359-371.

Greenfield, A.M.R., Ghent, E.D., Russell, J.K., 2013. Geothermobarometry of spinel peridotites from southern British Columbia: implications for the thermal conditions in the upper mantle. Canadian Journal of Earth Sciences 50, 1019-1032.

Grégoire, M., Bell, D.R., Le Roex A.P., 2003. Garnet lherzolites from the Kaapval Carton (South Africa): trace element evidence for a metasomatic history. Journal of Petrology 44, 629-657.

Griffin, W.L., Doyle, B.J., Ryan, C.G., 1999. Layered mantle lithosphere in the Lac de Gras area, Slave Craton: composition, structure and origin. Journal of Petrology 40, 705-727.

Griffin, W.L., O'Reilly, S.Y., 2007. Cratonic lithospheric mantle: is anything subducted?. Episodes 30, 43-53.

Gudfinnsson, G.H., Presnall, D.C, 2005. Continuous gradations among primary carbonatitic, kimberlitic, melilititic, basaltic, picritic and komatiitic melts in equilibrium with garnet lherzolite at 3-8 GPa. Journal of Petrology 46, 1645-1659.

Hammouda, T., Keshav, S., 2015. Melting in the mantle in the presence of carbon: review of experiments and discussion on the origin of carbonatites. Chemical geology 418, 171-188.

Heaman, L.M., Creaser, R.A., Cookenboo, H.O., 2002. Extreme enrichment of high field strength elements in Jericho eclogite xenoliths: a cryptic record of Paleoproterozoic subduction, partial melting, and metasomatism beneath the Slave Craton, Canada. Geology 30, 507-510.

Hellebrand, E., Snow, J.E., Dick, H.J., Hofmann, A.W., 2001. Coupled major and trace elements as indicators of the extent of melting in mid-ocean-ridge peridotites. Nature 410, 677-681.

Henderson, P., 1984. General geochemical properties and abundances of the rare earth elements, in: Henderson, P. (Ed), Rare Earth Element Geochemistry. Elsevier, Amsterdam, pp. 1-32

Hirose, K., 1997. Partial melt compositions of carbonate peridotites at 3 GPa and role of CO_2 in alkali-basalt magma generation. Geophysical Research Letters 24, 2837-2840.

Hoernle, K., Zhang, Y., Graham, D., 1995. Seismic and geochemical evidence for large-scale mantle upwelling beneath the eastern Atlantic and western and central Europe. Nature 374, 34-39.

Hughes, H.S.R., McDonald, I., Faithfull, J.W., Downes, H., 2015. Trace-element abundances in the shallow lithospheric mantle of the North Atlantic Craton margin: implications for melting and metasomatism beneath Northern Scotland. Mineralogical Magazine 79, 877-907.

Ionov, D.A., 1998. Trace element composition of mantle-derived carbonates and coexisting phases in peridotite xenoliths from alkali basalts. Journal of Petrology 39, 1931-1941.

Ionov, D.A., Bodinier, J.-L., Mukasa, S.B., Zanetti, A., 2002. Mechanisms and sources of mantle metasomatism: major and trace element compositions of peridotite xenoliths from Spitsbergen in the context of numerical modelling. Journal of Petrology 43, 2219-2259.

Ionov, D.A., Doucet, L.S., Ashchepkov, I.V., 2010. Composition of the lithospheric mantle in the Siberian Craton: new constraints from fresh peridotites in the Udachnaya-East Kimberlite. Journal of Petrology 51, 2177-2210.

Jacob, D.E., Schimickler, B., Schulze, D.J., 2003. Trace element geochemistry of coesite-bearing eclogites from the Roberts Victor kimberlite, Kaapval Craton. Lithos 71, 337-351.

Karner, J.M., Papike, J.J., Sutton, S.R., Burger, P.V., Shearer, C.K., Le, L., Newville, M., Choi, Y., 2010. American Mineralogist 95, 410-413.

Kelemen, P.B., Hart, S.R., Bernstein, S., 1998. Silica enrichment in the continental upper mantle via melt/rock reaction. Earth and Planetary Science Letters 164, 387-406.

Klemme, S., Vanderlaan, S.R., Foley, S.F., Gunther, D., 1995. Experimentally determined trace and minor element partitioning between clinopyroxene and carbonatite melt under upper-mantle conditions. Earth and Planetary Science Letters 133, 439-448.

Köhler T.P., Brey, G.P., 1990. Calcium exchange between olivine and clinopyroxene calibrated as a geothermobarometer for natural peridotites from 2 to 60 kb with applications. Geochimica et Cosmochimica Acta 54, 2375-2388.

Lenoir, X. Carlos, C.J., Bodinier J.-L., Dautria J-M., 2000. Contrasting lithospheric mantle domains beneath the Massif Central (France) revealed by geochemistry of peridotite xenoliths. Earth and Planetary Science Letters 181, 359-375.

Liu, J., Scott, J.M., Martin, C.E., Pearson D.G., 2015. The longevity of Archean mantle residues in the convecting upper mantle and their role in young continent formation. Earth and Planetary Science Letters 424, 109-118.

Lustrino, M., Wilson M., 2007. The circum-Mediterranean anorogenic Cenozoic igneous province. Earth-Science Reviews 81, 1-65.

Lustrino, M., Duggen, S., Rosenberg, C.L., 2011. The central-western Mediterranean: anomalous igneous activity in an anomalous collisional tectonic setting. Earth-Science Reviews 104, 1-40.

Marchesi, C., Garrido, C.J., Bosch, D., Bodinier, J-L., Gervilla, F., Hidas, K., 2013. Mantle refertilization by melts of crustal-derived garnet pyroxenite: evidence from the Ronda peridotite massif, southern Spain. Earth and Planetary Science Letters 362, 66-75.

McCoy-West, A.J., Bennett, V.C., Puchtel, I.S., Walker, R.J., 2013. Extreme persistence of cratonic lithosphere in the southwest Pacific: Paleoproterozoic Os isotopic signatures in Zealandia. Geology 41, 231-234.

McLennan, S. M., 2001. Relationships between the trace element composition of sedimentary rocks and upper continental crust. Geochemistry Geophysics Geosystems 2, 1021-1024.

Medaris, L.G., 1999. Garnet peridotites in Eurasian high-pressure and ultrahigh-pressure terranes: a diversity of origins and thermal histories. International Geology Review 41, 799-815.

Mercier, J.-C.C., Nicolas, A., 1975. Texture and fabrics of upper-mantle peridotites as illustrated by xenoliths from basalts. Journal of Petrology 16, 454-487.

Milani, L., Beccaluva, L., Coltorti, M., 1999. Petrogenesis and evolution of the Euganean magmatic complex, north eastern Italy. European Journal of Mineralogy 11, 379-399.

Morimoto, N., 1988. Nomenclature of pyroxenes. American Mineralogist 73, 1123-1133.

Morten, L., Taylor, L.A., Durazzo, A., 1989. Spinel in harzburgite and lherzolite inclusions from the San Giovanni Ilarione Quarry, Lessini Mountains, Veneto Region, Italy. Mineralogy and Petrology 40, 73-89.

Muttoni, G., Garzanti, E., Alfonsi, L., Birilli, S., Germani, D., Lowrie, W., 2001. Motion of Africa and Adria since the Permian: paleomagnetic and paleocliamtic constraints from northern Libya. Earth and Planetary Science Letters 192, 159-174.

Niu, Y., 2004. Bulk-rock major and trace element compositions of abyssal peridotites: implications for mantle melting, melt extraction and post-melting processes beneath mid-ocean ridges. Journal of Petrology 45, 2423-2458.

O'Neill, H. St C., Wall, V.J., 1987. The olivine-orthopyroxene-spinel oxygen geobarometer, the nickel curve, and the oxygen fugacity of the Earth's upper mantle. Journal of Petrology, 28, 1169-1191.

O'Reilly, S.Y., Chen, D., Griffin, W.L., Ryan, C.G., 1977. Minor elements in olivine from spinel lherzolite xenoliths: implications for thermobarometry. Mineralogical Magazine, 61, 257-269.

Panza, G.F., Suhaldoc, P., 1990. Properties of the lithosphere in collisional belts in the Mediterranean-A review. Tectonophysics 182, 39-46.

Pearson, D.G., Shirey, S.B., Carlson, R.W., Boyd, F.R., Pokhilenko, N.P., Shimizu, N., 1995. Re-Os, Sm-Nd, and Rb-Sr isotope evidence for thick Archean lithospheric mantle beneath the Siberian craton modified by multistage metasomatism. Geochimica et Cosmochimica Acta 59, 959-997.

Pearson, D.G., Canil, D., Shirley, S.B., 2003. Mantle samples included in volcanic rocks: xenoliths and diamonds, in: Holland, H.D., Turekian, K.K. (eds) Treatise on Geochemistry-2nd edition, Elsevier, Amsterdam, 171-275.

Pelorosso, B., Bonadiman, C., Coltorti, M., Faccini, B., Melchiorre, M., Nftalos, T., Grégoire M., 2016. Pervasive, tholeiitic refertilisation and heterogeneous metasomatism in Northern Victoria Land lithospheric mantle (Antarctica). Lithos 248-251, 493-505.

Pokhilenko, N.P., Agashev, A.M., Litasov, K.D., Pokhilenko, L.N., 2015. Carbonatite metasomatism of peridotite lithospheric mantle: implications for diamond formation and carbonatite-kimberlite magmatism. Russian Geology and Geophysics 56, 280-295.

Schmid, S.M., Pfiffer, O.A., Schoenborn, G., Froitzheim, N., Kissling, E., 1997. Integrated cross section and tectonic evolution of the Alps along the eastern traverse. Results of NRP20; Deep Structure of the Swiss Alps (Eds.), 289-304.

Schmid, S.M., Bernoulli, D., Fugenschuh, B., Matenco, L., Schefer, S., Schuster, R., Tschler, M., Ustaszewski, K., 2008. The Alpine-Carpathian-Dinaridic orogenic system: correlation and evolution of tectonic units. Swiss Journal of Geosciences 101, 139-183.

Scott, J.M., Waight, T.E., van der Meer, Q.H.A., Palin, J.M., Cooper, A.F., Münker, C., 2014a. Metasomatized ancient lithospheric mantle beneath the young Zealandia microcontinent and its role in HIMU-like intraplate magmatism. Geochemistry, Geophysics, Geosystems 15, 3477- 3501.

Scott, J.M., Hodgkinson, A., Palin, J.M, Waight, T.E., van der Meer, Q.H.A., Cooper, A.F., 2014b. Ancient melt depletion overprinted by young carbonatitic meatsomatism in the New Zealand lithospheric mantle. Contributions to Mineralogy and Petrology 167, 1-17.

Scott, J.M., Liu, J., Pearson, D.G., Waight, T.E., 2016. Mantle depletion and metasomantism recorded in orthopyroxene in highly depleted peridotites. Chemical Geology 441, 280-291.

Sen, G., Frey, F.A., Schimizu, N., Leeman, W.P., 1993. Evolution of the lithosphere beneath Oahu, Hawaii: rare earth element abundances in mantle xenoliths. Earth and Planetary Science Letters 119, 53-69.

Siena, F., Coltorti, M., 1989. Lithospheric mantle evolution: evidences from ultramafic xenoliths in the Lessinean volcanics (Northern Itlay). Chemical Geology 77, 347-364.

Siena, F., Coltorti, M., 1993. Thermobarometric evolution and metasomatic processes of upper mantle in different tectonic settings: evidence from spinel peridotite xenoliths. European Journal of Mineralogy 5, 1073-1090.

Simon, N.S.C., Irvine, G.J., Davies, G.R., Pearson, D.G., Carlson, R.W., 2003. The origin of garnet and clinopyroxene in "depleted" Kaapval peridotites. Lithos 71, 289-322.

Simon, N.S.C., Carlson R. W., Pearson, D.G., Davies G.R., 2007. The origin and the evolution of the Kaapval cratonic lithospheric mantle. Journal of Petrology 48, 589-625.

Spengler, D., Van Roermund, H.L.M., Drury, M.R., Ottolini, L., Mason, P.R.D., Davies, G.R., 2006. Deep origin and hot melting of an Archaean orogenic peridotite massif in Norway. Nature 440, 913-917.

Stagno, V., Frost, D.J., 2010. Carbon speciation in the asthenosphere: experimental measurements of the redox conditions at which carbonate-bearing melts coexist with graphite or diamond in peridotite assemblages. Earth and Planetary Science Letters 300, 72-84.

Streckeisen, A., 1974. Classification and nomenclature of plutonic rocks recommendations of the IUGS subcommission on the systematics of Igneous Rocks. Geologische Rundschau 63, 773-786.

Sun, J., Liu C.-Z., Wu F.-Y., Yang Y.-H., Chu Z.-Y., 2012. Metasomatic origin of clinopyroxene in Archean mantle xenoliths from Hebi, North China Craton: trace-element and Sr-isotope constraints. Chemical Geology 328, 123-136.

Sun, C., Liang, Y., 2014. An assessment of sub-solidus re-equilibration on REE distribution among mantle minerals olivine, orthopyroxene, clinopyroxene, and garnet in peridotites. Chemical Geology 372, 80-91.

Sun, S.S., McDonough, W.F., 1989. Chemical and isotopic systematics of oceanic basalts: implications for mantle composition and processes. In: Saunders, A.D, Norry, M.J. (Eds). Magmatism in the Oceanic Basins. Geological Society London, Special Publications 42, 313-346.

Takahashi, E., 1987. Origin of basaltic magmas-implications from peridotite melting experiments and an olivine fractionation model. Bulletin of the Volcanological Society of Japan 30, 17-40.

Taylor, W.R., 1998. An experimental test of some geothermometer and geobarometer formulations for upper mantle peridotites with application to the thermobarometry of fertile lherzolite and garnet websterite. Neues Jahrbuch für Mineralogie-Abhandlungen 172, 381-408.

Tang, Y.J., Zhang, H.F., Ying, J.F., Zhang, J., Liu, X.M., 2008. Refertilization of ancient lithospheric mantle beneath the central North China Craton: evidence from petrology and geochemistry of peridotite xenoliths. Lithos 101, 435-452.

Tang, Y.J., Zhang, H.F., Deloule, E., Su, B.X., Ying, J.F., Xiao, Y., Hu., Y., 2012. Slab-derived lithium isotopic signatures in mantle xenoliths from northeastern North China Craton. Lithos 149, 79-90.

Tang, Y.J., Zhang, H.F., Ying, J.F., Su, B.X., 2013. Widespread refertilization of cratonic and circum-cratonic lithospheric mantle. Earth-Science Reviews 118, 45-68.

Tang, M., McDonough, W.F., Ash, R.D., 2017. Europium and strontium anomalies in the MORB source mantle. Geochimica et Cosmochimica Acta 197, 132-141.

von Blankenburg, F., Davies, J.H., 1995. Slab breakoff: amodel for syncollisional magmatism and tectonics in the Alps. Tectonics 14, 120-131.

Walter, M.J., 2003. Melt extraction and compositional variability in mantle lithosphere. The Mantle & Core. Treatise of Geochemistry-2nd edition. Elsevier, Amsterdam, 363-394.

Wells, P.R.A., 1977. Pyroxene thermometry in simple and complex systems. Contributions to Mineralogy and Petrology 62, 129-139.

Wilson, M., Patterson, R., 2001. Intraplate magmatism related to short-wavelength convective instabilities in the upper mantle: evidence from the Tertiary Quaternary volcanic province of western and central Europe. Geological Society of America Special Paper 352, 37-58.

Wood, B.J., Banno, S., 1973. Garnet-orthopyroxene and orthopyroxene-clinopyroxene relationship in simple and complex system. Contributions to Mineralogy and Petrology 42, 109-124.

Zampieri, D., 1995. Tertiary extension in the southern Trento Platform, southern Alps, Italy. Tectonics 14, 645-657.

Zhang, H.F., Goldstein, S.L., Zhou, X.H., Sun, M., Cai, Y., 2009a. Comprehensive refertilization of lithospheric mantle beneath the North China Craton: further Os-Sr-Nd isotopic constraints. Journal of the Geological Society, London 166, 249-259.

Zhang, H.F., Sun, Y.L., Tang, Y.J., Xiao, Y., Zhang, W.H., Zhao, X.M., Santosh, M., Menzies, M.A., 2012. Melt-peridotite interaction in the Pre-Cambrian mantle beneath the western North China Craton: petrology, geochemistry and Sr, Nd and Re isotopes. Lithos 149, 100-114.

APPENDIX A4

Table A4.1: Representative major element (wt.%) compositions of olivine from Marosticano (MG) spinel peridotites and host lava.

Sample	**MG1**	**MG1**	**MG1**	**MG1**	**MG1**	**MG1**	**MG1**	**MG1**	**MG1**	**MG6**	**MG6**	**MG6**	**MG6**	**MG6**	**MG6**	**MG6**	**MG16**	**MG16**	**MG13**
	Lh	Lh	Lh	Lh	Lh	Lh	Lh	Lh	Lh	Lh	Lh	Lh	Lh	Lh	Lh	Lh	Lh	Lh	Hz
SiO_2	40.87	41.08	41.04	39.82	40.19	40.71	40.95	40.68	40.95	40.56	41.21	41.00	40.91	40.94	41.20	40.85	40.68	40.98	40.57
FeO	7.83	7.84	8.28	8.08	7.95	7.91	8.05	7.76	7.75	8.34	8.47	8.32	8.62	8.62	8.62	8.38	7.83	7.93	8.84
MnO	0.15	0.09	0.12	0.12	0.14	0.11	0.13	0.09	0.11	0.15	0.13	0.12	0.12	0.12	0.12	0.13	0.13	0.10	0.14
MgO	51.58	51.25	51.07	51.84	51.74	51.08	51.40	51.42	50.84	51.24	50.74	50.94	50.70	50.75	50.48	50.26	51.74	51.69	50.80
CaO	0.04	0.06	0.05	0.05	0.09	0.07	0.04	0.04	0.33	0.03	0.07	0.06	0.04	0.08	0.07	0.07	0.06	0.03	0.04
NiO	0.41	0.46	0.33	0.43	0.34	0.40	0.41	0.41	0.40	0.39	0.38	0.37	0.39	0.36	0.39	0.40	0.41	0.41	0.43
Tot	100.96	100.83	100.92	100.42	100.61	100.44	101.04	100.47	100.48	100.77	101.08	100.88	100.83	100.95	100.92	100.17	100.89	101.14	100.85
Si	0.99	0.99	0.99	0.97	0.98	0.99	0.99	0.99	0.99	0.98	0.99	0.99	0.99	0.99	1.00	1.00	0.98	0.99	0.98
Fe	0.16	0.16	0.17	0.16	0.16	0.16	0.16	0.16	0.16	0.17	0.17	0.17	0.17	0.17	0.17	0.17	0.16	0.16	0.18
Mn	0.00	0.00	0.00	0.00	0.00	0.00	0.00	0.00	0.00	0.00	0.00	0.00	0.00	0.00	0.00	0.00	0.00	0.00	0.00
Mg	1.86	1.84	1.84	1.88	1.87	1.85	1.85	1.86	1.84	1.85	1.83	1.84	1.83	1.83	1.82	1.82	1.86	1.86	1.84
Ni	0.01	0.01	0.01	0.01	0.01	0.01	0.01	0.01	0.01	0.01	0.01	0.01	0.01	0.01	0.01	0.01	0.01	0.01	0.01
Fo	92.15	92.09	91.66	91.96	92.06	92.01	91.92	92.19	92.12	91.63	91.44	91.60	91.29	91.30	91.26	91.44	92.17	92.07	91.10

Abbreviations: Lh= lherzolite; Hz= harzburgite; Bsn= basanite. Fo= 100 x $Mg/(Mg+Fe)_{mol}$

Table A4.1 (continued): Representative major element (wt.%) compositions of olivine from Marosticano (MG) spinel peridotites and host lava.

Sample	MG13	MG13	MG13	MG13	MG13	MG13	MG13	MG13	MG13	MG14	MG14	MG14	MG14	MG14
	Hz	Hz	Hz	Hz	Hz	Hz	Hz	Hz	Hz	Hz	Hz	Hz	Hz	Hz
SiO_2	40.87	40.18	41.15	40.80	40.80	40.79	40.71	40.47	40.38	41.75	41.30	40.31	40.10	41.39
FeO	8.87	8.88	9.35	8.93	9.14	8.87	9.01	9.06	8.84	7.33	7.43	7.55	7.68	7.57
MnO	0.11	0.11	0.18	0.15	0.15	0.08	0.14	0.12	0.10	0.13	0.09	0.13	0.10	0.11
MgO	51.11	50.65	50.24	50.26	50.23	50.80	50.74	50.72	50.53	50.88	51.01	51.31	52.05	51.12
CaO	0.04	0.04	0.07	0.03	0.08	0.04	0.04	0.05	0.03	0.10	0.04	0.07	0.13	0.13
NiO	0.42	0.45	0.41	0.37	0.34	0.39	0.37	0.36	0.40	0.42	0.42	0.35	0.40	0.37
Tot	101.50	100.34	101.46	100.58	100.83	101.03	101.03	100.83	100.30	100.63	100.31	99.82	100.48	100.71
Si	0.99	0.98	0.99	0.99	0.99	0.99	0.99	0.98	0.99	1.01	1.00	0.98	0.97	1.00
Fe	0.18	0.18	0.19	0.18	0.19	0.18	0.18	0.18	0.18	0.15	0.15	0.15	0.16	0.15
Mn	0.00	0.00	0.00	0.00	0.00	0.00	0.00	0.00	0.00	0.00	0.00	0.00	0.00	0.00
Mg	1.84	1.84	1.81	1.82	1.82	1.83	1.83	1.84	1.84	1.83	1.84	1.87	1.88	1.84
Ni	0.01	0.01	0.01	0.01	0.01	0.01	0.01	0.01	0.01	0.01	0.01	0.01	0.01	0.01
Fo	91.13	91.04	90.54	90.93	90.74	91.08	90.94	90.89	91.06	92.52	92.44	92.37	92.35	92.33

Abbreviations: Lh= lherzolite; Hz= harzburgite; Bsn= basanite. Fo= 100 x $Mg/(Mg+Fe)_{mol}$

Table A4.2: Representative major element (wt.%) compositions of orthopyroxene from Marosticano (MG) spinel peridotites.

Sample	MG1	MG1	MG1	MG1	MG1	MG1	MG1	MG1	MG1	MG1	MG1	MG1	MG6	MG6	MG6	MG6	MG6	MG6	MG6	MG6
	Lh	Lh	Lh	Lh	Lh	Lh	Lh	Lh	Lh	Lh	Lh	Lh	Lh	Lh	Lh	Lh	Lh	Lh	Lh	Lh
SiO_2	57.00	56.40	56.30	56.24	56.54	54.64	56.54	56.55	56.98	56.57	57.03	56.61	55.97	56.58	56.25	56.73	55.31	56.42	53.55	55.24
Al_2O_3	2.23	2.62	2.51	2.54	2.48	2.09	2.50	2.35	2.35	2.32	2.37	2.20	2.53	2.55	2.64	2.56	2.73	2.40	4.18	3.38
Fe_2O_3	0.22	0.46	0.58	0.72	0.28	1.16	0.45	0.08	0.29	0.42	0.18	0.33	0.62	0.28	0.67	0.37	0.92	0.30	0.72	0.50
FeO	4.93	4.79	4.64	4.53	4.88	3.92	4.73	4.93	4.94	4.87	5.09	4.83	4.97	5.43	4.95	5.09	4.78	5.09	5.04	5.20
MnO	0.11	0.06	0.09	0.11	0.05	0.14	0.12	0.13	0.07	0.08	0.08	0.10	0.14	0.14	0.13	0.13	0.11	0.07	0.10	0.11
MgO	35.18	35.25	35.26	35.01	34.78	35.62	35.25	34.71	35.22	35.26	35.17	35.15	35.07	34.82	35.39	35.13	35.12	34.89	33.35	33.42
CaO	0.53	0.57	0.60	0.52	0.51	0.44	0.52	0.51	0.54	0.63	0.54	0.50	0.56	0.50	0.60	0.60	0.61	0.56	0.72	1.74
Na_2O	0.08	0.06	0.13	0.32	0.16	0.08	0.11	0.07	0.10	0.03	0.04	0.08	0.07	0.04	0.04	0.06	0.09	0.05	0.11	0.07
Cr_2O_3	0.40	0.56	0.52	0.50	0.52	0.35	0.48	0.43	0.42	0.37	0.43	0.36	0.36	0.37	0.43	0.50	0.50	0.29	1.24	0.80
Tot	100.74	100.85	100.69	100.57	100.28	98.50	100.78	99.82	100.96	100.63	101.01	100.19	100.33	100.75	101.13	101.21	100.24	100.09	99.03	100.52
Si	1.94	1.92	1.92	1.92	1.93	1.89	1.92	1.94	1.94	1.93	1.94	1.94	1.91	1.93	1.91	1.92	1.89	1.93	1.86	1.90
Al	0.09	0.11	0.10	0.10	0.10	0.09	0.10	0.10	0.09	0.09	0.10	0.09	0.10	0.10	0.11	0.10	0.11	0.10	0.17	0.14
Fe III	0.01	0.01	0.02	0.02	0.01	0.03	0.01	0.00	0.01	0.01	0.01	0.01	0.02	0.01	0.02	0.01	0.02	0.01	0.02	0.01
Fe II	0.14	0.14	0.13	0.13	0.14	0.11	0.14	0.14	0.14	0.14	0.14	0.14	0.14	0.16	0.14	0.14	0.14	0.15	0.15	0.15
Mn	0.00	0.00	0.00	0.00	0.00	0.00	0.00	0.00	0.00	0.00	0.00	0.00	0.00	0.00	0.00	0.00	0.00	0.00	0.00	0.00
Mg	1.78	1.79	1.79	1.78	1.77	1.84	1.79	1.78	1.78	1.79	1.78	1.79	1.79	1.77	1.79	1.78	1.79	1.78	1.73	1.71
Ca	0.02	0.02	0.02	0.02	0.02	0.02	0.02	0.02	0.02	0.02	0.02	0.02	0.02	0.02	0.02	0.02	0.02	0.02	0.03	0.06
Na	0.01	0.00	0.01	0.02	0.01	0.01	0.01	0.01	0.01	0.00	0.00	0.01	0.01	0.00	0.00	0.00	0.01	0.00	0.01	0.01
Cr	0.01	0.02	0.01	0.01	0.01	0.01	0.01	0.01	0.01	0.01	0.01	0.01	0.01	0.01	0.01	0.01	0.01	0.01	0.03	0.02
mg#	92.41	92.29	92.33	92.24	92.31	92.59	92.38	92.51	92.31	92.23	92.24	92.39	91.79	91.57	91.82	91.98	91.65	92.02	91.16	91.26

Abbreviations: Lh= lherzolite; Hz= harzburgite. mg#= 100 x $Mg/(Mg+Fe)_{mol}$

Table A4.2 (continued): Representative major element (wt.%) compositions of orthopyroxene from Marosticano (MG) spinel peridotites.

Sample	MG6	MG16	MG16	MG16	MG16	MG16	MG16	MG16	MG16	MG16	MG16	MG16	MG13	MG13	MG13	MG13	MG13	MG13	MG13	MG13
	Lh	Lh	Lh	Lh	Lh	Lh	Lh	Lh	Lh	Lh	Lh	Lh	Hz	Hz	Hz	Hz	Hz	Hz	Hz	Hz
SiO_2	56.65	57.03	57.42	57.11	57.16	56.87	57.20	56.80	56.72	57.04	57.03	56.89	56.57	56.25	56.36	56.82	56.57	56.72	56.53	57.23
Al_2O_3	2.43	1.88	1.82	1.76	2.15	1.74	1.68	3.01	2.27	1.74	1.74	1.75	2.29	2.29	2.34	1.78	2.20	1.97	2.08	1.93
Fe_2O_3	0.46	0.42	0.15	0.27	0.37	0.48	0.15	0.08	0.44	0.23	0.09	0.54	0.25	0.44	0.31	0.24	0.36	0.27	0.19	0.18
FeO	5.15	4.68	4.84	4.80	4.77	4.56	4.79	5.03	4.65	4.88	4.89	4.57	5.45	5.34	5.47	5.60	5.43	5.38	5.41	5.68
MnO	0.15	0.15	0.11	0.12	0.07	0.12	0.10	0.13	0.13	0.09	0.10	0.09	0.07	0.11	0.14	0.11	0.11	0.15	0.13	0.09
MgO	35.15	35.48	35.22	35.34	35.63	35.66	35.28	34.51	34.75	35.13	34.93	35.66	34.65	34.84	34.58	34.69	34.92	34.85	34.60	34.92
CaO	0.51	0.54	0.59	0.55	0.55	0.53	0.49	0.71	1.30	0.61	0.55	0.58	0.51	0.50	0.43	0.55	0.38	0.47	0.53	0.50
Na_2O	0.08	0.12	0.13	0.09	0.07	0.08	0.09	0.13	0.14	0.10	0.11	0.11	0.09	0.06	0.09	0.08	0.08	0.07	0.05	0.06
Cr_2O_3	0.29	0.45	0.46	0.48	0.38	0.42	0.50	0.63	0.59	0.39	0.39	0.49	0.50	0.50	0.49	0.52	0.46	0.50	0.54	0.39
Tot	100.89	100.76	100.74	100.53	101.18	100.48	100.28	101.07	101.00	100.21	99.85	100.70	100.40	100.33	100.24	100.40	100.52	100.40	100.06	100.98
Si	1.93	1.94	1.95	1.95	1.94	1.94	1.96	1.93	1.93	1.95	1.96	1.93	1.94	1.93	1.93	1.95	1.93	1.94	1.94	1.95
Al	0.10	0.08	0.07	0.07	0.09	0.07	0.07	0.12	0.09	0.07	0.07	0.07	0.09	0.09	0.10	0.07	0.09	0.08	0.08	0.08
Fe III	0.01	0.01	0.00	0.01	0.01	0.01	0.00	0.00	0.01	0.01	0.00	0.01	0.01	0.01	0.01	0.01	0.01	0.01	0.01	0.01
Fe II	0.15	0.13	0.14	0.14	0.14	0.13	0.14	0.14	0.13	0.14	0.14	0.13	0.16	0.15	0.16	0.16	0.16	0.15	0.16	0.16
Mn	0.00	0.00	0.00	0.00	0.00	0.00	0.00	0.00	0.00	0.00	0.00	0.00	0.00	0.00	0.00	0.00	0.00	0.00	0.00	0.00
Mg	1.78	1.80	1.79	1.80	1.80	1.81	1.80	1.75	1.76	1.79	1.79	1.81	1.77	1.78	1.77	1.77	1.78	1.78	1.77	1.77
Ca	0.02	0.02	0.02	0.02	0.02	0.02	0.02	0.03	0.05	0.02	0.02	0.02	0.02	0.02	0.02	0.02	0.01	0.02	0.02	0.02
Na	0.01	0.01	0.01	0.01	0.01	0.01	0.01	0.01	0.01	0.01	0.01	0.01	0.01	0.00	0.01	0.01	0.01	0.01	0.00	0.00
Cr	0.01	0.01	0.01	0.01	0.01	0.01	0.01	0.02	0.02	0.01	0.01	0.01	0.01	0.01	0.01	0.01	0.01	0.01	0.02	0.01
mg#	91.78	92.54	92.63	92.55	92.51	92.65	92.71	92.33	92.40	92.45	92.59	92.56	91.55	91.48	91.42	91.37	91.49	91.66	91.67	91.39

Abbreviations: Lh= lherzolite; Hz= harzburgite. mg#= 100 x $Mg/(Mg+Fe)_{mol}$

Table A4.2 (continued): Representative major element (wt.%) compositions of orthopyroxene from Marosticano (MG) spinel peridotites.

Sample	MG13	MG13	MG13	MG14	MG14	MG14	MG14	MG14	MG14
	Hz	Hz	Hz	Hz	Hz	Hz	Hz	Hz	Hz
SiO_2	57.11	56.81	57.05	56.51	56.32	55.21	56.58	57.20	56.13
Al_2O_3	1.87	1.88	1.98	2.40	2.39	2.27	2.60	2.38	2.16
Fe_2O_3	0.19	0.45	0.25	0.60	0.52	1.49	0.50	0.19	0.74
FeO	5.48	5.45	5.56	4.42	4.53	3.70	4.22	4.84	4.29
MnO	0.07	0.12	0.13	0.16	0.11	0.12	0.06	0.12	0.14
MgO	34.93	35.15	34.92	35.59	35.39	36.56	34.61	35.20	35.72
CaO	0.45	0.41	0.49	0.58	0.60	0.62	1.49	0.64	0.51
Na_2O	0.08	0.09	0.07	0.09	0.06	0.06	0.25	0.09	0.08
Cr_2O_3	0.48	0.39	0.45	0.42	0.37	0.39	0.51	0.35	0.42
Tot	100.68	100.76	100.91	100.78	100.30	100.42	100.85	101.03	100.18
Si	1.95	1.94	1.94	1.92	1.92	1.88	1.92	1.94	1.92
Al	0.08	0.08	0.08	0.10	0.10	0.09	0.10	0.10	0.09
Fe III	0.01	0.01	0.01	0.02	0.01	0.04	0.01	0.01	0.02
Fe II	0.16	0.16	0.16	0.13	0.13	0.11	0.12	0.14	0.12
Mn	0.00	0.00	0.00	0.00	0.00	0.00	0.00	0.00	0.00
Mg	1.78	1.79	1.77	1.80	1.80	1.85	1.75	1.78	1.82
Ca	0.02	0.02	0.02	0.02	0.02	0.02	0.05	0.02	0.02
Na	0.01	0.01	0.01	0.01	0.00	0.00	0.02	0.01	0.01
Cr	0.01	0.01	0.01	0.01	0.01	0.01	0.01	0.01	0.01
mg#	91.65	91.39	91.46	92.67	92.59	92.62	92.89	92.58	92.68

Abbreviations: Lh= lherzolite; Hz= harzburgite. mg#= 100 x $Mg/(Mg+Fe)_{mol}$

Table A4.3: Representative major element (wt.%) compositions of clinopyroxene from Marosticano (MG) spinel peridotites and host lava.

Sample	**MG1**	**MG1**	**MG1**	**MG1**	**MG1**	**MG1**	**MG6**	**MG6**	**MG6**	**MG16**	**MG16**	**MG16**	**MG16**	**MG16**	**MG16**	**MG13**	**MG13**	**MG14**	**MG14**	**MG14**
Host rock	Lh	Lh	Lh	Lh	Lh	Lh	Lh	Lh	Lh	Lh	Lh	Lh	Lh	Lh	Lh	Hz	Hz	Hz	Hz	Hz
SiO_2	53.61	53.45	52.88	53.30	52.71	53.41	53.72	53.29	53.22	55.30	53.67	53.60	53.70	53.52	53.03	54.20	54.84	52.16	52.72	52.96
TiO_2	0.11	0.22	0.39	0.10	0.15	0.12	0.07	0.10	0.06	0.04	0.03	0.04	0.07	0.06	0.07	0.58	0.50	0.04	0.03	0.12
Al_2O_3	3.38	1.91	2.01	3.79	4.38	3.92	2.83	3.18	3.19	4.53	2.36	2.54	2.42	1.73	3.11	0.82	0.63	3.12	2.56	3.79
Fe_2O_3	0.47	0.27	0.58	0.44	0.74	0.45	0.50	0.53	0.37	-1.01	0.20	0.17	-0.08	0.29	0.61	0.52	-0.05	0.60	0.73	0.50
FeO	2.03	1.99	1.76	2.17	1.91	2.08	2.23	2.03	2.06	3.85	2.65	2.74	2.71	2.51	2.02	2.20	2.92	1.90	1.91	2.15
MgO	16.63	17.73	17.70	16.37	15.76	16.21	17.25	16.79	16.73	17.02	18.11	17.86	17.75	18.10	17.86	19.54	19.20	17.93	18.44	17.39
CaO	21.25	22.08	22.66	20.76	20.58	20.80	21.83	22.01	21.86	19.60	21.27	21.14	21.38	21.49	19.97	20.82	20.50	22.23	21.80	20.40
Na_2O	1.41	0.62	0.60	1.52	1.89	1.62	1.00	1.08	1.03	0.76	0.55	0.61	0.49	0.53	1.20	0.56	0.52	0.35	0.49	1.18
Cr_2O_3	1.02	1.54	1.56	1.18	1.44	1.39	0.72	0.93	0.95	1.14	1.53	1.01	1.57	1.20	1.64	0.89	1.18	1.22	1.37	1.52
Tot	99.95	99.85	100.17	99.64	99.60	100.04	100.23	100.02	99.52	101.48	100.40	99.79	100.06	99.52	99.59	100.33	100.27	99.61	100.11	100.05
Si	1.93	1.94	1.91	1.93	1.91	1.93	1.94	1.93	1.93	1.97	1.94	1.94	1.95	1.95	1.92	1.95	1.98	1.89	1.90	1.91
Ti	0.00	0.01	0.01	0.00	0.00	0.00	0.00	0.00	0.00	0.00	0.00	0.00	0.00	0.00	0.00	0.02	0.01	0.00	0.00	0.00
Al	0.14	0.08	0.09	0.16	0.19	0.17	0.12	0.14	0.14	0.19	0.10	0.11	0.10	0.07	0.13	0.04	0.03	0.13	0.11	0.16
Fe III	0.01	0.01	0.02	0.01	0.02	0.01	0.01	0.01	0.01	-0.03	0.01	0.01	0.00	0.01	0.02	0.01	0.00	0.02	0.02	0.01
Fe II	0.06	0.06	0.05	0.07	0.06	0.06	0.07	0.06	0.06	0.12	0.08	0.08	0.08	0.08	0.06	0.07	0.09	0.06	0.06	0.07
Mg	0.89	0.96	0.96	0.88	0.85	0.87	0.93	0.90	0.91	0.91	0.97	0.97	0.96	0.98	0.96	1.05	1.03	0.97	0.99	0.93
Ca	0.82	0.86	0.88	0.81	0.80	0.80	0.84	0.85	0.85	0.75	0.82	0.82	0.83	0.84	0.77	0.80	0.79	0.87	0.84	0.79
Na	0.10	0.04	0.04	0.11	0.13	0.11	0.07	0.08	0.07	0.05	0.04	0.04	0.03	0.04	0.08	0.04	0.04	0.03	0.03	0.08
Cr	0.03	0.04	0.05	0.03	0.04	0.04	0.02	0.03	0.03	0.03	0.04	0.03	0.05	0.03	0.05	0.03	0.03	0.04	0.04	0.04
mg#	92.22	93.33	93.10	91.79	91.38	91.95	91.85	92.12	92.47	91.44	91.89	91.62	92.33	92.01	92.37	92.76	92.26	92.75	92.57	92.12

Abbreviations: Lh= lherzolite; Hz= harzburgite. mg#= 100 x $Mg/(Mg+Fe)_{mol}$

Table A4.3 (continued): Representative major element (wt.%) compositions of clinopyroxene from Marosticano (MG) spinel peridotites and host lava.

Sample	**MG14**	**MG14**	**MG14**	**MG14**
Host rock	Hz	Hz	Hz	Hz
SiO_2	53.69	52.47	53.42	53.50
TiO_2	0.11	0.13	0.06	0.10
Al_2O_3	2.18	3.31	2.78	1.94
Fe_2O_3	0.21	0.35	0.12	0.48
FeO	2.17	2.36	2.60	2.20
MgO	18.23	17.76	17.87	18.59
CaO	21.66	20.75	20.97	21.71
Na_2O	0.52	0.68	0.62	0.48
Cr_2O_3	1.33	1.34	1.19	1.08
Tot	100.13	99.17	99.68	100.09
Si	1.94	1.91	1.94	1.93
Ti	0.00	0.00	0.00	0.00
Al	0.09	0.14	0.12	0.08
Fe III	0.01	0.01	0.00	0.01
Fe II	0.07	0.07	0.08	0.07
Mg	0.98	0.96	0.97	1.00
Ca	0.84	0.81	0.82	0.84
Na	0.04	0.05	0.04	0.03
Cr	0.04	0.04	0.03	0.03
mg#	93.18	92.11	92.13	92.52

Abbreviations: Lh= lherzolite; Hz= harzburgite. mg#= 100 x $Mg/(Mg+Fe)_{mol}$

Table A4.4: Representative major element (wt.%) compositions of spinel from Marosticano (MG) spinel peridotites.

Sample	MG1	MG1	MG6	MG6	MG16	MG16	MG16	MG16	MG13	MG13	MG13	MG13	MG13	MG14	MG14	MG14	MG14	MG14
	Lh	Lh	Lh	Lh	Lh	Lh	Lh	Lh	Hz	Hz	Hz	Hz	Hz	Hz	Hz	Hz	Hz	Hz
TiO_2	0.11	0.58	0.08	0.07	0.06	0.06	0.09	0.07	2.52	3.07	1.78	1.51	0.04	0.06	0.02	0.05	0.07	0.03
Al_2O_3	32.50	31.98	41.76	41.52	25.64	25.35	25.68	26.28	17.97	15.41	26.64	22.21	24.89	34.30	34.43	35.60	35.31	35.17
Fe_2O_3	5.84	6.64	2.37	2.63	5.05	5.69	4.99	4.37	5.79	5.32	5.19	7.10	7.73	4.56	4.16	3.86	4.31	3.89
FeO	10.28	11.36	8.66	8.99	11.42	11.30	11.77	12.33	14.26	14.91	13.46	9.19	10.97	10.08	10.61	10.20	10.34	10.14
MgO	17.79	17.31	19.46	19.40	16.13	16.16	15.79	15.41	14.68	14.56	16.08	17.68	15.92	18.06	17.73	18.09	18.00	17.91
NiO	0.16	0.28	0.20	0.18	0.21	0.16	0.17	0.18	0.18	0.17	0.20	0.17	0.18	0.24	0.24	0.26	0.26	0.25
Cr_2O_3	34.35	33.50	27.15	27.72	42.20	42.08	41.04	40.88	44.64	47.13	37.59	40.57	38.77	34.02	34.26	33.00	32.99	32.78
Tot	101.10	101.69	99.74	100.55	100.79	100.86	99.60	99.53	100.23	101.23	101.05	98.55	98.54	101.38	101.51	101.13	101.33	100.26
Ti	0.00	0.01	0.00	0.00	0.00	0.00	0.00	0.00	0.06	0.07	0.04	0.03	0.00	0.00	0.00	0.00	0.00	0.00
Al	1.09	1.08	1.36	1.34	0.90	0.89	0.91	0.93	0.66	0.56	0.93	0.79	0.89	1.14	1.15	1.18	1.17	1.18
FeIII	0.13	0.14	0.05	0.05	0.11	0.13	0.11	0.10	0.13	0.12	0.12	0.16	0.18	0.10	0.09	0.08	0.09	0.08
Fe II	0.24	0.27	0.20	0.21	0.28	0.28	0.29	0.31	0.37	0.39	0.33	0.23	0.28	0.24	0.25	0.24	0.24	0.24
Mg	0.76	0.74	0.80	0.79	0.71	0.71	0.71	0.69	0.68	0.67	0.71	0.80	0.72	0.76	0.75	0.76	0.75	0.76
Ni	0.00	0.01	0.00	0.00	0.01	0.00	0.00	0.00	0.00	0.00	0.01	0.00	0.00	0.01	0.01	0.01	0.01	0.01
Cr	0.77	0.76	0.59	0.60	0.99	0.99	0.97	0.97	1.09	1.16	0.88	0.97	0.93	0.76	0.76	0.73	0.73	0.74
mg#	66.29	63.15	75.87	74.84	63.57	62.89	62.67	62.18	56.61	56.19	60.58	65.92	60.27	68.73	68.14	69.63	68.65	69.46
cr#	41.48	41.26	30.37	30.91	52.47	52.67	51.73	51.05	62.47	67.23	48.61	55.07	51.07	39.94	40.02	38.34	38.52	38.46

Abbreviations: Lh= lherzolite; Hz= harzburgite. mg#= 100 x $Mg/(Mg+Fe)_{mol}$ cr#=100 x $Cr/(Cr+Al)_{mol}$

Table A4.5: Trace element (ppm) abundances of representative orthopyroxenes in MG spinel peridotites.

Sample	MG1	MG1	MG6	MG6	MG16	MG16	MG13	MG13	MG14	MG14	MG14
	Lh	Lh	Lh	Lh	Lh	Lh	Hz	Hz	Hz	Hz	Hz
Cs	0.01	b.d.l.	b.d.l.	0.02	b.d.l.	b.d.l.	0.02	0.01	b.d.l.	b.d.l.	b.d.l.
Rb	0.05	0.02	b.d.l.	0.04	b.d.l.	0.03	0.88	0.02	b.d.l.	b.d.l.	b.d.l.
Ba	0.29	0.01	0.03	0.33	0.40	0.12	1.93	0.11	0.01	0.01	0.01
Th	0.07	0.02	0.04	0.32	0.07	0.01	0.07	0.02	0.10	0.25	0.04
U	0.02	0.01	0.03	0.24	0.01	b.d.l.	0.01	0.01	0.01	0.02	0.01
Nb	0.05	0.02	0.06	0.32	0.09	0.04	0.60	0.08	0.01	0.01	b.d.l.
Ta	0.01	b.d.l.	b.d.l.	0.03	0.01	b.d.l.	0.02	0.01	b.d.l.	b.d.l.	b.d.l.
La	0.09	0.01	0.05	0.44	0.21	0.02	0.21	0.03	0.07	0.05	0.03
Ce	0.20	0.06	0.08	0.61	0.84	0.12	0.69	0.10	0.16	0.14	0.09
Pr	0.02	b.d.l.	b.d.l.	0.05	0.14	0.03	0.08	0.02	0.02	0.02	0.01
Sr	1.03	0.24	0.63	5.43	2.32	0.80	3.72	0.59	0.79	0.59	0.42
Nd	0.08	0.02	0.01	0.07	0.51	0.16	0.29	0.08	0.05	0.04	0.06
Zr	0.69	0.92	0.52	1.27	1.86	4.01	3.05	2.59	0.06	0.11	0.10
Hf	0.02	b.d.l.	0.01	0.07	0.04	0.03	0.03	0.03	b.d.l.	b.d.l.	b.d.l.
Sm	0.01	b.d.l.	0.01	0.05	0.09	0.06	0.07	0.02	0.01	0.02	b.d.l.
Eu	b.d.l.	0.01	b.d.l.	0.01	0.03	0.02	0.03	0.01	b.d.l.	b.d.l.	b.d.l.
Gd	0.01	0.01	0.02	0.09	0.09	0.08	0.08	0.05	0.01	0.01	0.03
Tb	b.d.l.	b.d.l.	b.d.l.	b.d.l.	0.01	0.01	0.01	0.01	b.d.l.	b.d.l.	b.d.l.
Dy	0.02	0.03	0.05	0.09	0.05	0.11	0.10	0.10	0.01	0.01	0.01
Y	0.21	0.25	0.30	0.68	0.44	0.72	0.61	0.55	0.07	0.11	0.10
Ho	b.d.l.	0.01	0.01	0.01	0.02	0.03	0.02	0.02	b.d.l.	0.01	b.d.l.
Er	0.02	0.03	0.03	0.08	0.04	0.11	0.07	0.06	0.01	0.01	0.02
Tm	b.d.l.	0.01	0.01	0.02	0.01	0.02	0.01	0.02	b.d.l.	b.d.l.	0.01
Yb	0.07	0.06	0.07	0.20	0.05	0.12	0.12	0.10	0.02	0.03	0.02
Lu	0.01	0.01	0.02	0.02	0.01	0.02	0.02	0.02	b.d.l.	b.d.l.	b.d.l.

Abbreviations: Lh= lherzolite; Hz= harzburgite; b.d.l= below detection limit.

Table A4.6: Trace element (ppm) abundances of representative clinopyroxenes in MG spinel peridotites.

Sample	MG1 Lh group-1	MG1 Lh group-1	MG6 Lh group-1	MG6 Lh group-1	MG16 Lh group-2	MG16 Lh group-2	MG16 Lh group-2	MG14 Hz group-1	MG14 Hz group-1	MG14 Hz group-1	MG14 Hz group-1	MG14 Hz group-1
Cs	0.01	0.34	b.d.l.	0.03	0.01	0.01	b.d.l.	0.01	0.13	0.03	0.05	0.02
Rb	0.05	8.3	0.02	0.95	0.5	1.47	0.88	0.44	1.88	0.81	1.36	0.52
Ba	0.97	5.33	1.38	1.8	1.8	5.18	6.8	5.1	1.46	0.43	1.31	0.54
Th	1.99	1.63	1.66	1.01	0.72	0.59	0.47	1.4	2.57	3.03	2.3	2.31
U	0.55	0.41	0.63	0.26	0.02	0.06	0.05	0.17	0.35	0.14	0.23	0.11
Nb	0.34	3.4	0.4	0.34	1.92	0.95	0.39	0.45	0.67	2.2	2.53	2.17
Ta	0.06	0.2	0.03	0.03	0.09	0.05	0.05	0.01	0.02	0.08	0.1	0.13
La	12.4	21.2	12.9	13.9	22.1	25.6	17.6	15	16.1	13.8	14.9	11.8
Ce	26.1	55.3	16.8	21.9	77.9	84.2	64.4	36.9	39.3	36.5	38.6	36.8
Pr	2.55	5.61	1.37	1.91	12.2	13.6	10.9	3.93	4.01	4.32	4.25	4.42
Sr	162	323	160	215	170	219	219	105	90.5	118	94.6	106
Nd	8.67	18.05	4.11	5.97	51.6	54.8	46.8	12.3	12.8	14.1	14.2	15.2
Zr	28	58.4	8.19	8.69	136	165	159	4.98	5.1	10.8	9.13	16.8
Hf	0.46	0.98	0.28	0.3	1.85	2.42	2.45	0.18	0.15	0.23	0.17	0.39
Sm	1.38	3.18	0.59	0.79	8.93	10	9.13	1.76	1.71	1.94	1.89	2.33
Eu	0.51	1.43	0.22	0.52	2.27	2.59	2.28	0.51	0.46	0.86	0.65	0.89
Gd	1.15	2.12	0.88	1.13	6.7	7.07	6.72	1.01	1.01	1.3	1.08	1.69
Tb	0.15	0.32	0.13	0.15	0.79	0.8	0.79	0.16	0.12	0.15	0.17	0.19
Dy	1.02	1.65	0.67	0.98	4.09	4.17	4.65	0.89	0.83	1.04	1.01	1.29
Y	4.96	8.07	4.23	4.79	18.8	19.83	18.85	5.18	4.73	5.54	5.62	6.4
Ho	0.2	0.28	0.15	0.16	0.67	0.75	0.69	0.17	0.16	0.2	0.18	0.23
Er	0.47	0.74	0.44	0.42	1.73	1.91	1.76	0.58	0.54	0.54	0.54	0.59
Tm	0.09	0.12	0.08	0.08	0.22	0.26	0.24	0.09	0.09	0.07	0.07	0.1
Yb	0.51	0.57	0.5	0.56	1.17	1.43	1.32	0.56	0.61	0.63	0.68	0.61
Lu	0.08	0.11	0.08	0.07	0.16	0.2	0.18	0.06	0.06	0.08	0.08	0.11

Abbreviations: Lh= lherzolite; Hz= harzburgite; b.d.l.= below detection limit. Group-1 and group-2 as in the main text.

Chapter 5. Final remarks

The Cenozoic Southalpine Magmatic Province or VVP is the widest magmatic domain in the Adria plate, therefore it represents a crucial area to clarify the relationship between the Cenozoic magmatism and its mantle source. In this thesis petrological, geochemical, and geochronological studies of i) basic and acidic magmatic products, and ii) the mantle xenoliths hosted in the alkaline basaltic lavas helped to reconstruct the dynamic processes occurred during Europe/Adria plate interactions and to constrain nature and evolution of the mantle domain underlying the northern sector of the Adria plate.

5.1 A new geodynamic model for the Adria/Europe scenario from VVP $^{40}Ar/^{39}Ar$ geochronological data

The new high resolution $^{40}Ar/^{39}Ar$ radioisotopic age of basic and acidic magmatic products from four VVP magmatic districts (Val d'Adige, Lessini Mts., Marosticano, and Euganean Hills) allowed to depict i) the temporal evolution of the Cenozoic magmatism occurred in the southeastern Southalpine domain and ii) a new interpretation of the geodynamics processes occurred after the Adria/Europe collision, which concides with the closure of Vardar ocean (Late Cretaceous). In accordance with the biostratigraphic data and literature radioisotopic ages, the new $^{40}Ar/^{39}Ar$ data indicate that the VVP magmatic activity was discontinuous and took place in several pulses, covering a time-span of 30 Ma (from late Paleocene to early Miocene). The oldest magmatic activity (i.e., late Paleocene in age) was not dated because of the pervasive alteration of the subaqueous volcanic products. The oldest $^{40}Ar/^{39}Ar$ age obtained is Lutetian (~45 Ma; middle Eocene) from a basanitic lava flow of Lessini Mts. district. The other Lessini Mts. sample of this study is from basanitic neck of Monte Purga di Bolca cutting several lava flows and recording a younger age (~39 Ma; Bartonian) confirming that volcanism in this district lasted at least 7 Ma and occurred in several pulses. The Val d'Adige district records similar $^{40}Ar/^{39}Ar$ ages (~41-42 Ma) similar to those obtained for the Lessini Mts., while the magmatic activities of the eastern VVP districts (i.e., Euganean Hills and Marosticano) are younger. In particular, Euganean Hills acidic and basic samples yielded age of ~32 Ma, introducing for the first time the occurrance of Oligocene subaerial basaltic volcanism, beside the middle Eocene subaqueous activity. Finally, the $^{40}Ar/^{39}Ar$ ages of the Marosticano basanitic samples indicate that magmatic activity took place in early Miocene (~22 Ma).

These geochronological results depict a possible new Adria/Europe geodynamic scenario. The Alpine magmatism has been generally interpreted as an effect of European slab

breakoff with upwelling of plume-like mantle diapirs through a slab window. Such gaps were inferred thanks to the discontinuous high velocity (i.e., cold material) anomalies revealed by the seismic tomography images. However, recently, high-resolution isotropic and anisotropic tomographic profiles show that the subducting European slab is continuous from the Western Alps to the Central Alps and nearly vertical. In addition, recent numerical modelling reveal that magmatism induced by slab breakoff is uncommon as in general the breakoff occurred too deeply to generate any decompressional melting of dry upwelling asthenosphere or a thermal perturbation within the overriding lithosphere. These recent observations seem to rule out the slab breakoff as the possible triggering mechanism of the VVP magmatism. Therefore, another alternative geodynamic model is proposed. The European slab became progressively steeper and retreated toward west in response to rollback mechanisms. The effects of retreating slabs is well documented by analytical laboratory solutions, 3D experiments and numerical modeling, which demonstrate that near the lateral edge of the slab the astenospheric material located below the slab escapes laterally producing vigorous toroidal/poloidal mantle flow (i.e., horizontal and vertical rotational vortex-like components of mantle motion). Likewise, the retreatment of the European slab could have caused the upwelling of a toroidal/poloidal flow, which drove the decompression melting in the mantle wedge beneath the VVP and induced the magmatism. The migration and rejuvenation of the magmatism southeastward within the VVP could be due to overriding Adria plate moving faster than the retreating European slab.

The geochemistry of the most primary rocks from Val d'Adige, Lessini Mts., Marosticano, and Euganean Hills districts was analyzed to constrain nature and evolution of the mantle source beneath this region. The trace element patterns of VVP mafic samples have i) a typical OIB signature (i.e., enrichment in LREE compared with HREE) and ii) positive Ba, Sr, and P anomalies, probably inherited by a carbonatite metasomatized mantle source. Such metasomatized peridotitic source has been already hypothesized for the VVP alkaline magmas. In addition, on-craton mantle peridotites with fingerprint of carbonatitic/CO_2-rich silicate melt metasomatism were discovered in the Marosticano district and investigated in this thesis.

5.2. Cratonic and circumcratonic mantle portions of the Southerneastern Alps domain: evidence from VVP mantle peridotites

The petrological characterization of a new occurance of anhydrous spinel mantle peridotites from Marosticano district (NE VVP) revealed an unexpected nature of a lithospheric mantle sector beneath this area, including evidence for its metasomatic modification and evolution. This study, not only enlarge the knowledge of spatial heterogeneity within the local mantle portion, but also introduce a cratonic component in the geodynamic evolution of the Adria plate system. In fact, Marosticano clinopyroxene-bearing harzburgites and lherzolites, exhibit high contents in restitic components (i.e., Mg, Ni, Cr) similar to those observed for the on-craton peridotites worlwide. The Fo = 91.5 and cr# = 60.0 of Marosticano olivine and spinel, respectively, suggest high degrees of partial melting (>25%) occurring at high melting temperature typical of old mantle thermal regime (i.e., Archean or Early Proterozoic mantle), that would imply the clinopyroxene consumption in the spinel stability field. Therefore, the observed Marosticano clinopyroxene are secondary in nature with a metasomatic legacy as expected from clinopyroxene of peridotites from on-craton setting. In fact, i) similarities in major elements with clinopyroxene equilibrated with carbonatite combined with ii) enrichment in Th, U, Rb, and LREE, but depletion in both HREE and HFSE (e.g., Ta, Zr and Hf), and iii) REE patterns that mimic those of clinopyroxene equilibrated with a synthetic carbonatitic melt at 1100-1150°C and 1.5-2.0 GPa suggest that clinopyroxenes in both lherzolites and harzburgites were formed by the interaction between restitic peridotite and carbonatitic/CO_2-rich silicatic metasomatic melts. The metasomatic melt could be also responsible for the equilibrium temperatures (1033-1117 °C) and oxidizing conditions [$\Delta \log fO_2$ (FMQ)= -0.6 +1.1], anomalously high for a proper cratonic environment but similar to the off-craton VVP xenoliths. Calculated dissolved CO_2 mole fractions for the inferred metasomatic agent are close to 1.0, indicating that CO_2 was the largest component of such melt and it played an oxidizing role. In this frame, the positive Eu anomaly exhibited by some Marosticano clinopyroxene may be the adjustment effect of the interplay between crystal chemistry and redox conditions during metasomatism, as it was demonstrated that with the increase of fO_2 Eu^{3+} became more compatible than Eu^{2+} in the augite structure and can partition into the crystallizing pyroxene.

These features (i.e., the cratonic signature and the carbonatitic/CO_2-rich silicatic metasomatism) are not reported for any other VVP xenolith population. According to

literature, all the other mantle VVP mantle portions (i.e., Val d'Adige and Lessini Mts.) exhibit characteristics of off-craton lithospheric mantle variably affected by Na-alkaline silicatic metasomatism. However, on- and off-craton VVP mantle portions show similarities in Re-Os ages, which ranging between 1.9 to 2.1 Ga, with a unique value at 3.1 Ga for the entire VVP domain, suggesting a "hidden" cratonic signature for Val d'Adige and Lessini Mts. mantle domains. As it is known the Archean/Proterozoic cratonic roots could be modify by mechanical disruption (lithospheric thinning and incipient rifting) and by episodic rejuvenation events.

Taking all these results into account, a new geodynamic picture of the Adria plate mantle domain is proposed in this thesis. The Marosticano domain could be interpreted as the vestige of an Archean/Proterozoic cratonic keel, whose signature was not erased by the carbonatitic/CO_2-rich silicatic metasomatism, whereas Lessini Mts. and Val d'Adige xenoliths are remnants of circumcratonic domains compositionally rejuvenated by infiltration of asthenospheric-derived melts, which upwelling could be induced by the retreatment of the European slab after the Adria/Europe collision.